

Characterization of Target Gene Regulation by the Two Epstein-Barr Virus Oncogene LMP1 Domains Essential for B-cell Transformation

Bidisha Mitra¹⁻³, Nina Rose Beri¹⁻³, Rui Guo¹⁻³, Eric M. Burton¹⁻³, Laura A. Murray-Nerger¹⁻³ and Benjamin E. Gewurz^{1-3*}

¹ Division of Infectious Diseases, Department of Medicine, Brigham and Women's Hospital, 181 Longwood Avenue, Boston MA 02115, USA

² Center for Integrated Solutions in Infectious Disease, Broad Institute of Harvard and MIT, Cambridge, MA 02142, USA

³ Department of Microbiology, Harvard Medical School, Boston, Massachusetts 02115, USA

*Correspondence: bgewurz@bwh.harvard.edu

Abstract:

The Epstein-Barr virus (EBV) oncogene latent membrane protein 1 (LMP1) mimics CD40 signaling and is expressed by multiple malignancies. Two LMP1 C-terminal cytoplasmic tail regions, termed transformation essential sites (TES) 1 and 2, are critical for EBV transformation of B lymphocytes into immortalized lymphoblastoid cell lines (LCL). However, TES1 versus TES2 B-cell target genes have remained incompletely characterized, and whether both are required for LCL survival has remained unknown. To define LCL LMP1 target genes, we profiled transcriptome-wide effects of acute LMP1 CRISPR knockout (KO) prior to cell death. To then characterize specific LCL TES1 and TES2 roles, we conditionally expressed wildtype, TES1 null, TES2 null or double TES1/TES2 null LMP1 alleles upon endogenous LMP1 KO. Unexpectedly, TES1 but not TES2 signaling was critical for LCL survival. The LCL dependency factor cFLIP, which plays obligatory roles in blockade of LCL apoptosis, was highly downmodulated by loss of TES1 signaling. To further characterize TES1 vs TES2 roles, we conditionally expressed wildtype, TES1 and/or TES2 null LMP1 alleles in two Burkitt models. Systematic RNAseq analyses revealed gene clusters that responded more strongly to TES1 versus TES2, that respond strongly to both or that are oppositely regulated. Robust TES1 effects on cFLIP induction were again noted. TES1 and 2 effects on expression of additional LCL dependency factors, including BATF and IRF4, and on EBV super-enhancers were identified. Collectively, these studies suggest a model by which LMP1 TES1 and TES2 jointly remodel the B-cell transcriptome and highlight TES1 as a key therapeutic target.

Key Words: gammaherpesvirus; lymphoproliferative disease; tumor virus; B-cell oncogenesis; interferon regulatory factor; BATF; NF-kB; super-enhancer; dependency factor, apoptosis.

Short title: The LMP1 TES1 and TES2 host target gene landscape

1 Introduction:

2 Epstein-Barr virus (EBV) is a gamma-herpesvirus that persistently infects most adults
3 worldwide. EBV causes 200,000 cancers per year, including Burkitt lymphoma, Hodgkin
4 lymphoma, post-transplant lymphoproliferative disease (PTLD), and HIV/AIDS associated
5 lymphomas. EBV also causes a range of epithelial cell tumors, including gastric and
6 nasopharyngeal carcinomas, as well as T and NK cell lymphomas(1). The key EBV oncogene
7 latent membrane protein 1 (LMP1) is expressed in most of these tumors, where it drives growth
8 and survival pathway signaling.

9 To colonize the B-cell compartment and establish lifelong infection, EBV uses a series of
10 viral latency genome programs, in which different combinations of latency genes are expressed.
11 These include six Epstein-Barr nuclear antigens (EBNA) and the membrane oncoproteins
12 LMP1, LMP2A and LMP2B. LMP1 mimics aspects of signaling by the B-cell co-receptor CD40
13 (2-5), whereas LMP2A rewires surface B-cell immunoglobulin receptor signaling (6). All nine
14 latency oncoproteins are expressed in the EBV B-cell transforming latency III program, which
15 are expressed in immunoblastic lymphomas of immunosuppressed hosts. These include PTLN
16 and primary central nervous system lymphoma. The latency II program is observed in EBV+
17 Hodgkin lymphoma, where the Reed-Sternberg tumor cells express EBNA1, LMP1 and LMP2A.
18 Latency II is also frequently observed in T and NK cell lymphomas and in nasopharyngeal
19 carcinoma. Host genome NF- κ B activating mutations are frequently observed in EBV-negative
20 Hodgkin lymphoma, but to a much lesser extent in EBV+ tumors, underscoring LMP1's key role
21 in activating growth and survival signaling (7).

22 LMP1 localizes to lipid rafts, where it signals constitutively in a ligand-independent
23 fashion to activate NF- κ B, MAP kinase, STAT3, PI3K, interferon and P62 pathways. LMP1 is
24 comprised of a short N-terminal cytoplasmic tail, six transmembrane (TM) domains and a 200
25 residue C-terminal cytoplasmic tail (2-5). LMP1 TM domains drive homotypic aggregation, lipid
26 raft association and constitutive signaling (8, 9). The LMP1 C-terminal tail functionally mimics
27 signaling from activated CD40 receptors, to the point that the CD40 tail can essentially be
28 replaced by that of LMP1 in transgenic mice studies. However, while CD40/LMP1 knockin mice
29 had relatively normal B-cell development and evidence of intact CD40 function, including
30 germinal center formation and class switch recombination, T-cell independent B-cell activation
31 was also observed (10). These experiments suggest that the LMP1 C-terminal tail mimics CD40
32 signaling, but has also evolved additional functions.

33 Reverse genetic studies identified two LMP1 C-terminal cytoplasmic tail domains that
34 are critical for EBV-mediated conversion of primary human B-cells into immortalized,
35 continuously growing lymphoblastoid cell lines (LCL). Transformation effector site 1 (TES1),
36 also called C-terminal activating region 1 (CTAR1), spans LMP1 residues 186-231.
37 TES1/CTAR1 contains a PXQXT motif that engages tumor necrosis factor receptor associated
38 factors (TRAFs). TES1 activates canonical NF- κ B, non-canonical NF- κ B, MAP kinase, PI3K and
39 STAT3 pathways (3, 4, 11-15). TES2, which spans residues 351-386 and is also referred to as
40 CTAR2, activates canonical NF- κ B, MAPK, IRF7 and P62 pathways (3-5, 16-20). TRAF6 is
41 critical for LMP1 TES2-driven canonical NF- κ B, MAPK and p62 pathway activation (21-26).
42 Canonical NF- κ B signaling is critical for TES2/CTAR2 driven target gene regulation in a 293 cell
43 conditional expression model (27). Signaling from a third LMP1 C-terminal tail region, CTAR3,
44 activates JAK/STAT and SUMOylation pathways (28-30) potentially important *in vivo* but that
45 are not essential for EBV-driven B-cell transformation (31). ChIP-seq analyses demonstrated a

46 complex NF- κ B binding landscape in LCLs, in which constitutive LMP1 signaling stimulates
47 different combinations of the NF- κ B transcription factors RelA, RelB, cRel, p50 and p52 to bind
48 B-cell enhancers and promoters (32).

49 LMP1 is the only EBV oncogene that can independently transform rodent fibroblasts,
50 driving anchorage independent growth and loss of contact inhibition (33-35). LMP1 expression
51 drives aberrant B-cell growth in transgenic B-cell models, particularly in combination with LMP2
52 upon disruption of cell mediated immunity (36-39). While not critical for the first 8 days of EBV-
53 driven B-cell outgrowth (40), LMP1 is critical for EBV-mediated conversion of primary human B-
54 cells into immortalized LCLs (41, 42). A longstanding question has remained why TES1 and
55 TES2 are each essential for EBV-mediated LCL establishment. Whether either or both are
56 required for LCL survival is also unknown. Experiments using the EBV second site mutagenesis
57 method (43) demonstrated that TES1 is critical for initiation of EBV-infected lymphoblastoid cell
58 outgrowth (44). By contrast, TES2 is critical for long-term LCL growth, although TES2 null EBV
59 infected lymphoblastoid cells could be propagated on epithelial feeders (44, 45). It remains
60 incompletely understood the extent to which TES1 and TES2 play overlapping versus non-
61 redundant roles.

62 To gain insights into non-redundant, additive or synergistic roles, we profiled
63 transcriptome-wide changes in response to acute LMP1 knockout (KO). To then gain insights
64 into specific TES1 and TES2 roles, we also profiled LCL LMP1 KO with rescue wildtype, TES1
65 null, TES2 null or TES1/2 null LMP1 cDNA, newly identifying that only TES1 is required for LCL
66 survival. The key LCL dependency factor cFLIP was highly downmodulated by loss of TES1
67 signaling. As multiple latency III genes often target the same host cell targets, we also
68 constructed Burkitt B-cell models with conditional expression of wildtype, TES1 and/or TES2
69 null LMP1. Systematic RNAseq analyses identified multiple modes of target gene regulation in
70 response to LMP1 signaling, providing new insights into independent versus shared TES1 and 2
71 roles. Cross-comparison with CRISPR screen datasets defined dependency factors identified a
72 subset of LMP1 target genes critical for LCL proliferation. Similarly, differential TES1 and TES2
73 contributions to the regulation of genes targeted by viral super-enhancers were identified.

74

75

76 **Results:**

77 **CRISPR analysis of LCL LMP1 Target Genes**

78 To characterize LMP1 target genes in LCLs, we used CRISPR to knockout LMP1 in the well-
79 characterized LCL GM12878, a Tier 1 Encode project cell line that we have used extensively for
80 CRISPR analyses, and which we confirmed to have the latency III program (25, 46). GM12878
81 with stable Cas9 expression were transduced with lentivirus expressing a control single guide
82 RNA (sgRNA) targeting a human genome intergenic region or LMP1. Immunoblot confirmed
83 efficient LMP1 depletion by 48 hours post-puromycin selection of transduced LCLs (**Fig. 1A**).
84 CRISPR LMP1 editing rapidly downmodulated the LMP1/NF- κ B target genes TRAF1 and IRF4
85 and decreased non-canonical pathway processing of the p100 NF- κ B precursor into the active
86 p52 transcription factor subunit, suggesting successful on-target effects of LMP1 knockout (KO)
87 (**Fig. 1A**). At this early timepoint post-CRISPR editing, LCLs remained viable (**Fig. S1A**),
88 whereas LMP1 KO triggers LCL growth arrest and cell death shortly thereafter. We therefore
89 used this early 2-day post-puromycin selection timepoint to perform systematic RNAseq
90 analyses of control vs LMP1 KO LCLs. At a multiple hypothesis testing adjusted p-value <0.05
91 and fold change of >2 cutoff, acute LMP1 KO significantly altered the levels of around 3400 host
92 genes.

93 Genes differentially expressed in LMP1 KO vs control cells could be broadly characterized
94 into two k-means clusters, in which LMP1 KO either downregulated 1,476 or upregulated 1926
95 host genes (**Fig. 1B, Table S9**). Kyoto Encyclopedia of Genetic Elements (KEGG) pathway
96 Enrichr analysis (47) identified that cytokine receptor signaling, NF- κ B signaling and TNF
97 signaling as enriched amongst genes rapidly downmodulated by LMP1 KO (**Fig. 1C**). As
98 examples of cluster 1 NF- κ B target genes, interferon regulatory factor 4 (IRF4) and CFLAR,
99 which encodes c-FLIP, were strongly downmodulated by LMP1 KO (**Fig. 1D**). By contrast,
100 KEGG highlighted that autophagy, p53 signaling and protein-processing in the endoplasmic
101 reticulum as enriched amongst cluster 2 genes (**Fig. 1C**). As examples from these enriched
102 pathways, LMP1 KO highly induced expression of the autophagy suppressor DEPP1 and the
103 p53 target and tumor suppressor cyclin dependent kinase inhibitor 2A (CDKN2A) (**Fig. 1D-F**).

104 We next integrated our RNAseq dataset with published CRISPR analysis of host
105 dependency factors essential for EBV+ LCL, but not Burkitt B-cells (25), to gain insights into key
106 LMP1 roles in LCL growth and survival. This analysis identified that mRNA abundances of 37 of
107 the 87 CRISPR-defined LCL selective dependency factors significantly changed upon LMP1
108 KO, suggesting multiple LMP1 roles in support of LCL survival (**Fig. 1G and S1B**). Of these, it is
109 notable that multiple key suppressors of LCL intrinsic and extrinsic apoptotic pathways were
110 rapidly lost upon LCL LMP1 KO. For instance, our published CRISPR analyses highlighted non-
111 redundant roles for the transcription factors IRF4 and BATF in blockade of the intrinsic
112 apoptosis pathway and for CFLAR-encoded cFLIP in extrinsic apoptosis pathway inhibition (25),
113 each of whose mRNAs rapidly decreased upon LCL LMP1 KO. Likewise, LMP1 KO strongly
114 downmodulated expression of MDM2, an LCL-selective dependency factor (25) that targets p53
115 for proteasomal degradation and that prevents LCL p53-dependent apoptosis(48). Furthermore,
116 NF- κ B blockade triggers LCL apoptosis(49) and the LCL dependency factor NFKB2, which
117 encodes the NF- κ B transcription factor subunit p52, was also highly downmodulated by LMP1
118 KO (**Fig. 1F-G**). STRING network analysis also underscored that each of these assemble into a
119 network with 23 other LMP1-regulated LCL dependency factors (**Fig. 1H**).

120 Since LMP1 is highly expressed in Hodgkin lymphoma Reed-Sternberg tumor cells, we next
121 analyzed effects of LMP1 KO on Hodgkin lymphoma KEGG pathway genes (**Fig. S1C**).
122 Interestingly, LMP1 KO strongly downmodulated expression of the T-cell tropic chemokines
123 CCL22 and CCL17, consistent with several prior reports linking LMP1 to their expression (50,
124 51). These findings raise the possibility that LMP1-driven chemokine expression may contribute
125 to the striking enrichment of T-cells characteristic of the Hodgkin Reed-Sternberg
126 microenvironment. However, volcano plot analysis also highlighted that LMP1 KO increased
127 expression of CD274, which encodes the checkpoint inhibitor PD-L1, further implicating LMP1 in
128 T-cell regulation.

129 Given widespread effects of LMP1 KO on LCL host gene expression, we next characterized
130 effects of LMP1 KO on viral latency III genes. Mapping of RNAseq reads onto the GM12878
131 EBV transcriptome identified that LMP1 depletion significantly downmodulated mRNAs
132 encoding EBNA3A, 3C and EBNA-LP, though interestingly not those encoding EBNA2 or
133 EBNA3B (**Fig. 1I**). While it has been reported that LMP1 regulates its own mRNA expression
134 (52, 53), we did not observe changes in LMP1 mRNA abundance upon LMP1 CRISPR KO. We
135 note that CRISPR editing often results in insertions or deletions, causing functional protein
136 knockout without necessarily changing mRNA levels of the edited gene. However, it is plausible
137 a compensatory response to LMP1 knockout occurred on the mRNA level at this early
138 timepoint, potentially balancing loss of NF- κ B induced LMP1. Taken together, our RNAseq
139 analyses raise the possibility that secondary effects of LMP1 KO on Epstein-Barr nuclear
140 antigens may also contribute to changes in the host transcriptome and cell death upon LMP1
141 KO.

142

143 **TES1 but not TES2 signaling is critical for LCL survival**

144 While TES1 and TES2 signaling are each critical for B-cell transformation, it has remained
145 unknown whether either or both are necessary for proliferation of fully transformed LCLs.
146 Likewise, knowledge has remained incomplete about shared versus non-redundant TES1 and
147 TES2 roles in LCL host gene regulation. To gain insights into these key questions, we
148 engineered Cas9+ GM12878 LCLs with conditional expression of wildtype (WT) LMP1, or with
149 well characterized point mutants that abrogate signaling from the TES1 TRAF binding domain
150 (TES1m, residues 204PQQAT208 -> **AQAAT**), from TES2 (TES2m, 384YYD386 -> ID) (45, 54,
151 55) (**Fig. 2A**). A silent mutation in the CRISPR protospacer adjacent motif (PAM) was used to
152 abrogate CRISPR editing of these LMP1 rescue cDNA constructs. For cross-comparison, we
153 also established conditional TES1/TES2 double mutant (DM) cell lines with both mutations, to
154 profile responses to other LMP1 regions, potentially including CTAR3 or unfolded protein
155 responses induced by LMP1 induction (56, 57) (**Fig. 2A**). LCLs were then transduced with
156 lentivirus expressing a control sgRNA targeting a human intergenic region or LMP1. Conditional
157 LMP1 expression was then induced by addition of 400 ng/ml doxycycline, such that the rescue
158 cDNA was induced as endogenous EBV-encoded LMP1 was depleted. We confirmed similar
159 levels of LMP1 expression across this series and achieved similar LMP1 levels as in unedited
160 GM12878 LCLs (**Fig. 2B**). Importantly, we validated that WT LMP1 rescued physiological levels
161 of LMP1 target TRAF1 expression and p100/p52 processing (**Fig. 2B**). TES1 is responsible for
162 the majority of LMP1-mediated TRAF1 induction and p100/p52 processing (54, 58) and as
163 expected, conditional TES1m and DM expression failed to rescue physiological levels of TRAF1
164 or p100/p52 processing in GM12878 with endogenous LMP1 KO. By contrast, TES2m induced

165 levels of TRAF1 and p100/p52 processing in LMP1 KO levels approaching those in unedited
166 GM12878 (**Fig. 2B**), validating our LCL LMP1 KO/rescue system.

167 We next tested the effects of LMP1 WT, TES1m, TES2m or DM rescue cDNA expression on
168 GM12878 proliferation. Whereas signaling from both TES1 and TES2 are required for EBV-
169 driven primary human B-cell growth transformation, we unexpectedly found that LCLs require
170 signaling only from TES1 for growth and survival: LMP1 KO LCLs with WT vs TES2m rescue
171 cDNA proliferated indistinguishably. By contrast, LCLs with TES1m or DM rescue cDNA
172 expression failed to proliferate (**Fig. 2C**). To characterize this unexpected result further, we next
173 measured effects of endogenous LMP1 KO and rescue LMP1 cDNA expression on LCL
174 survival. Consistent with our growth curve analysis, LMP1 KO LCLs with TES1m or DM rescue
175 cDNA exhibited widespread cell death, as judged by uptake of the vital dye 7-aminoactinomycin
176 D (7-AAD) by FACS analysis (**Fig. 2D-E**). Consistent with apoptosis as the cell death pathway
177 triggered by loss of TES1 signaling in LCLs, levels of Annexin V and executioner caspase 3/7
178 activity were significantly higher in LMP1 KO GM12878 with TES1m or DM than with WT or
179 TES2m rescue cDNA expression (**Fig. 2F-G and S2**). Taken together, these data newly
180 suggest that TES1 signaling is necessary for LCL growth and survival in a manner that is not
181 redundant with TES2, and that cannot be rescued by TES2 signaling alone.

182

183 **Identification of TES1 versus TES2 roles in LCL gene regulation**

184 To gain insights into overlapping versus non-redundant TES1 and TES2 LCL roles, we
185 performed biological triplicate RNAseq analyses to cross-compare GM12878 transcriptomes at
186 day 6 post endogenous LMP1 KO and with doxycycline-induced WT, TES1m or TES2m rescue
187 cDNA expression. We selected this early timepoint as it is just prior to the divergence of the
188 growth curves (**Fig. 2C, Table S10-11**) and the onset of apoptosis. K-means analysis identified
189 six clusters in which host gene expression differed between LMP1 KO LCLs with WT, TES1m or
190 TES2m cDNA rescue. KEGG analysis highlighted pathways most highly enriched in each
191 cluster (**Fig. 3A**). Notably, apoptosis pathway genes were the most highly enriched in cluster 4
192 genes, which were expressed at lower levels in cells with TES1m than with WT or TES2m
193 rescue cDNA expression, suggesting that TES1 signaling may induce their expression.
194 Apoptosis genes were also enriched amongst cluster 5 genes, where levels were lower in cells
195 with TES2m expression, suggesting that TES2 signaling may induce their expression (**Fig. 3A**).

196 Given this apoptosis signal, we next analyzed the KEGG apoptosis gene set responses to
197 WT, TES1m or TES2m cDNA rescue (**Fig. 3B**). Interestingly, a cluster of genes were more
198 highly expressed in cells with WT and TES2m than with TES1m expression, including the anti-
199 apoptotic genes CFLAR, BCL2 and BIRC3, which encodes the cIAP2 ubiquitin ligase, which
200 counteracts TNF-driven cell death. BCL2 and BIRC3 were not defined as LCL dependency
201 factors by genome-wide CRISPR analysis, whereas CFLAR was (25). Intriguingly, while a small
202 number of the 87 LCL dependency factors (25) were more highly downmodulated in LMP1 KO
203 LCLs with TES1 rescue than with TES2 rescue, CFLAR was the LCL dependency factor most
204 highly depleted from with TES1m rescue (nearly 8-fold) (**Fig. 3C, S3A**). By contrast, CFLAR
205 was only mildly depleted (<0.5 fold) in cells with TES2m rescue (**Fig. 3C**). We validated that
206 CFLAR-encoded c-FLIP was highly downmodulated on the protein level in LMP1 KO LCLs with
207 TES1m or DM LMP1 rescue, but not in LCLs with WT or TES2m rescue at an early timepoint
208 prior to cell death (**Fig. 3D**). The LCL dependency factors NFKB2 and CCND2 were also more

209 highly downmodulated in LMP1 KO cells with TES1 than TES2 cDNA rescue but not to the
210 same extent as CFLAR (**Fig. 3C**), suggesting that their loss may not be responsible for
211 apoptosis in the absence of TES1 signaling. Collectively, these analysis underscore distinct
212 TES1 versus TES2 signaling roles in control of LCL apoptosis pathway gene expression.

213 To gain further insights into potential TES1 vs TES2 roles in regulation of genes with
214 relevance to Hodgkin Reed-Sternberg cells, we analyzed KEGG Hodgkin lymphoma pathway
215 gene expression in LMP1 KO GM12878 rescued with WT, TES1m or TES2m LMP1. This
216 analysis highlighted that many KEGG Hodgkin lymphoma pathway genes are jointly induced by
217 TES1 and TES2 signaling in LCLs, including CCL22, BCL3, cRel, IRF4, STAT3, STAT6 and
218 CD70, each of which have prominent roles in Hodgkin lymphoma pathogenesis (**Fig. S3B**).
219 Interestingly, the Hodgkin lymphoma therapeutic target CD27 was expressed at lower level with
220 TES1m rescue but more highly expressed in cells with TES2m rescue, suggesting that TES1
221 and TES2 signaling may jointly balance its expression.

222 On the transcriptome-wide level, multiple well characterized LMP1 target genes were more
223 highly expressed in LCLs rescued with WT LMP1 than with TES1m cDNA, establishing these as
224 key TES1 LCL target genes. These included CD40, TRAF1, EBI3 and ICAM1 (**Fig. 4A**), which
225 was previously established as a TES1 target genes in studies of cell lines with LMP1 over-
226 expression, including BL-41 Burkitt and BJAB diffuse large B-cell lymphoma models(54).
227 Notably, this approach also newly suggests a large number of B-cell targets whose upregulation
228 or downregulation is dependent on TES1 signaling. These include CFLAR and TLR6 (which
229 encodes Toll-like receptor 6), which were significantly more highly expressed in LMP1 KO LCLs
230 with WT LMP1 cDNA rescue. By contrast, the mRNA encoding the histone loader DAXX, which
231 can serve as an epigenetic suppressor of EBV gene expression (59, 60) and DNA damage
232 pathway TP53 (which encodes p53), were expressed at considerably higher in LMP1 KO LCLs
233 with TES1m than WT LMP1 rescue cDNA (**Fig. 4A**). This result suggests that TES1 may
234 repress their expression. Enrichr analysis of genes more highly expressed with WT LMP1
235 rescue highlighted TNF and NF- κ B signaling as enriched KEGG pathways, whereas p53
236 signaling and apoptosis were amongst the pathways most highly enriched in genes more highly
237 expressed with TES1m rescue (**Fig. 4B**).

238 Volcano plot and KEGG pathway analysis highlighted LCL genes differentially expressed in
239 LMP1 KO LCLs with WT vs TES2m rescue (**Fig. 4C-D**). KEGG pathways enriched amongst
240 genes more highly expressed with WT LMP1 rescue again included antigen presentation and
241 cytokine/receptor interaction, but also included systemic lupus erythematosus (SLE). Pathways
242 enriched amongst genes more highly expressed with TES2m rescue instead included cyclic
243 GMP protein kinase G (cGMP-PKG) signaling and phosphatidylinositol signaling (**Fig. 4D**).
244 Notably, TP53 (which encodes p53) was also more highly expressed in LMP1 KO LCLs with
245 TES2m than WT LMP1 rescue, suggesting that both TES1 and 2 signaling regulate its
246 expression. By comparison, CFLAR expression was similar in LMP1 KO LCLs with WT and
247 TES2m rescue, further establishing it as a TES1 target in LCLs (**Fig. 4C**).

248 Direct cross-comparison of genes in LCLs with TES1m vs TES2m rescue further identified
249 roles of TES1 versus TES2 signaling on LCL target gene expression. The oncogenic kinase
250 CLK2, which has roles in splicing regulation, was the host gene most highly expressed in LMP1
251 KO with TES2m rescue than in cells with TES1m rescue, newly indicating that it is strongly
252 induced by TES1 or strongly inhibited by TES1 (**Fig. 4E**). Enrichr analysis indicated that multiple
253 KEGG metabolism pathways were the most highly enriched in cells with TES2m rescue,

254 including fructose/mannose metabolism, HIF1 signaling and AMPK signaling (**Fig. 4E-F**). In
255 support, the glycolytic enzyme PFKFB4 and the kinase PDK1, which regulates flux of glycolytic
256 products to mitochondrial metabolism pathways at the level of pyruvate, were more highly
257 expressed with TES2m rescue, suggesting that they are either driven by TES1 or repressed by
258 TES2 signaling (**Fig. 4F**). Cell cycle regulation was the KEGG pathway most enriched amongst
259 genes more highly expressed with TES1m rescue. The cyclin dependent kinase (CDK)
260 substrate and cytokinesis regulator PRC1, as well as the CDK1 kinase and mitosis regulator
261 PKMYT1, were amongst the genes most highly differentially expressed in TES1m rescue (**Fig.**
262 **4E-F**), suggesting that TES2 drives or that TES1 instead inhibits their expression.

263

264 **B-cell genes induced by conditional expression LMP1 in EBV-negative Burkitt cells**

265 As a complementary approach to our loss-of-function CRISPR KO LCL analyses, we next
266 profiled B-cell responses to conditional LMP1 expression. A goal of this approach was to identify
267 LMP1-specific effects on host gene expression, since LMP1 KO significantly altered expression
268 of several EBV latency III genes. Furthermore, EBNA and LMP latency III oncoproteins often
269 jointly target host genes. Therefore, to study LMP1-specific effects in isolation of other latency III
270 genes, we engineered EBV-negative Akata and BL-41 Burkitt B-cell lines with doxycycline-
271 inducible WT, TES1m, TES2m or DM LMP1 alleles. The Akata cell line was originally
272 established from a human EBV+ Burkitt tumor (61), but an EBV-negative subclone that
273 spontaneously lost the viral genome was isolated shortly thereafter (62), which we used for
274 these studies. Similarly, the BL-41 cell line was established from an EBV-negative human
275 Burkitt lymphoma tumor (63). BL-41 were used for early microarray analysis of latency III or
276 LMP1 effects on a subset of human genes (49). We validated that WT and point mutant LMP1
277 were expressed to similar extents across the panel. As expected, TES1m and DM exhibited
278 impaired non-canonical NF- κ B pathway activation, as judged by p100:p52 processing (**Fig S4A-**
279 **B**). LMP1 signaling was also validated by FACS analysis of ICAM-1 and Fas upregulation.
280 Consistent with a published study (54), TES1 signaling more strongly induced ICAM-1 and Fas
281 in both Burkitt cell lines, even though BL-41 had somewhat higher basal NF- κ B activity than
282 Akata, as judged by Fas and ICAM-1 levels in uninduced cells (**Fig. S4C-J**).

283 We then profiled effects of conditional WT, TES1m, TES2m or DM expression for 24 hours
284 on the Akata transcriptome using biological triplicate RNAseq datasets. K-means heatmap
285 analysis with n=6 clusters revealed strikingly distinct patterns of host gene responses to WT,
286 TES1m, TES2m and DM LMP1 signaling (**Fig. 5A, Table S1-4**). Cluster 1 genes were highly
287 upregulated by WT LMP1, to a lesser extent by TES2m (in which only TES1 signals), and more
288 modestly by TES1m (in which only TES2 signals). This result suggests that TES1 signaling
289 contributes more strongly than TES2 to their expression. Notably, CFLAR was a cluster I gene
290 target, consistent with our finding that TES1 drives CFLAR expression in LCLs, as was the
291 interferon stimulated gene IFIT1 (**Fig. 5B**). KEGG pathways enriched amongst Cluster 1 genes
292 included TLR signaling, chemokine signaling, IFN signaling and NLR signaling (**Fig. 5C**).
293 Cluster 1 also contained well described LMP1 target genes, including TRAF1, which we
294 validated by immunoblot (**Fig. S4A**), consistent with a prior study(54). Notably, MAP3K7, which
295 encodes the kinase TAK1 is also a Cluster 1 gene. Since TAK1 is critical for TES2/canonical
296 NF- κ B and MAP kinase signaling (26), this result suggests an important mechanism of cross-
297 talk between TES1 and TES2. Likewise, the Cluster I gene IRF7 binds to and is activated by
298 TES2 (64-67), again suggesting cross-talk between LMP1 pathways. STAT1 and STAT3 are

299 also Cluster 1 genes, raising the question of whether these STATs may drive interferon
300 stimulated gene induction downstream of LMP1.

301 Cluster 2 genes were induced by WT, TES1m or TES2m LMP1 to a similar extent (**Fig. 5C**),
302 suggesting that they redundantly respond to TES1 or TES2 signaling. GO analysis highlighted
303 enrichment of NF- κ B signaling in this cluster, and which included mRNAs encoding four NF- κ B
304 transcription factor subunits, as well as the NF- κ B induced inhibitors I κ B α , I κ B δ and I κ B ϵ . mRNA
305 fold changes for *NFBK2*, which encodes non-canonical pathway NF- κ B p52 transcription factor
306 are shown in **Fig. 5C** and are consistent with our LCL rescue analysis, which identified similarly
307 important roles for both TES1 and TES2 in support of NFKB2 expression (**Fig. 3C**). Consistent
308 with a prior study (54), Fas and ICAM-1 are Cluster 2 genes similarly induced on the mRNA
309 level by TES1m and TES2m, though interestingly, plasma membrane ICAM-1 levels were lower
310 in cells expressing TES1m (**Fig. S4C-F**). This result raises the possibility that TES1 signaling
311 may play a role in ICAM-1 post-transcriptional regulation and/or trafficking.

312 Cluster 3 genes were expressed at lower levels in cells expressing TES1m, even as
313 compared with cells expressing LMP1 DM, suggesting that unopposed TES2 signaling results in
314 their downregulation (**Fig. 5B and S4A**). Cluster 3 genes were enriched for multiple KEGG
315 metabolism pathways, including oxidative phosphorylation (**Fig. S5A**). Cluster 4 contained a
316 smaller subset of host genes, downregulated by TES1 signaling, including in the WT LMP1
317 context. This gene set was enriched for SNARE interactions in vesicular transport and
318 sphingolipid metabolism (**Fig. S5B**). Cluster 5 mRNAs were instead upregulated by unopposed
319 TES2 signaling (**Fig. 5B, S5C**) and enriched for the KEGG ubiquitin mediated proteolysis
320 pathway. Finally, Cluster 6 genes were repressed by TES1 and TES2 signaling in an additive
321 manner (**Fig. 5D**). This gene set was enriched for mismatch and base excision repair,
322 nucleotide metabolism, cystine and methionine metabolism. TES1 and TES2 signaling may
323 additively recruit the same repressors or may instead recruit co-repressors to these sites.

324 We next used RNAseq to profile BL-41 Burkitt cells. RNAseq was performed at 24 hours
325 post-expression of WT, TES1m, TES2m or DM LMP1. K-means analysis with n=6 clusters
326 again revealed categories of genes that respond differently to LMP1 alleles (**Fig. S6A, Table**
327 **S5-8**). As observed in Akata, Cluster 1 genes were most highly induced by WT, and to a lesser
328 extent by TES1m or TES2m, suggesting that TES1/2 additively or synergistically induce their
329 expression. Cluster 1 genes contained multiple pro-inflammatory factors, including chemokines
330 and the interferon pathway transcription factors STAT1, IRF4, IRF5 and IRF9 (**Fig. S6A-B**). As
331 observed in Akata, cluster 2 genes were induced more strongly by TES2m than by TES1m, and
332 to a somewhat higher level by WT LMP1, suggesting that these are predominantly TES1 target
333 genes (**Fig. S6C**). Consistent with our LCL and Akata cell analyses, CFLAR was a Cluster 2
334 gene more highly induced by LMP1 alleles with TES1 signaling, further underscoring it as a key
335 TES1 target gene (**Fig. S6C**). By contrast, BL-41 Cluster 4 genes were instead suppressed by
336 unopposed TES1 signaling even relative to levels observed in cells with LMP1 DM expression,
337 suggesting that TES2 may block TES1 repressive effects on these host targets (**Fig. S6D**).
338 Cluster 6 genes were enriched for the antigen presentation pathway and were most highly
339 induced by TES2m, suggesting positive TES1 and potentially also negative TES2 roles in their
340 induction (**Fig. S6E**). While concordant to a large degree, we speculate that observed
341 differences between LMP1 effects on Akata versus BL-41 host gene expression may likely
342 reflect the somewhat higher basal NF- κ B levels observed in BL-41, and perhaps also
343 differences in driver mutations pathways frequently found in EBV+ vs EBV- Burkitt lymphomas

344 (68, 69). Nonetheless, both models highlight distinct clusters of host B-cell target genes that
345 differ in responses to TES1, TES2 or combined TES1/2 signaling.

346

347 **LMP1 WT, TES1, TES2 and DM target genes**

348 We next cross-compared the most highly differentially-expressed genes across the LMP1
349 conditions. At a fold-change >2 and adjusted p value <0.05 cutoff, WT LMP1 highly upregulated
350 1021 and downregulated 518 Akata genes, respectively. The most highly upregulated genes
351 included multiple interferon stimulated genes, TRAF1, FAS and CFLAR (**Fig. 6A**). Interestingly,
352 WT LMP1 decreased expression of the recombinase RAG1 and RAG2 mRNAs, as well as
353 MME, which encodes CD10, a plasma membrane protein that we and others have found is
354 downmodulated by EBV latency III (70-72). Enrichr analysis identified that EBV infection was
355 the KEGG pathway most highly upregulated by WT LMP1 (**Fig. 6B**), reflecting the major LMP1
356 contribution to latency III datasets used in KEGG. Likewise, NF- κ B and TLR signaling were also
357 highly enriched, whereas downmodulated genes were enriched in the term primary
358 immunodeficiency. Highly concordant effects were observed in the BL-41 cell context, where the
359 same KEGG pathways were the most enriched amongst LMP1 upregulated genes (**Fig. S7A-C**,
360 **Table S5**). Cross-comparison of expression patterns in Akata and BL-41 with WT vs DM LMP1
361 expression again revealed highly concordant results (**Fig. 6C-D and S7D-F**), further validating a
362 range of host genes as targets of TES1 and 2 signaling.

363 To gain insights into how TES2 signaling shapes LMP1 genome-wide targets, we next
364 cross-compared transcriptomes from Akata expressing WT vs TES1 mutant LMP1. At a fold-
365 change >2 and adjusted p-value <0.05 cutoff, 561 genes were more highly expressed in WT
366 than LMP1 TES1m, whereas 201 were less highly expressed. Interestingly, multiple interferon
367 stimulated genes, including IFIT1, IFI6, STAT1 and IFI44 were amongst the most highly
368 upregulated in WT LMP1 expressing cells (**Fig. 6E**). Enrichr analysis identified TNF, Nod-like
369 receptor (NLR) and JAK/STAT signaling to be the most highly enriched KEGG pathways
370 amongst genes more highly expressed in WT LMP1+ cells, whereas oxidative phosphorylation
371 was the most highly enriched KEGG pathway amongst genes more highly expressed in cells
372 expressing the TES1 mutant (**Fig. 6F**). Similar analyses on BL-41 cell datasets again revealed
373 large numbers of differentially expressed genes in WT vs TES1m LMP1 expressing cells (**Fig.**
374 **S8A-B**).

375 To then gain insights into how TES1 signaling shapes LMP1 genome-wide target gene
376 effects, we cross-compared Akata differentially expressed genes at 24 hours post expression of
377 WT vs TES2 mutant LMP1. At a fold-change >2 and adjusted p value <0.05 cutoff, 275 genes
378 were more highly expressed in Akata with WT than TES2 mutant LMP1, whereas 118 were less
379 highly expressed. Once again, multiple interferon stimulated genes (ISG), including STAT1, IFI6
380 and OAS1 were more highly expressed in WT cells. Enrichr analysis identified sphingolipid
381 signaling and metabolism to be most highly enriched KEGG pathways amongst genes
382 upregulated genes, whereas TCA cycle was the most significant KEGG pathway amongst
383 genes more highly expressed with TES2 mutant LMP1 expression (**Fig. 6G-H**). Similar numbers
384 of genes were differentially regulated between WT and TES2m expressing cells in the BL-41
385 context, where Toll-like receptor signaling was the most highly enriched term amongst genes
386 more highly expressed in WT LMP1+ cells (**Fig S8C-D**). These analyses are consistent with a
387 model in which TES1 and TES2 signaling additively or synergistically upregulate ISGs. Direct

388 cross-comparison of TES1 vs TES2 signaling in Akata and BL41 further revealed pathways
389 selectively targeted by either (**Fig. S8E-H**). In the Akata environment, cells expressing TES2m
390 more highly induced ISGs, including IFIT1, IFI6, OAS, IFI44 and DDX58 (**Fig. S8E**). Enrichr
391 analysis indicated that TES1 signaling most strongly induced the Nod-like receptor (NLR),
392 necroptosis and chemokine signaling KEGG pathways. By contrast, TES2 signaling (from the
393 TES1 mutant) most highly induced growth hormone and multiple amino acid metabolism KEGG
394 pathways (**Fig. S8F**). In BL-41 cells, interferon stimulated genes were not as highly induced by
395 TES2m (**Fig. S8G**). Since non-canonical NF- κ B activity can strongly impact B cell type I
396 interferon pathways (73), we suspect that differences in basal NF- κ B activity in BL-41 may
397 compensate to some extent to reduce this phenotype. Instead, cell adhesion molecules and
398 TNF signaling were most highly enriched. For instance, CFLAR was significantly more highly
399 induced by TES1 signaling, as was OTULIN, a deubiquitinating enzyme that controls TNF/NF-
400 κ B canonical pathway. FoxO and Toll-like receptor signaling were the most highly enriched
401 KEGG pathways induced by TES2 signaling (by the TES1 mutant) in BL-41, with FOXO
402 signaling the most selectively induced by TES1 mutant LMP1 (**Fig. S8H, Table S10**).

403 We next directly cross-compared results from our LCL and Burkitt systems. Volcano plot
404 analysis identified host cell genes whose expression was induced by Akata WT LMP1
405 expression but decreased by LCL LMP1 KO, suggesting that they are bone fide LMP1 targets
406 (**Fig. S9A**, orange circles and **Tables S1, 9**). This gene set included CFLAR, TRAF1, EBI3,
407 CCL2, CD40, consistent with prior studies (27, 49, 54, 74-77). Similarly, genes whose
408 expression was suppressed by Akata WT LMP1 expression but induced by LCL LMP1 KO were
409 identified as LMP1-repressed host targets (**Fig. S9A**, green circles). We similarly cross-
410 compared data from our Akata LMP1 expression and LCL LMP1 rescue datasets. Key targets of
411 TES1 signaling, whose expression was significantly lower in Akata with TES1 mutant than WT
412 LMP1 and also in LCLs rescued by TES1 mutant versus WT LMP1, included CFLAR, TRAF1,
413 NFKB2 and CCL22 (**Fig. S9B**). Likewise, key TES2 targets more highly induced by WT than by
414 TES2 mutant in both contexts included CCL22 and EBI3, whereas CR2, which encodes the
415 EBV B-cell receptor complement receptor 2, was instead more highly expressed in cells with
416 TES2m than WT LMP1 expression, suggesting it is repressed by TES2 signaling (**Fig. S9C**).
417 Taken together, these findings serve to validate a class of host genes as LMP1 targets in the
418 LCL context, although we cannot exclude that they are regulated through secondary effects.

419

420 **LMP1 TES1 and TES2 roles in LCL Dependency Factor BATF and IRF4 Expression**

421 We next characterized LMP1 pathways important for BATF and IRF4 induction, given their
422 key LCL but not Burkitt B-cell dependency factor roles (25, 78, 79). Notably, BATF and Jun
423 family members bind cooperatively with IRF transcription factors to AP1-IRF composite DNA
424 elements (AICE) (80), and JunB is the Jun family member predominantly expressed in LCLs
425 (**Fig. 8A**). WT and TES2m LMP1 upregulated IRF4 mRNA abundance to a similar extent in
426 Akata, whereas TES1m did so to a somewhat lesser extent. By contrast, TES1m and TES2m
427 each upregulated BATF, but not quite as strongly as WT LMP1 (**Fig. 8B**). Taken together with
428 the LCL LMP1 knockout data, these results suggest that LMP1 TES1 and TES2 signaling each
429 support expression of the host transcription factors that bind to AICE.

430 We next examined the contribution of LMP1 NF- κ B pathways to B cell IRF4 and BATF
431 expression. LMP1 CRISPR knockout in GM12878 LCLs or in latency III Jijoye Burkitt cells

432 significantly reduced BATF and to IRF4 expression at the protein level, though effects on IRF4
433 were more subtle at this early timepoint (**Fig. S10A**). LMP1 induction of IRF4 and BATF was
434 strongly impaired by induction of either TES1m or TES2m in Akata or in LCLs, relative to levels
435 in cells with WT LMP1 (**Fig. 8B and S10B**). To test canonical NF- κ B pathway roles in IRF4 and
436 BATF induction, we then induced LMP1 in the absence or presence of a small molecule
437 antagonist of the kinase IKK β , which is critical for canonical NF- κ B pathway signaling. IKK β
438 inhibition blocked their residual induction by TES1m and TES2m (**Fig. 8C-D**). The IKK β inhibitor
439 also reduced BATF and IRF4 expression in GM12878 (**Fig. S10C**). Similar results were
440 obtained in Akata cells that co-induced LMP1 with an I κ B α super-repressor (I κ B α -SR), in which
441 I κ B α serine 32 and 36 to alanine point mutations prevent its canonical pathway phosphorylation
442 and proteasomal degradation (**Fig. S10D**). Furthermore, CRISPR KO of the canonical NF- κ B
443 pathway kinase TAK1 significantly impaired IRF4 induction by WT and also TES2m LMP1 (**Fig.**
444 **8E**). Taken together, these results suggests that canonical NF- κ B pathways driven by both
445 TES1 and TES2 signaling are each important for BATF and IRF4 expression (**Fig. 8F**).

446

447

448 **LMP1 TES1 and TES2 roles in EBV Super-Enhancer target induction**

449 The five LMP1-activated NF- κ B transcription factor subunits and four EBNA target a set of
450 LCL host genome enhancers termed EBV super-enhancers (EBV SE). EBV SE are
451 characterized by occupancy by all five NF- κ B subunits, EBNA2, LP, 3A and 3C and markedly
452 higher and broader histone H3K27ac ChIP-seq signals than at typical LCL enhancers (**Fig. 9A**).
453 SE are critical for cell identity and oncogenic states (81), and EBV SE are important for LCL
454 growth and survival (82-84). However, little has remained known about the extent to which
455 LMP1 TES1 versus TES2 signaling contribute to EBV SE. To gain insights, we therefore
456 interrogated EBV SE gene target responses, we first plotted EBV SE gene target responses to
457 GM12878 LMP1 CRISPR KO. At the early timepoint of 48 hours after LMP1 editing, expression
458 of SE targets TRAF1, PRDM1 (which encodes the transcription repressor BLIMP1) and GPR15
459 (which encodes a G-protein coupled chemokine receptor) each significantly decreased, though
460 most other EBV SE gene targets did not significantly change at this early timepoint (**Fig. 9B**, red
461 circles). This data suggests that EBV SE are robust to short-term perturbations of LMP1
462 expression, perhaps given persistence of the established epigenetic landscape built at these
463 key sites.

464 To then identify the extent to which LMP1 is sufficient to alter expression of these LCL EBV
465 SE targets, we next visualized effects of WT, TES1m or TES2m rescue of LMP1 KO LCLs.
466 Potentially because this analysis could be done at a later timepoint post LMP1 CRISPR editing
467 (day 6 post LMP1 KO), we observed stronger effects on EBV SE target gene expression.
468 Rescue with TES1 mutant LMP1 caused significant loss of CFLAR, BCL2 and TRAF1 relative to
469 levels with WT rescue, whereas rescue with either TES mutant significantly lowered levels of
470 CD86 and BIRC3 messages from levels observed with WT rescue (**Fig. 9C-D**). As a
471 complementary approach, we also analyzed effects of conditional LMP1 induction in our Burkitt
472 models on EBV SE target gene expression. In Akata B cells, WT LMP1 induction was sufficient
473 to significantly upregulate the abundance of the majority of EBV SE target gene mRNAs (**Fig.**
474 **S11A**). This result suggests that while EBNA-2, LP, 3A and 3C also target these sites in LCLs,
475 LMP1 can independently alter expression of most EBV SE targets, albeit not necessarily to the

476 same extent as latency III. By contrast, Akata TES1m or TES2m induction less strongly induced
477 most EBV SE targets (**Fig. 9 and S11B-C**). A similar pattern was observed in BL-41 cells (**Fig.**
478 **11D-F**). Taken together, our results indicate that TES1 and TES2 likely play key joint roles in the
479 induction of EBV SE target genes.

480

481

482 Discussion:

483 Why the LMP1 C-terminal tail TES1 and TES2 domains are each necessary for lymphoblastoid
484 B-cell immortalization, and whether each are necessary for transformed cell survival have
485 remained longstanding questions. To gain insights into key LMP1 B-cell roles, we used a novel
486 LCL LMP1 KO with conditional LMP1 rescue system to identify that signaling by TES1, but not
487 TES2, is required for LCL survival. We performed the first systematic B-cell transcriptome-wide
488 analyses to identify effects of LMP1 knockout in the absence or presence of rescue by WT, TES1
489 mutant or TES2 mutant LMP1, at early timepoints where cells remained viable. These highlighted
490 key LMP1 TES1 and TES2 roles in support of LCL dependency factor and EBV super-enhancer
491 targets gene expression. As a complimentary approach to identify host B-cell genome-wide
492 targets of LMP1 signaling, we also profiled EBV-negative Burkitt B-cell responses to conditional
493 expression of wildtype LMP1, or LMP1 point mutants abrogated for signaling by TES1 or TES2.
494 These further highlighted host target genes that responded more strongly to TES1 than TES2,
495 that were similarly upregulated by either TES1 or TES2, that were downmodulated by either TES
496 in a manner that is negatively regulated by the other, that were induced by TES2 but dampened
497 by TES1, or that were inhibited by both TES1 and TES2 (**Fig. 10**).

498 LMP1 knockout rapidly altered expression of ~3400 LCL genes. We do not suspect that these
499 changes were secondary to cell death, as we performed profiling on viable cells at an early
500 timepoint post-CRISPR editing. Conditional expression of WT LMP1 rescued LCL survival,
501 confirming on-target CRISPR effects on EBV genomic LMP1. Our rescue approach identified that
502 loss of TES1, but not TES2 signaling, triggered LCL apoptosis, as judged by upregulation of
503 caspase 3 and 7 activity and by FACS analysis for plasma membrane Annexin V. Disruption of
504 cell death signaling is a hallmark of cancer (85), and enrichment analysis identified that the KEGG
505 apoptosis pathway was highly altered by loss of TES1. Notably, LMP1 has thus far remained an
506 undruggable target. Therefore, these results suggest that small molecule or peptide inhibitors that
507 block TES1 signaling may have therapeutic benefit, even in the absence of effects on TES2, for
508 instance in the setting of EBV-driven post-transplant and central nervous system lymphomas,
509 which frequently express the latency III program and which are modeled by LCLs. It will be of
510 interest to determine whether TES1 signaling has similarly important roles in apoptosis blockade
511 in other EBV-infected tumor contexts, including in Hodgkin lymphoma Reed-Sternberg tumor cells
512 and in nasopharyngeal carcinoma, where little is presently known about TES1 vs TES2 roles.

513 The key LCL dependency factor CFLAR, which encodes the extrinsic apoptosis pathway
514 inhibitor c-FLIP, was highly downmodulated upon loss of TES1 signaling, to a significantly
515 greater extent than upon loss of TES2 signaling. We previously identified that c-FLIP is required
516 for LCL survival and is required to block the extrinsic apoptosis pathway that is otherwise
517 triggered by TNF α signaling, likely in response to EBV oncogenic stress (25), though this
518 remains the only study characterizing cFLIP roles downstream of LMP1. Therefore, our data
519 newly identified CFLAR as a key TES1 target gene and suggests that TES1 signaling is
520 required for LCL survival, at least in part due to obligatory roles in blockade of apoptosis at the
521 level of cFLIP induction. Our data raises the interesting question of why CFLAR expression is
522 particularly dependent on TES1 signaling, to a much greater extent than TES2. It is plausible
523 that a TES1-driven non-canonical NF- κ B pathway is particularly important for cFLIP
524 transcription. However, TES1 signaling also strongly activates canonical NF- κ B pathways (13,
525 15, 86), which may be critical for CFLAR induction. Alternatively, MAP kinases activated by
526 TES1 may also support CFLAR expression.

527 We also highlight LMP1 TES1 and TES2 roles in support of additional LCL dependency factors,
528 in particular BATF and IRF4. In contrast to CFLAR, TES1 and TES2 signaling were each found
529 to be important for BATF and IRF4 expression, both in LCL and Burkitt cell models. TES1 and
530 TES2 driven canonical NF- κ B signaling supported BATF induction in EBV-negative Burkitt cells,
531 where EBNA2 is not expressed. BATF and IRF4 expression rapidly decreased upon LMP1 KO
532 in LCLs, even upon rescue by LMP1 signaling from only one TES domain. Thus, in LCLs,
533 EBNA2 and LMP1-stimulated canonical NF- κ B jointly induce this critical LCL dependency factor.
534 LMP1 canonical NF- κ B pathways were also critical for inducing IRF4, which binds with BATF to
535 composite AICE DNA sites. As EBNA2 also supports BATF (87) and EBNA3C also supports
536 IRF4 expression (88), our results further highlight BATF and IRF4 as major hubs of EBV
537 oncoprotein cross-talk.

538 We previously used ChIP-seq to characterize the LCL NF- κ B genomic binding landscape (32).
539 Rather than identifying readily recognizable LMP1 canonical versus non-canonical NF- κ B target
540 genes, this study identified complex patterns of occupancy by the five NF- κ B transcription factor
541 subunits at LCL enhancers and promoters. However, LCL enhancers often target multiple
542 genes, often from long distances (82), complicating cross-comparison with this study.
543 Furthermore, concurrent LMP1 TES1 and TES2 signaling yields up to 13 distinct NF- κ B
544 transcription factor dimers in LCL nuclei (32), including dimers such as cRel:p52 that are under
545 control of both NF- κ B pathways. Conditional expression of TES1m or TES2m should yield a
546 considerably less complex NF- κ B. Therefore, a future objective will therefore be to perform NF-
547 κ B ChIP-seq in using the conditional TES1m and TES2m conditional Burkitt models reported
548 here, as these may yield less complex patterns of NF- κ B occupancy.

549 Our analyses highlight independent, shared and antagonistic LMP1 TES1 and TES2 roles in B-
550 cell genome-wide target gene regulation (**Fig. 10**). How independent or combined TES1 and
551 TES2 signaling have different effects on clusters of target genes will be important to define. Our
552 results suggest multiple testable models. For instance, with regards to genes which were induced
553 weakly by TES2 signaling, somewhat more by TES1 signaling but more highly by WT LMP1, we
554 speculate that TES1 and TES2 may cross-talk at the epigenetic level. For example, our results
555 are consistent with a model in which TES1 signaling increases chromatin accessibility at these
556 sites, including the genes encoding IFIT1 and CXCL9. Once accessible, both TES1 and TES2
557 signal-dependent pathways may then additively or perhaps synergistically upregulate these sites.
558 Alternatively, TES1 signaling could be needed to dismiss a repressor, such that these sites can
559 then be stimulated by both LMP1 domains. TES1 signaling may also activate a key positive
560 regulator such as BCL3 (89), which then functions together with transcription factors activated by
561 TES1 and TES2 pathways. By contrast, a large number of genes appeared to be additively
562 repressed by TES1 and TES2 signaling. TES1 and TES2 may recruit co-repressors to these sites,
563 may additively recruit the same repressor or may reduce chromatin accessibility.

564 We also identified a cluster of LMP1 response genes, in which unopposed TES2 signaling
565 caused target gene downregulation (**Fig. 10**). In Akata cells, this cluster (Cluster 3) was
566 enriched for metabolism genes, raising the possibility that another key TES1 signaling role is to
567 support metabolic pathway remodeling by EBV, such as glutathione metabolism or OXPHOS
568 (90-93). It is possible that TES2 induces a repressor that targets these sites, but that TES1
569 signaling serves to blunt its induction. Alternatively, TES1 signaling may induce an activator that
570 counter-balances TES2-driven repressor activity. Or, TES2 signaling may reduce chromatin
571 accessibility at these sites in the absence of TES1. By contrast, genes in Akata Cluster 5 were

572 upregulated by unopposed TES2 signaling, but not by WT LMP1 or unopposed TES1 signaling
573 (**Figure 10**). TES1 signaling may instead recruit repressors or alter chromatin accessibility at
574 these sites. Epigenetic analyses of histone repressive marks, such as ChIP studies of H3K9me3
575 and H3K27me3, as well as ATAC-seq studies of DNA packaging, should help to differentiate
576 between these and other possibilities.

577 Our studies provide insights into TES1 and TES2 roles in regulation of B-cell EBV SE targets.
578 Although EBV SE are highly co-occupied by all five LMP1-activated NF- κ B subunits, individual
579 TES1 and TES2 roles in EBV SE target gene regulation has remained unstudied. Interestingly,
580 while either TES1 or TES2 signaling was sufficient to induce many EBV SE targets, TES1
581 induced a larger number, perhaps because it highly induces both canonical and non-canonical
582 pathways and therefore activates all 5 NF- κ B subunits. By contrast, LMP1 KO perturbed
583 expression of only a small number of EBV SE targets in LCLs, likely because of the early
584 timepoint profiled prior to cell death, which left little time for epigenetic remodeling of these sites.

585 WT or DM LMP1 expression caused highly concordant changes in host gene expression in
586 Akata and BL-41 Burkitt models. We speculate that differences in response to signaling by
587 TES1 or TES2 alone may have instead arisen from distinct host genome mutation landscapes
588 between these two human tumor derived models, which alter the basal NF- κ B level.
589 Nonetheless, since EBV can infect a wide range of B-cells, including of distinct differentiation or
590 activation states that alter NF- κ B states, differences between Akata and BL-41 provide insights
591 into how LMP1 may function in differing human B-cell contexts, and suggest that LMP1 may
592 have evolved signaling by both TES domains to increase robustness across the spectrum of
593 infected B-cell states.

594 LMP1 polymorphisms have been observed across EBV strains, in particular between type I and
595 II EBV (94). In addition, LMP1 C-terminal tail polymorphisms have been observed in several
596 analyses of EBV genomes isolated from Hodgkin lymphoma and nasopharyngeal carcinoma
597 tumor cells, though the roles of these variant LMP1 sequences remain controversial. Amongst
598 the best studied is a 30 base pair deletion present in the EBV CAO and 1510 strains isolated
599 from Asian NPC tumors, which causes loss of LMP1 residues 343-352 (95, 96). This 30bp
600 deletion has also been reported as enriched in EBV genomes isolated from Hodgkin tumor
601 samples (96-99). A meta-analysis of 31 observational studies suggested a possible association
602 between this LMP1 C-terminal tail deletion and nasopharyngeal carcinoma susceptibility, but
603 was limited by small sample size and considerable variation between studies (100). Deletion of
604 these residues, which comprise the last eight residues between the TES1/CTAR1 and the first
605 two residues of TES2/CTAR2, enhance rodent fibroblast transformation by LMP1 (101) and may
606 reduce immunogenicity (102), but were not found to enhance LMP1-mediated NF- κ B activation
607 (103). These strains also have multiple additional LMP1 amino acid polymorphisms, which are
608 instead implicated in enhanced NF- κ B activation, and were mapped to the LMP1
609 transmembrane domains (103). Little information is presently available about how these
610 polymorphisms alter LMP1 target gene expression. It will therefore be of interest to use the
611 approaches presented here to characterize how LMP1 polymorphisms present in tumor-derived
612 EBV strains may alter transcriptome responses to TES1 and TES2 signaling.

613 In summary, we identified LMP1 genome-wide B-cell targets and characterized their responses
614 to signaling by TES1 and/or TES2. Signaling by TES1, but not TES2 was identified to be critical
615 for blockade of LCL apoptosis, and CLFAR was identified as the LCL dependency factor most
616 strongly impacted by shutoff of TES1 signaling as opposed to TES2. CRISPR KO approaches

617 highlighted LCL genes that are highly sensitive to perturbation of TES1 and/or TES2 signaling.
618 K-means analysis highlighted gene clusters with distinct expression responses to signaling by
619 one or both LMP1 transformation essential domains in the latency III LCL versus EBV-negative
620 Burkitt B-cell contexts. These studies highlight multiple levels by which TES1 and TES2
621 signaling alter LMP1 target gene expression, including by additive vs opposing roles.
622 Collectively, these studies provide new insights into key non-redundant versus joint TES1 and
623 TES2 roles in B-cell target gene regulation and highlight TES1 signaling as a key
624 lymphoblastoid B-cell therapeutic target.

625

626

627 **Acknowledgements:**

628 This work was supported by NIH R01 CA228700 and AI164709, U01 CA275301, P01
629 CA269043 and a Burroughs Wellcome Career Award in Medical Sciences to B.E.G, T32
630 T32AI007245 and an American Cancer Society Post-doctoral Fellowship to E.M.B,
631 T32AI007061 to N.B., T32 T32AI007245 and F32 AI172329 to L.A.M.N and NIH K99
632 1K99DE031016 to R.G. All RNAseq and proteomics datasets will be published in the GEO
633 omnibus GSE228158, GSE228167, GSE228178 and GSE240732 upon manuscript publication.

634

635 **AUTHOR CONTRIBUTIONS**

636 B.M and E.M.B performed the experiments. B.M, N.R.B., R.G, E.M.B and L.A.M.N performed
637 bioinformatics analyses. B.M and B.E.G designed the experiments. B.M and B.E.G wrote the
638 manuscript. All authors analyzed the results, read and approved the manuscript.

639

640

641

642

643

644

645

646

647

648

649

650

651

652 **Figure Legends:**

653 **Fig. 1. Characterization of LMP1 KO effects on GM12878 LCL target gene regulation**

654 (A) Immunoblot analysis of whole cell lysates (WCL) from GM12878 LCLs transduced with
655 lentiviruses that express control or LMP1 targeting single guide RNAs (sgRNAs). Transduced
656 cells were puromycin selected for 0 vs 2 days, as indicated. Blots for LMP1, for LMP1 target
657 genes TRAF1 and IRF4, and for LMP1-driven non-canonical NF- κ B pathway p100/p52
658 processing are shown. Blots are representative of n=3 experiments.

659 (B) K-means heatmap analysis of GM12878 LCLs transduced as in (A) with lentivirus
660 expressing control or LMP1 sgRNA and puromycin selected for 48 hours. The heatmap depicts
661 relative Z-scores in each row from n=3 independent RNAseq replicates, divided into two
662 clusters. The Z-score scale is shown at bottom, where blue and red colors indicate lower versus
663 higher relative expression, respectively. Two-way ANOVA P-value cutoff of <0.01 and >2-fold
664 gene expression cutoffs were used.

665 (C) Enrichr analysis of KEGG pathways most highly changed in GM12878 expressing control
666 versus LMP1 sgRNA (LMP1 KO), as in (A). The X-axis depicts the -Log₁₀ adjusted p-value (adj
667 p-value) scale. The top three most enriched KEGG pathways are shown.

668 (D) Abundances of two representative Cluster 1 genes from n=3 RNAseq analyses in cells with
669 control vs LMP1 sgRNA. p-values were determined by one-sided Fisher's exact test. *p<0.05,
670 **p<0.01.

671 (E) Abundances of two representative Cluster 2 genes from n=3 RNAseq analyses in cells with
672 control vs LMP1 sgRNA. p-values were determined by one-sided Fisher's exact test.
673 ***p<0.001.

674 (F) Volcano plot analysis of host transcriptome-wide GM12878 genes differentially expressed in
675 cells with control versus LMP1 sgRNA expression, as in (B), using data from n=3 RNAseq
676 datasets.

677 (G) Scatter plot cross comparison of log₂ transformed fold change mRNA abundances in
678 GM12878 expressing LMP1 vs. control sgRNA (Y-axis) versus log₂ transformed fold change
679 abundances of sgRNAs at Day 21 versus Day 1 post-transduction of GM12878 LCLs in a
680 genome-wide CRISPR screen (25) (X-axis).

681 (H) String analysis of genes shown in (G). Pathway identifiers for each gene and interaction are
682 colored coded.

683 (I) Volcano plot analysis of EBV mRNA values in GM12878 expressing LMP1 vs control
684 sgRNAs, as in (B). p-value <0.05 and >2-fold change mRNA abundance cutoffs were used.

685

686 **Fig. S1. Characterization of LMP1 KO effects on GM12878 LCL target gene regulation.**

687 (A) Relative mean + standard deviation (SD) live cell numbers from CellTitreGlo analysis of n=3
688 replicates of Cas9+ GM12878 LCLs, transduced with lentiviruses that expressed control or LMP1
689 sgRNAs and puromycin selected, for 2 versus 4 days.

690 (B) Scatter plot analysis cross-comparing the significance of changes in LCL dependency factor
691 expression upon GM12878 LMP1 KO versus the CRISPR screen significance score for selection
692 against sgRNAs in LCL vs Burkitt dependency factor analysis (25). Shown on the Y-axis are -

693 log₁₀ transformed P-values from RNAseq analysis of GM12878 LCLs transduced with
694 lentiviruses expressing LMP1 versus control sgRNA (as in **Fig. 1F**), versus -log₁₀ transformed P-
695 values from CRISPR LCL vs Burkitt cell dependency factor analysis (25). Higher Y-axis scores
696 indicate more significant differences in expression for the indicated genes in GM12878 with LMP1
697 vs control sgRNA. Higher X-axis scores indicate a stronger selection against sgRNA targeting the
698 indicated genes in GM12878 LCLs versus P3HR1 Burkitt cells over 21 days of cell culture. Shown
699 are genes with p<0.05 in both analyses.

700 (C) Volcano plot analysis visualizing KEGG Hodgkin lymphoma pathway gene -Log₁₀ (P-value)
701 on the y-axis versus log₂ transformed fold change in mRNA abundances on the x-axis of
702 GM12878 genes in cells expressing LMP1 versus control sgRNA (as in **Fig. 1F**). P-value <0.05
703 and >2-fold change mRNA abundance cutoffs were used.

704

705

706 **Fig. 2. Loss of TES1 but not TES2 signaling triggers LCL apoptosis.**

707 (A) Schematic diagram of LMP1 WT with TES1 and TES2 domains highlighted. Wildtype (WT)
708 or point mutants abrogated for signaling from TES1 (TES1m), TES2 (TES2m) or double
709 TES1/TES2 mutant (DM) are shown.

710 (B) Immunoblot analysis of WCL from GM12878 LCLs that expressed control or LMP1 sgRNAs
711 and puromycin selected for 3 days, then induced for expression with the indicated LMP1 rescue
712 cDNA construct for 6 days. Blots are representative of n = 3 experiments.

713 (C) Growth curve analysis of GM12878 LCLs at the indicated day post expression of control or
714 LMP1 sgRNAs and the indicated LMP1 WT, TES1m, TES2m or DM rescue cDNA. Shown are
715 mean ± SD from n=3 independent experiments. **p<0.01.

716 (D) FACS analysis of 7-AAD vital dye uptake in GM12878 on day 7 post- expression of LMP1
717 sgRNAs and the indicated LMP1 rescue cDNA. Shown are percentages of 7-AAD+ cells within
718 the indicated gates. Representative of n=3 experiments.

719 (E) Mean ± SD of fold change 7-AAD values from n=3 independent experiments of GM12878
720 with the indicated control or LMP1 sgRNA and rescue cDNA expression, as in (D). Values in
721 GM12878 with control sgRNA and no LMP1 rescue cDNA were set to 1.

722 (F) FACS analysis of plasma membrane annexin V abundance in GM12878 on day 7 post-
723 expression of control or LMP1 sgRNAs and the indicated LMP1 rescue cDNA. Shown are
724 percentages of 7-AAD+ cells within the indicated gates. Representative of n=3 experiments.

725 (G) Mean ± SD of fold-change caspase 3/7 activity levels, as determined by caspase 3/7 Glo
726 assay, from n=3 independent experiments of GM12878 with the indicated control or LMP1
727 sgRNA and rescue cDNA expression. Values in GM12878 with control sgRNA and no LMP1
728 rescue cDNA were set to 1.

729

730 **Fig. S2. Loss of TES1 but not TES2 signaling triggers LCL apoptosis.**

731 Mean ± SD of fold change plasma membrane Annexin V values from n=3 independent
732 experiments, using GM12878 with the indicated control or LMP1 sgRNA and rescue cDNA
733 expression. Values in GM12878 with control sgRNA and no LMP1 rescue cDNA were set to 1.

734

735 **Fig. 3. Characterization of host genome-wide TES1 vs TES2 LCL target genes**

736 (A) RNAseq K-means heatmap analysis of GM12878 LCLs transduced with lentivirus
737 expressing LMP1 sgRNA and induced for WT, TES1m or TES2m rescue cDNA expression for 6
738 days. The heatmap depicts relative Z-scores in each row from n=3 independent RNAseq
739 datasets, divided into six clusters. The Z-score scale is shown at bottom, where blue and red
740 colors indicate lower versus higher relative expression, respectively. Two-way ANOVA P-value
741 cutoff of <0.05 and >2-fold gene expression cutoffs were used. The top three most highly
742 enriched KEGG pathways amongst genes within each cluster are shown at right.

743 (B) Heatmap analysis of KEGG apoptosis pathway gene relative row Z-scores from RNAseq
744 analysis as in (A). The Z-score scale is shown at bottom, where blue and red colors indicate
745 lower versus higher relative expression, respectively. Two-way ANOVA P-value cutoff of <0.05
746 and >2-fold gene expression cutoffs were used.

747 (C) Scatter plot analysis cross comparing log2 transformed fold change of LCL dependency
748 factor mRNA abundances in GM12878 expressing LMP1 sgRNA together with TES2 mutant
749 versus wildtype cDNA rescue (Y-axis) and TES1 mutant versus wildtype cDNA rescue (X-axis)
750 from triplicate RNAseq datasets, as in (A). This analysis highlighted that CFLAR and to a lesser
751 extent NFKB2 and CCND2 mRNAs were more highly downmodulated by TES1m than TES2m
752 rescue, relative to levels in cells with WT LMP1 rescue. Shown are genes differentially regulated
753 by >2 fold with either TES1m or TES2m rescue, relative to levels with WT LMP1 rescue.

754 (D) Immunoblot analysis of c-FLIP and load control GAPDH expression in WCL from GM12878
755 LCLs with the indicated control or LMP1 sgRNA and LMP1 rescue cDNA expression.
756 Representative of n=3 experiments.

757

758 **Figure S3. Characterization of TES1 vs TES2 LCL dependency factor and Hodgkin**
759 **lymphoma pathway targets.**

760 (A) Heatmap analysis of CRISPR defined LCL dependency factor gene relative row Z-scores
761 from RNAseq of GM12878 expressing LMP1 sgRNA and the indicated rescue cDNA, as in **Fig.**
762 **3**. The Z-score scale is shown at bottom, where blue and red colors indicate lower versus higher
763 relative expression, respectively. Two-way ANOVA P-value cutoff of <0.05 and >2-fold gene
764 expression cutoffs were used.

765 (B) Heatmap analysis of KEGG Hodgkin Lymphoma pathway gene relative row Z-scores from
766 RNAseq of GM12878 expressing LMP1 sgRNA and the indicated rescue cDNA, as in **Fig. 3**.
767 Two-way ANOVA P-value cutoff of <0.05 and >2-fold gene expression cutoffs were used.

768

769 **Fig. 4. Characterization of LCL pathways targeted by TES1 vs TES2 signaling**

770 (A) Volcano plot analysis of host transcriptome-wide GM12878 genes differentially expressed in
771 LMP1 KO GM12878 with WT vs TES1 mutant cDNA rescue. Higher X-axis fold changes
772 indicate higher expression with WT LMP1 rescue, whereas lower X-axis fold changes indicate
773 higher expression with TES1m rescue. Data are from n=3 RNAseq datasets, as in **Fig. 3**.

774 (B) Enrichr analysis of KEGG pathways most highly enriched in RNAseq data as in (A) amongst
775 genes more highly expressed in LMP1 KO GM12878 with WT than TES1m rescue (red) vs
776 amongst genes more highly expressed with TES1m than WT rescue (blue).

777 (C) Volcano plot analysis of host transcriptome-wide GM12878 genes differentially expressed in
778 LMP1 KO GM12878 with WT vs TES2 mutant cDNA rescue. Higher X-axis fold changes
779 indicate higher expression with WT LMP1 rescue, whereas lower X-axis fold changes indicate
780 higher expression with TES2m rescue. Data are from n=3 RNAseq datasets, as in **Fig. 3**.

781 (D) Enrichr analysis of KEGG pathways most highly enriched in RNAseq data as in (C) amongst
782 genes more highly expressed in LMP1 KO GM12878 with WT than TES2m rescue (red) vs
783 amongst genes more highly expressed with TES2m than WT rescue (blue).

784 (E) Volcano plot analysis of host transcriptome-wide GM12878 genes differentially expressed in
785 LMP1 KO GM12878 with TES1 vs TES2 mutant cDNA rescue. Higher X-axis fold changes
786 indicate higher expression with TES1m rescue, whereas lower X-axis fold changes indicate
787 higher expression with TES2m rescue. Data are from n=3 RNAseq datasets, as in **Fig. 3**.

788 (F) Enrichr analysis of KEGG pathways most highly enriched in RNAseq data as in (E) amongst
789 genes more highly expressed in LMP1 KO GM12878 with TES1m than TES2m rescue (red) vs
790 amongst genes more highly expressed with TES2m than TES1m rescue (blue).

791

792 **Fig. 5. Characterization of host genome-wide Akata B-cell LMP1 target genes.**

793 (A) K-means heatmap analysis of RNAseq datasets from n=3 replicates generated in EBV-
794 Akata Burkitt cells with conditional LMP1 WT, TES1m, TES2m or DM expression induced by
795 250 ng/ml doxycycline for 24 hours. The heatmap visualizes host gene Log₂ Fold change
796 across the four conditions, divided into six clusters. A two-way ANOVA P value cutoff of <0.01
797 and >2-fold gene expression were used. # of genes in each cluster is indicated at right.

798 (B) Heatmaps of representative Cluster 1 differentially regulated genes (top), with column
799 maximum (max) colored red and minimum (min) colored blue, as shown by the scalebar. Also
800 shown are expression values of two representative Cluster 1 genes (lower left) and Enrichr
801 analysis of KEGG pathways significantly enriched in Cluster 1 gene sets (lower right). p-values
802 were determined by one-sided Fisher's exact test. ***p<0.001.

803 (C) Heatmaps of representative Cluster 2 differentially regulated genes (top), as in (B). Also
804 shown are expression values of two representative Cluster 2 genes (lower left) and Enrichr
805 analysis of KEGG pathways significantly enriched in Cluster 2 gene sets (lower right). p-values
806 were determined by one-sided Fisher's exact test. *p<0.05, **p<0.01, ***p<0.001.

807 (D) Heatmaps of representative Cluster 6 differentially regulated genes (top), as in (B). Also
808 shown are expression values of two representative Cluster 6 genes (lower left) and Enrichr
809 analysis of KEGG pathways significantly enriched in Cluster 6 gene sets (lower right). p-values
810 were determined by one-sided Fisher's exact test. *p<0.05, ***p<0.001.

811

812 **Fig. S4. Validation of LMP1 WT, TES1m, TES2m and DM conditional expression system in**
813 **EBV-negative Akata Burkitt B-cells.**

814 (A) Immunoblot analysis of WCL from Akata cells induced for LMP1 WT, TES1m, TES2m or DM
815 expression by addition of 250 ng/ml doxycycline (Dox) for 24 hours, as indicated. For cross-
816 comparison, WCL from equal numbers of Mutu I Burkitt lymphoma (latency I, lacks LMP1
817 expression) and GM12878 were also included at right. Blots are representative of n = 3
818 experiments.

819 (B) Immunoblot analysis of WCL from BL-41 cells induced for WT, TES1m, TES2m or DM
820 LMP1 by addition of 250 ng/ml Dox for 24 hours, as indicated. For cross-comparison, WCL from
821 equal numbers of Mutu I Burkitt and GM12878 were also included at right. Blots are
822 representative of n = 3 experiments.

823 (C) FACS analysis of plasma membrane (PM) ICAM-1 abundance in Akata cells induced for
824 LMP1 by 250 ng/ml Dox for 24 hours, as indicated. Y-axis are histogram cell counts, X-axis
825 represents PM ICAM-1 abundance. For comparison, levels in GM12878 LCLs or latency I Mutu
826 I Burkitt cells are shown.

827 (D) PM ICAM-1 Mean Fluorescence Intensity (MFI) + standard deviation (SD) from n=3
828 replicates in Akata cells with the indicated LMP1 expression, as in (C). p-values were
829 determined by one-sided Fisher's exact test. **p<0.001, ***p<0.0001.

830 (E) FACS analysis of PM Fas abundance in Akata cells induced for LMP1 by 250ng/ml of Dox
831 for 24 hours as indicated. For comparison, GM12878 LCLs or latency I Mutu I Burkitt cells were
832 also analyzed.

833 (F) PM Fas MFI + SD from n=3 replicates in Akata cells with the indicated LMP1 expression, as
834 in (E). P-values were determined by one-sided Fisher's exact test. **p<0.001, ***p<0.0001.

835 (G) FACS analysis of PM ICAM-1 in BL-41 cells induced for LMP1 expression by 250ng/ml Dox
836 for 24 hours, as indicated. For comparison, GM12878 and Mutu I were also analyzed. p-values
837 were determined by one-sided Fisher's exact test. **p<0.001, ***p<0.0001.

838 (H) PM ICAM-1 MFI + SD from n=3 replicates in BL-41 cells with the indicated LMP1
839 expression, as in (G). P-values were determined by one-sided Fisher's exact test. **p<0.001,
840 ***p<0.0001.

841 (I) FACS analysis of PM Fas levels in BL-41 cells induced for LMP1 expression by 250 ng/ml
842 dox for 24 hours, as indicated. GM12878 and Mutu I were analyzed for cross-comparison. p-
843 values were determined by one-sided Fisher's exact test. **p<0.001, ***p<0.0001.

844 (J) PM Fas MFI + SD from n=3 replicates of BL-41-LMP1 with the indicated LMP1 expression,
845 as in (I). Mutu I and GM12878 were analyzed for comparison. p-values were determined by
846 one-sided Fisher's exact test. **p<0.001, ***p<0.0001.

847

848 **Fig. S5. Characterization of host genome-wide Akata B-cell LMP1 target genes, related to**
849 **Figure 4.**

850 (A) Heatmaps of representative **Figure 4** Cluster 3 differentially regulated genes (top), with
851 column maximum colored red and minimum colored blue, as shown by the scalebar. Also
852 shown are expression values of two representative Clusters 3 genes (lower left) and Enrichr
853 analysis of KEGG pathways most significantly enriched Cluster 3 gene sets (lower right). p-
854 values were determined by one-sided Fisher's exact test. **p<0.01.

855 (B) Heatmaps of representative **Figure 4** Cluster 4 differentially regulated genes (top), with
856 column maximum colored red and minimum colored blue, as shown by the scalebar. Also
857 shown are expression values of two representative Clusters 4 genes (lower left) and Enrichr
858 analysis of KEGG pathways most significantly enriched Cluster 4 gene sets (lower right). p-
859 values were determined by one-sided Fisher's exact test. *p<0.05, **p<0.01, ***p<0.001.

860 (C) Heatmaps of representative **Figure 4** Cluster 5 differentially regulated genes (top), with
861 column maximum colored red and minimum colored blue, as shown by the scalebar. Also

862 shown are expression values of two representative Cluster 5 genes (lower left) and Enrichr
863 analysis of KEGG pathways most significantly enriched Cluster 5 gene sets (lower right). p-
864 values were determined by one-sided Fisher's exact test. * $p < 0.05$, *** $p < 0.001$.

865

866 **Fig. S6. RNAseq analysis of BL-41 B-cell responses to WT, TES1, TES2 or DM LMP1.**

867 (A) K-means heatmap analysis of RNAseq datasets from $n=3$ replicates generated in EBV- BL-
868 41 Burkitt cells with conditional LMP1 WT, TES1m, TES2m or DM expression induced by 250
869 ng/ml doxycycline for 24 hours. The heatmap visualizes host gene Log₂ Fold change across the
870 four conditions, divided into six clusters. A two-way ANOVA P value cutoff of <0.01 and >2 -fold
871 gene expression were used. # of genes in each cluster is indicated at right.

872 (B) Heatmaps of representative Cluster 1 differentially regulated genes (top), with column
873 maximum (max) colored red and minimum (min) colored blue, as shown by the scalebar. Also
874 shown are expression values of two representative Cluster 1 genes (lower left) and Enrichr
875 analysis of KEGG pathways significantly enriched in Cluster 1 gene sets (lower right). p-values
876 were determined by one-sided Fisher's exact test. *** $p < 0.001$.

877 (C) Heatmaps of representative Cluster 2 differentially regulated genes (top). Also shown are
878 expression values of two representative Cluster 2 genes (lower left) and Enrichr analysis of
879 KEGG pathways significantly enriched in Cluster 2 gene sets (lower right). p-values were
880 determined by one-sided Fisher's exact test. *** $p < 0.001$.

881 (D) Heatmaps of representative Cluster 4 differentially regulated genes (top). Also shown are
882 expression values of two representative Cluster 4 genes (lower left) and Enrichr analysis of
883 KEGG pathways significantly enriched in Cluster 4 gene sets (lower right). p-values were
884 determined by one-sided Fisher's exact test. * $p < 0.05$, *** $p < 0.001$.

885 (E) Heatmaps of representative Cluster 6 differentially regulated genes (top). Also shown are
886 expression values of two representative Cluster 6 genes (lower left) and Enrichr analysis of
887 KEGG pathways significantly enriched in Cluster 6 gene sets (lower right). p-values were
888 determined by one-sided Fisher's exact test. * $p < 0.05$, ** $p < 0.01$, *** $p < 0.001$.

889

890 **Fig. 6. Characterization of Akata B-cell pathways targeted by TES1 vs TES2 signaling.**

891 (A) Volcano plot analysis of host transcriptome-wide genes differentially expressed in Akata
892 cells conditionally induced for WT LMP1 expression for 24h by 250 ng/ml Dox versus in mock
893 induced cells. Higher X-axis fold changes indicate genes more highly expressed in cells with
894 WT LMP1 expression, whereas lower X-axis fold changes indicate higher expression in cells
895 mock induced for LMP1. Data are from $n=3$ RNAseq datasets, as in **Fig. 5**.

896 (B) Enrichr analysis of KEGG pathways most highly enriched in RNAseq data as in (A) amongst
897 genes more highly expressed in Akata with WT LMP1 (red) vs amongst genes more highly
898 expressed with mock LMP1 induction (blue).

899 (C) Volcano plot analysis of host transcriptome-wide genes differentially expressed in Akata
900 cells conditionally induced for WT vs DM LMP1 expression for 24h by 250 ng/ml Dox. Higher X-
901 axis fold changes indicate genes more highly expressed in cells with WT LMP1 expression,
902 whereas lower X-axis fold changes indicate higher expression in cells with DM LMP1. Data are
903 from $n=3$ RNAseq datasets, as in **Fig. 5**.

904 (D) Enrichr analysis of KEGG pathways most highly enriched in RNAseq data as in (C) amongst
905 genes more highly expressed in Akata with WT LMP1 (red) vs amongst genes more highly
906 expressed with DM LMP1 induction (blue).

907 (E) Volcano plot analysis of host transcriptome-wide genes differentially expressed in Akata
908 cells conditionally induced for WT vs TES1m LMP1 expression for 24h by 250 ng/ml Dox.
909 Higher X-axis fold changes indicate genes more highly expressed in cells with WT LMP1
910 expression, whereas lower X-axis fold changes indicate higher expression in cells with TES1m
911 LMP1. Data are from n=3 RNAseq datasets, as in **Fig. 5**.

912 (F) Enrichr analysis of KEGG pathways most highly enriched in RNAseq data as in (E) amongst
913 genes more highly expressed in Akata with WT LMP1 (red) vs amongst genes more highly
914 expressed with TES1m LMP1 induction (blue).

915 (G) Volcano plot analysis of host transcriptome-wide genes differentially expressed in Akata
916 cells conditionally induced for WT vs TES2m LMP1 expression for 24h by 250 ng/ml Dox.
917 Higher X-axis fold changes indicate genes more highly expressed in cells with WT LMP1
918 expression, whereas lower X-axis fold changes indicate higher expression in cells with TES2m
919 LMP1. Data are from n=3 RNAseq datasets, as in **Fig. 5**.

920 (H) Enrichr analysis of KEGG pathways most highly enriched in RNAseq data as in (G) amongst
921 genes more highly expressed in Akata with WT LMP1 (red) vs amongst genes more highly
922 expressed with TES2m LMP1 induction (blue).

923

924 **Fig. S7. Cross-comparison of WT and DM LMP1 effects on Akata vs BL-41**
925 **transcriptomes.**

926 (A) Volcano plot analysis of host transcriptome-wide genes differentially expressed in BL-41
927 cells conditionally induced for WT LMP1 expression for 24h by 250 ng/ml Dox versus in mock
928 induced cells. Higher X-axis fold changes indicate genes more highly expressed in cells with
929 WT LMP1 expression, whereas lower X-axis fold changes indicate higher expression in cells
930 mock induced for LMP1. Data are from n=3 RNAseq datasets.

931 (B) Enrichr analysis of KEGG pathways most highly enriched in RNAseq data as in (A) amongst
932 genes more highly expressed in BL-41 with WT LMP1 (red) vs amongst genes more highly
933 expressed with mock LMP1 induction (blue).

934 (C) Volcano plot cross-comparison of Log2 transformed fold change of host mRNA levels in BL-
935 41 cells (X-axis) versus Akata cells (Y-axis) uninduced versus induced for WT LMP1 by 250
936 ng/ml Dox for 24 hours. Selected genes highly WT LMP1 induced in both Burkitt contexts are
937 highlighted in red, whereas selected genes suppressed by LMP1 in both Burkitt contexts are
938 highlighted in blue.

939 (D) Volcano plot analysis of host transcriptome-wide genes differentially expressed in BL-41
940 cells conditionally induced for DM versus WT LMP1 expression for 24h by 250 ng/ml Dox.
941 Higher X-axis fold changes indicate genes more highly expressed in cells with WT LMP1
942 expression, whereas lower X-axis fold changes indicate higher expression in cells induced for
943 DM LMP1. Data are from n=3 RNAseq datasets.

944 (E) Enrichr analysis of KEGG pathways most highly enriched in RNAseq data as in (D) amongst
945 genes more highly expressed in BL-41 with WT LMP1 (red) vs amongst genes more highly
946 expressed with DM LMP1 induction (blue).

947 (F) Volcano plot cross-comparison of Log₂ transformed fold change of host mRNA levels in BL-
948 41 cells (X-axis) versus Akata cells (Y-axis) induced for DM versus WT LMP1 by 250 ng/ml Dox
949 for 24 hours. Selected genes highly WT LMP1 induced in both Burkitt contexts relative to levels
950 in cells with DM LMP1 expression are highlighted in red, whereas selected genes suppressed
951 by WT LMP1 in both Burkitt contexts are highlighted in blue.

952

953 **Fig. S8. Cross-comparison of TES1 and TES2 LMP1 effects on Akata vs BL-41**
954 **transcriptomes.**

955 A) Volcano plot analysis of host transcriptome-wide genes differentially expressed in BL-41 cells
956 conditionally induced for TES1m vs WT LMP1 expression for 24h by 250 ng/ml Dox. Higher X-
957 axis fold changes indicate genes more highly expressed in cells with WT LMP1 expression,
958 whereas lower X-axis fold changes indicate higher expression induced for TES1m LMP1. Data
959 are from n=3 RNAseq datasets.

960 (B) Enrichr analysis of KEGG pathways most highly enriched in RNAseq data as in (A) amongst
961 genes more highly expressed in BL-41 with WT LMP1 (red) vs amongst genes more highly
962 expressed with TES1m LMP1 induction (blue).

963 (C) Volcano plot analysis of host transcriptome-wide genes differentially expressed in BL-41
964 cells conditionally induced for TES2m vs WT LMP1 expression for 24h by 250 ng/ml Dox.
965 Higher X-axis fold changes indicate genes more highly expressed in cells with WT LMP1
966 expression, whereas lower X-axis fold changes indicate higher expression induced for TES2m
967 LMP1. Data are from n=3 RNAseq datasets.

968 (D) Enrichr analysis of KEGG pathways most highly enriched in RNAseq data as in (A) amongst
969 genes more highly expressed in BL-41 with WT LMP1 (red) vs amongst genes more highly
970 expressed with TES2m LMP1 induction (blue).

971 (E) Volcano plot analysis of host transcriptome-wide genes differentially expressed in Akata
972 cells conditionally induced for TES1m vs TES2m LMP1 expression for 24h by 250 ng/ml Dox.
973 Higher X-axis fold changes indicate genes more highly expressed in cells with TES1m LMP1
974 expression, whereas lower X-axis fold changes indicate higher expression induced for TES2m
975 LMP1. Data are from n=3 RNAseq datasets.

976 (F) Enrichr analysis of KEGG pathways most highly enriched in RNAseq data as in (E) amongst
977 genes more highly expressed in Akata with TES1m LMP1 (red) vs amongst genes more highly
978 expressed with TES2m LMP1 induction (blue).

979 (G) Volcano plot analysis of host transcriptome-wide genes differentially expressed in BL-41
980 cells conditionally induced for TES1m vs TES2m LMP1 expression for 24h by 250 ng/ml Dox.
981 Higher X-axis fold changes indicate genes more highly expressed in cells with TES1m LMP1
982 expression, whereas lower X-axis fold changes indicate higher expression induced for TES2m
983 LMP1. Data are from n=3 RNAseq datasets.

984 (H) Enrichr analysis of KEGG pathways most highly enriched in RNAseq data as in (G) amongst
985 genes more highly expressed in BL-41 with TES1m LMP1 (red) vs amongst genes more highly
986 expressed with TES2m LMP1 induction (blue).

987

988 **Figure S9. Cross-comparison of host genes differentially expressed upon perturbation of**
989 **LCL LMP1 versus upon LMP1 induction in Akata cells.**

990

991 (A) Volcano plot analysis of host genes differentially expressed upon WT LMP1 induction in
992 Akata (X-axis) versus upon LMP1 KO in GM12878 (Y-axis). Shown are Log₂ transformed
993 mRNA fold change values for Akata cells mock induced versus induced for LMP1 WT
994 expression for 24 hours (X-axis) versus upon expression of LMP1 vs control sgRNA in
995 GM12878 for 48 hours. Genes more highly expressed in mock-induced Akata have higher x-
996 axis values, whereas genes more highly expressed in Akata induced for WT LMP1 have lower
997 x-axis values. Likewise, genes with higher expression with control sgRNA expression have
998 higher y-axis values, whereas genes with lower expression in GM12878 with LMP1 KO have
999 lower Y-axis values. P value <0.05 and >2-fold gene expression cutoffs were used.

1000 (B) Volcano plot analysis of host genes differentially expressed upon TES1m vs WT LMP1
1001 induction in Akata (X-axis) versus upon rescue of LMP1 KO GM12878 with TES1m versus WT
1002 LMP1 (Y-axis). Shown are Log₂ transformed mRNA fold change values for Akata cells induced
1003 for TES1m versus WT LMP1 expression for 24 hours (X-axis) versus upon rescue of GM12878
1004 LMP1 KO with TES1m vs WT LMP1 cDNA, as in **Fig 3**. Genes more highly expressed in Akata
1005 with TES1m than WT LMP1 expression have higher x-axis values, whereas genes more highly
1006 expressed in Akata induced for WT LMP1 than TES1m have lower x-axis values. Likewise,
1007 GM12878 genes with higher expression with TES1m rescue have higher y-axis values, whereas
1008 genes with lower expression in GM12878 with TES1m than WT rescue have lower Y-axis
1009 values. P value <0.05 and >2-fold gene expression cutoffs were used.

1010 (C) Volcano plot analysis of host genes differentially expressed upon TES2m vs WT LMP1
1011 induction in Akata (X-axis) versus upon rescue of LMP1 KO GM12878 with TES2m versus WT
1012 LMP1 (Y-axis). Shown are Log₂ transformed mRNA fold change values for Akata cells induced
1013 for TES2m versus WT LMP1 expression for 24 hours (X-axis) versus upon rescue of GM12878
1014 LMP1 KO with TES2m vs WT LMP1 cDNA, as in **Fig 3**. Genes more highly expressed in Akata
1015 with TES2m than WT LMP1 expression have higher x-axis values, whereas genes more highly
1016 expressed in Akata induced for WT LMP1 than TES2m have lower x-axis values. Likewise,
1017 GM12878 genes with higher expression with TES2m rescue have higher y-axis values, whereas
1018 genes with lower expression in GM12878 with TES2m than WT rescue have lower Y-axis
1019 values. P value <0.05 and >2-fold gene expression cutoffs were used.

1020

1021 **Fig. 8. Roles of TES1 and TES2 canonical NF-κB pathways in LCL dependency factor**
1022 **BATF and IRF4 expression.**

1023 (A) Schematic diagram of JUNB, BATF and IRF4 at an AP-1/IRF composite DNA site.

1024 (B) Mean + SD fold changes of IRF4, BATF and JUNB mRNA abundances from n=3 RNAseq
1025 replicates of Akata cells expressing the indicated LMP1 cDNA for 24 hours, as in Fig. 5. p-
1026 values were determined by one-sided Fisher's exact test. *p<0.05, ***p<0.001.

1027 (C) Schematic diagram of LMP1 TES1 and TES2 NF-κB pathways. TES1 and TES2 each
1028 activate canonical NF-κB pathways, whereas TES1 also activates non-canonical NF-κB.

1029 (D) Immunoblot analysis of WCL from Akata cells induced for LMP1 expression by 250 ng/ml
1030 Dox for 24 hours, either without or with 1 μM IKKβ inhibitor VIII. Shown below are relative fold
1031 changes + SD from n=3 replicates of IRF4 or BATF vs GAPDH load control densitometry
1032 values. Values in vehicle control treated WT LMP1 expressing cells were set to 1. P-values
1033 were determined by one-sided Fisher's exact test. **p<0.001, ***p<0.0001.

1034 (E) Immunoblot analysis of WCL from Cas9+ Akata cells expressing control or either of two
1035 *TAK1* targeting sgRNAs, induced for LMP1 expression by 250 ng/ml Dox for 24 hours. Shown
1036 below are relative foldchanges + SD from n=3 replicates of IRF4 or BATF vs GAPDH load
1037 control densitometry values. Levels in cells with control sgRNA (sgControl) and WT LMP1 were
1038 set to 1. **p<0.001, ***p<0.0001.

1039 (F) Model of additive TES1 and TES2 canonical NF- κ B pathway effects on BATF and IRF4
1040 induction.

1041

1042 **Fig. S10. Roles of TES1 and TES2 canonical NF- κ B pathways in BATF and IRF4**
1043 **induction.**

1044 (A) Immunoblot analysis of WCL from latency III Jijoye Burkitt cells or GM12878 LCL expressing
1045 LMP1 targeting sgRNA, as indicated. Shown below are relative fold changes + SD from n=3
1046 replicates of IRF4 or BATF vs GAPDH load control densitometry values, with values in sgRNA
1047 control expressing cells set to 1. P-values were determined by one-sided Fisher's exact test.
1048 **p<0.001, ***p<0.0001.

1049 (B) Relative +SD BATF and IRF4 mRNA levels from n=3 RNAseq replicates from LMP1 KO
1050 GM12878 with TES1m, TES2m or WT LMP1 rescue cDNA expression, as in **Fig 3-4**. BATF or
1051 IRF4 levels in cells with WT LMP1 rescue were defined as 1. ***p<0.0001.

1052 (C) Immunoblot analysis of WCL from GM12878 LCLs treated with vehicle control or 1 μ M IKK β
1053 inhibitor VIII for 24 hours. Shown below are relative foldchanges + SD from n=3 replicates of
1054 IRF4 or BATF vs GAPDH load control densitometry values. Levels in vehicle control treated WT
1055 LMP1 expressing cells were set to 1. P-values were determined by one-sided Fisher's exact
1056 test. **p<0.001, ***p<0.0001.

1057 (D) Immunoblot analysis of WCL from Akata cells induced for the indicated LMP1 construct
1058 expression, either without or together with an I κ B α super-repressor (I κ B α -S.R.) that blocks
1059 canonical NF- κ B signaling. Shown below are relative foldchanges + SD of IRF4 or BATF vs
1060 GAPDH load control densitometry values from n=3 replicates, with values in cells expressing
1061 WT LMP1 but not I κ B α - set to 1. P-values were determined by one-sided Fisher's exact test.
1062 **p<0.001, ***p<0.0001.

1063

1064 **Fig. 9. LMP1 TES1 and TES2 roles in EBV super-enhancer target gene regulation in**
1065 **GM12878 LCLs.**

1066 (A) Schematic diagram of typical LCL enhancers vs super-enhancers. Super-enhancers have
1067 significantly broader and taller histone 3 lysine 27 acetyl (H3K27Ac) peaks. EBV SE are host
1068 genomic enhancer sites bound by all five LMP1-activated NF- κ B transcription factor subunits,
1069 EBNA-2, LP, 3A, and 3C.

1070 (B) Volcano plot analysis of mRNA values in GM12878 expressing LMP1 vs control sgRNAs as
1071 in **Fig. 3**. Genes targeted by EBV super-enhancers (SE) are highlighted by red circles, whereas
1072 other LCL genes are indicated by blue circles. Genes more highly expressed with LMP1 KO
1073 have higher x-axis values, whereas those downmodulated by LMP1 KO have lower values. P
1074 value <0.05 and >2-fold gene expression cutoffs were used.

1075 (C) Volcano plot analysis of mRNA values in GM12878 expressing LMP1 sgRNA with TES1m
1076 versus WT LMP1 cDNA rescue, as in **Fig. 2-3**. Genes targeted by EBV super-enhancers (SE)

1077 are highlighted by red circles, whereas other LCL genes are indicated by blue circles. Genes
1078 more highly expressed with endogenous LMP1 KO and TES1m rescue have higher x-axis
1079 values, whereas those more highly expressed with WT LMP1 rescue have lower values. P value
1080 <0.05 and >2-fold gene expression cutoffs were used.

1081 (D) Volcano plot analysis of mRNA values in GM12878 expressing LMP1 sgRNA with TES2m
1082 versus WT LMP1 cDNA rescue, as in (C). Genes targeted by EBV super-enhancers (SE) are
1083 highlighted by red circles, whereas other LCL genes are indicated by blue circles. Genes more
1084 highly expressed with endogenous LMP1 KO and TES2m rescue have higher x-axis values,
1085 whereas those more highly expressed with WT LMP1 rescue have lower values. P value <0.05
1086 and >2-fold gene expression cutoffs were used.

1087 **Figure S11. LMP1 TES1 and TES2 roles in EBV super-enhancer target gene regulation in**
1088 **Akata and BL-41 Burkitt B-cells.**

1089 (A) Volcano plot analysis of Akata RNA-seq, comparing mRNA values in cells induced for LMP1
1090 WT vs. mock-induced for 24 hours. SE targeted genes highlighted by red circles and other B-
1091 cell genes indicated by blue circles. P value <0.05 and >2-fold gene expression cutoffs were
1092 used.

1093 (B) Volcano plot analysis of Akata RNA-seq, comparing mRNA values in cells induced for LMP1
1094 TES1m vs. mock-induced for 24 hours. SE targeted genes highlighted by red circles and other
1095 B-cell genes indicated by blue circles. P value <0.05 and >2-fold gene expression cutoffs were
1096 used.

1097 (C) Volcano plot analysis of Akata RNA-seq, comparing mRNA values in cells induced for LMP1
1098 TES2m vs. mock-induced for 24 hours. SE targeted genes highlighted by red circles and other
1099 B-cell genes indicated by blue circles. P value <0.05 and >2-fold gene expression cutoffs were
1100 used.

1101 (D) Volcano plot analysis of BL-41 RNA-seq, comparing mRNA values in cells induced for LMP1
1102 WT vs. mock-induced for 24 hours. SE targeted genes highlighted by red circles and other B-
1103 cell genes indicated by blue circles. P value <0.05 and >2-fold gene expression cutoffs were
1104 used.

1105 (E) Volcano plot analysis of BL-41 RNA-seq, comparing mRNA values in cells induced for LMP1
1106 TES1m vs. mock-induced for 24 hours. SE targeted genes highlighted by red circles and other
1107 B-cell genes indicated by blue circles. P value <0.05 and >2-fold gene expression cutoffs were
1108 used.

1109 (F) Volcano plot analysis of BL-41 RNA-seq, comparing mRNA values in cells induced for LMP1
1110 TES2m vs. mock-induced for 24 hours. SE targeted genes highlighted by red circles and other
1111 B-cell genes indicated by blue circles. P value <0.05 and >2-fold gene expression cutoffs were
1112 used.

1113

1114 **Fig. 10. Model highlighting different modes of LMP1 TES1 and TES2 cross-talk in B-cell target**
1115 **gene regulation.**

1116

1117 **Materials and Methods**

1118 **Cell lines, culture, and vectors.** HEK293T cells were purchased from ATCC and cultured in
1119 Dulbecco's modified Eagle medium (DMEM, Gibco) with 10% fetal bovine serum (FBS, Gibco).
1120 EBV-negative Akata and BL-41 cells were obtained from Elliott Kieff; GM12878 were purchased
1121 from Coriell. Mutu I was obtained from Jeff Sample and Jijoye was purchased from ATCC. All B-
1122 cell lines stably expressed *Streptococcus pyogenes* Cas9 and were grown in Roswell Park
1123 Memorial Institute (RPMI) 1640 (Life Technologies) with 10% fetal bovine serum (Gibco) and
1124 penicillin-streptomycin in a humidified chamber with 5% carbon dioxide. LMP1 wildtype, TES1
1125 alanine point mutant 204PQQAT208 -> AQQAT, TES2 384YYD386->ID mutant and double
1126 mutant LMP1 with both AQQAT and ID mutations were cloned into the pLIX-402 vector. pLIX-402
1127 uses a TET-On TRE promoter to drive transgene expression and a C-terminal HA-tag fusion.
1128 Lentivirus vectors were used to establish stable Cas9+/GM12878, Cas9+/EBV- Akata and
1129 Cas9+/EBV- BL-41 Burkitt cells. Cell lines were then maintained with 0.5 µg/mL puromycin or 25
1130 µg/mL hygromycin. For LMP1 inducible expression studies, 0.5X10⁶ cells/ml were plated on
1131 Day-1 in 2ml of fresh RPMI in a 12-well plate. Cell were treated with 250ng/ml (in Burkitt cell
1132 models) for 24 hours prior to sample collection for downstream analyses or with 400ng/ml
1133 doxycycline (in LCL LMP1 cDNA rescue model) (Sigma #D9891) to allow for LMP1 rescue upon
1134 CRISPR knockout of LMP1. The Iκβ Super-repressor (SR) lacking residues 1-67 has previously
1135 been reported (27).

1136 **Antibodies and Reagents.** Cell Signaling Technology (CST) TRAF1 (#4715, Rabbit mAb),
1137 p105/50 (#3035, Rabbit mAb), RelA (#8242, Rabbit mAb), phospho-RelA (Ser536) (3033, Rabbit
1138 mAb), RelB (#4922, Rabbit mAb), cRel (#4727, Rabbit mAb), IκBα (#9247, Mouse mAb), IRF4
1139 (#4964, Rabbit mAb), TAK1 (#4505, Rabbit mAb), V5 (#13202, Rabbit mAb), HRP-linked anti-
1140 mouse IgG(7076), FLIP (#8510, Rabbit mAb), HRP-linked anti-rabbit IgG (#7074) were used in
1141 this study at 1:1000 dilution. p100/52 (EMD Millipore #05-361, Mouse mAb, 1:1000), GAPDH
1142 (EMD Millipore #MAB374, Mouse mAb, 1:500) was used. S12 mouse monoclonal antibody
1143 against LMP1 was purified from hybridoma supernatant (104). The IKKβ inhibitor IKK-2 inhibitor
1144 VIII (ApexBio, #A3485), puromycin dihydrochloride (Thermo Fisher #A1113803), and hygromycin
1145 B (Millipore #400052).

1146 **Growth Curve Analysis:** For growth curve analysis, cells were counted and then normalized to
1147 the same starting concentration, using the CellTiterGlo (CTG) luciferase assay (Promega,
1148 Cat#G7570). Live cell numbers were quantitated at each timepoint by CTG measurements, and
1149 values were corrected for tissue culture passage. Fold change of live cell number at each
1150 timepoint was calculated as a ratio of the value divided by the input value. For the Caspase-Glo
1151 3/6 Assay (Promega #G8092), Caspase-Glo 3/7 reagent was added to the cells, mixed and
1152 incubated for 30 minutes followed by recording of the luminescence. Readings were normalized
1153 to respective CTG values of the samples that were performed and collected concurrently.

1154 **CRISPR/Cas9 editing.** B-cell lines with stable Cas9 expression were established as described
1155 previously (46). Briefly, HEK293T cells were plated at a density of 300,000 cells per well in 2 mL
1156 DMEM supplemented with 10% FBS on Day -1. The following day (Day 0) plated cells were
1157 transfected with the TransIT-LT1 Transfection Reagent (Mirus #2306), according to the
1158 manufacturer's protocol. Transfection media was replaced by RPMI 16 hours later (Day 1). B-
1159 cells were plated at 1.2X 10⁶ density in a 6-well plate on Day 1. Lentivirus collected on Day 2
1160 were added to the B-cells for spinoculation at 2000rpm for 2 hours at 37C and 4µg/ml of
1161 polybrene. Spinoculated cells were placed in in a humidified chamber with 5% carbon dioxide for
1162 6 hours, then pelleted and resuspended in fresh RPMI/FBS. 48 hours post-transduction,
1163 transduced cells were selected by addition of puromycin 3 µg/ml or 200 µg/ml hygromycin. Broad
1164 Institute pXPR-515 control sgRNA (targets a non-coding intergenic region), Avana or Brunello

1165 library sgRNAs, as listed in Table 1, were cloned into lentiGuide-Puro (Addgene, catalog #52963)
1166 or pLenti SpBsmBI sgRNA Hygro (Addgene, catalog #62205).

1167 **RNAseq.** Total RNA was isolated using RNeasy mini kit (Qiagen #74106) with in-column genomic
1168 DNA digestion step according to the manufacturer's protocol. To construct indexed libraries, 1 µg
1169 of total RNA was used for polyA mRNA selection using NEBNext Poly(A) mRNA Magnetic
1170 Isolation Module (Cat#E7490S), and library preparation with NEBNext Ultra RNA Library Prep
1171 with Sample Purification Beads (Cat#E7765S). Each experimental treatment was performed in
1172 biological triplicate. Libraries were multi-indexed (NEB 7335L and E7500S), pooled and
1173 sequenced on an Illumina NextSeq 500 sequencer using single 75 bp read length. Adaptor-
1174 trimmed Illumina reads for each individual library were mapped back to the human GRCh37.83
1175 transcriptome assembly using STAR2.5.2b (105). FeatureCounts was used to estimate the
1176 number of reads mapped to each contig (106). Only transcripts with at least 5 cumulative mapping
1177 counts were used in this analysis. DESeq2 was used to evaluate differential expression (DE)
1178 (107). DESeq2 uses a negative binomial distribution to account for overdispersion in
1179 transcriptome data sets. It is conservative and uses a heuristic approach to detect outliers while
1180 avoiding false positives. Each DE analysis was composed of a pairwise comparison between
1181 experimental group and the control group. Differentially expressed genes were identified after a
1182 correction for false discovery rate (FDR). For more stringent analyses, we set the cutoff for truly
1183 differentially expressed genes as adjusted p value (FDR corrected) < 0.05 and absolute fold
1184 change > 1.5. DE genes meeting this cutoff were selected and subject to downstream
1185 bioinformatics and functional analyses, including clustering, data visualization, GO annotation and
1186 pathway analysis. DE genes were also subjected to Enrichr analysis
1187 (<https://maayanlab.cloud/Enrichr/>) for pathway analysis. Heatmaps were generated by feeding
1188 the Variance-Stabilizing Transformed values of selected DE genes from DESeq2 into Morpheus
1189 (<https://software.broadinstitute.org/morpheus/>).

1190 **Immunoblot Analysis.** Cells were lysed in Laemelli buffer (0.2M Tris-HCL, 0.4 M Dithiothreitol,
1191 277mM SDS, 6mM Bromophenol blue and 10% glycerol v/v) and sonicated at 4°C for five seconds
1192 using a probe sonicator at 20% amplitude and boiled at 95°C for eight minutes. The whole cell
1193 lysates were resolved by 12% or 15% SDS-PAGE, transferred to nitrocellulose filters at 100V at
1194 4°C for 1.5 hour, blocked with 5% non-fat dried milk in 1X TBST for 30 min at room-temperature,
1195 and then probed with the indicated primary antibodies (diluted in 1x TBS-T with 0.02% sodium
1196 azide at recommended manufacturer concentrations) overnight at 4°C on a rotating platform. Blots
1197 were washed three times in TBST for ten minutes each, and then probed with horse-radish
1198 peroxidase (HRP)-conjugated secondary antibodies, at a dilution of 1:3000 in 1X TBST with 5%
1199 non-fat dried milk. Blots were then washed three times in TBST for ten minutes each, developed
1200 by ECL chemiluminescent substrate (Thermo Scientific, #34578) and imaged on Li-COR Odyssey
1201 workstation.

1202 **Flow cytometry analysis.** FACS was performed using a FACSCalibur instrument (BD). For
1203 ICAM-1 and FAS detection, cells were washed in PBS w/2%FBS, then stained on ice for 30 min
1204 with BioLegend PE-conjugated anti-CD54/ICAM-1 and APC-conjugated anti-CD95/Fas antibody,
1205 washed three times with PBS with 2%FBS and analyzed by FACS. 7-AAD viability assays were
1206 carried out using 7-AAD (Thermo Fisher, #A1310) where cells were harvested and washed twice
1207 in 1XPBS supplemented with 2% FBS (Gibco). Washed cells were incubated with 1ug/ml 7-AAD
1208 solution in 1X PBS/2%FBS buffer for five minutes at room temperature and protected from light.
1209 Stained cells were analyzed via flow cytometry. Annexin V assay was performed with harvesting
1210 1×10^6 cells and washed with 1X PBS twice to remove excess RPMI. 2×10^5 cells were then
1211 resuspended to be stained with 5ul of Annexin V-FITC (#640945, Biolegend) in 100ul of Annexin
1212 V binding buffer (10mM HEPES, 140mM NaCl and 2.5mM CaCl_2). Cells were incubated at room
1213 temperature for 15 minutes and protected from light before analyzed by FACS.

1214 **Bioinformatic analysis and Software:** All the growth curves and column charts were made with
1215 GraphPad Prism v.9. FACS data was analyzed by FlowJo V10.

1216 **Table 1. sgRNAs used in this study.**

Guide No.	Gene Target	sgRNA Sequence (5' -> 3')
#1	Control	TTGACCTTTACCGTCCCGCG
#1	LMP1	TCTATCTACAACAAACTGG
#1	TAK1	CACCGGCTTACTGCTGGTTGCAGGG
#2	TAK1	CACCGCGCAATGAGTTGGTGTTTAC

1217

1218 References

- 1219 1. Gewurz BE, Longnecker, R. & Cohen, J.L. . 2021. *Fields Virology*, 7 ed, vol 2. Wolters Kluwer.
- 1220 2. Stunz LL, Bishop GA. 2014. Latent membrane protein 1 and the B lymphocyte-a complex
1221 relationship. *Crit Rev Immunol* 34:177-98.
- 1222 3. Wang LW, Jiang S, Gewurz BE. 2017. Epstein-Barr Virus LMP1-Mediated Oncogenicity. *J Virol* 91.
- 1223 4. Kieser A, Sterz KR. 2015. The Latent Membrane Protein 1 (LMP1). *Curr Top Microbiol Immunol*
1224 391:119-49.
- 1225 5. Wang L, Ning S. 2021. New Look of EBV LMP1 Signaling Landscape. *Cancers (Basel)* 13.
- 1226 6. Fish K, Comoglio F, Shaffer AL, 3rd, Ji Y, Pan KT, Scheich S, Oellerich A, Doebele C, Ikeda M,
1227 Schaller SJ, Nguyen H, Muppidi J, Wright GW, Urlaub H, Serve H, Staudt LM, Longnecker R,
1228 Oellerich T. 2020. Rewiring of B cell receptor signaling by Epstein-Barr virus LMP2A. *Proc Natl*
1229 *Acad Sci U S A* 117:26318-26327.
- 1230 7. Weniger MA, Küppers R. 2021. Molecular biology of Hodgkin lymphoma. *Leukemia* 35:968-981.
- 1231 8. Soni V, Cahir-McFarland E, Kieff E. 2007. LMP1 TRAFficking activates growth and survival
1232 pathways. *Adv Exp Med Biol* 597:173-87.
- 1233 9. Kaykas A, Worringer K, Sugden B. 2002. LMP-1's transmembrane domains encode multiple
1234 functions required for LMP-1's efficient signaling. *J Virol* 76:11551-60.
- 1235 10. Rastelli J, Hömig-Hölzel C, Seagal J, Müller W, Hermann AC, Rajewsky K, Zimmer-Strobl U. 2008.
1236 LMP1 signaling can replace CD40 signaling in B cells in vivo and has unique features of inducing
1237 class-switch recombination to IgG1. *Blood* 111:1448-55.
- 1238 11. Meckes DG, Jr., Menaker NF, Raab-Traub N. 2013. Epstein-Barr virus LMP1 modulates lipid raft
1239 microdomains and the vimentin cytoskeleton for signal transduction and transformation. *J Virol*
1240 87:1301-11.
- 1241 12. Shair KH, Bendt KM, Edwards RH, Bedford EC, Nielsen JN, Raab-Traub N. 2007. EBV latent
1242 membrane protein 1 activates Akt, NFkappaB, and Stat3 in B cell lymphomas. *PLoS Pathog*
1243 3:e166.
- 1244 13. Greenfeld H, Takasaki K, Walsh MJ, Ersing I, Bernhardt K, Ma Y, Fu B, Ashbaugh CW, Cabo J,
1245 Mollo SB, Zhou H, Li S, Gewurz BE. 2015. TRAF1 Coordinates Polyubiquitin Signaling to Enhance
1246 Epstein-Barr Virus LMP1-Mediated Growth and Survival Pathway Activation. *PLoS Pathog*
1247 11:e1004890.
- 1248 14. Kung CP, Meckes DG, Jr., Raab-Traub N. 2011. Epstein-Barr virus LMP1 activates EGFR, STAT3,
1249 and ERK through effects on PKCdelta. *J Virol* 85:4399-408.
- 1250 15. Mainou BA, Everly DN, Jr., Raab-Traub N. 2007. Unique signaling properties of CTAR1 in LMP1-
1251 mediated transformation. *J Virol* 81:9680-92.
- 1252 16. Zhang L, Wu L, Hong K, Pagano JS. 2001. Intracellular signaling molecules activated by Epstein-
1253 Barr virus for induction of interferon regulatory factor 7. *J Virol* 75:12393-401.
- 1254 17. Floettmann JE, Rowe M. 1997. Epstein-Barr virus latent membrane protein-1 (LMP1) C-terminus
1255 activation region 2 (CTAR2) maps to the far C-terminus and requires oligomerisation for NF-
1256 kappaB activation. *Oncogene* 15:1851-8.
- 1257 18. Huen DS, Henderson SA, Croom-Carter D, Rowe M. 1995. The Epstein-Barr virus latent
1258 membrane protein-1 (LMP1) mediates activation of NF-kappa B and cell surface phenotype via
1259 two effector regions in its carboxy-terminal cytoplasmic domain. *Oncogene* 10:549-60.
- 1260 19. Voigt S, Sterz KR, Giehler F, Mohr AW, Wilson JB, Moosmann A, Kieser A. 2020. A central role of
1261 IKK2 and TPL2 in JNK activation and viral B-cell transformation. *Nat Commun* 11:685.
- 1262 20. Shkoda A, Town JA, Griese J, Romio M, Sarioglu H, Knöfel T, Giehler F, Kieser A. 2012. The
1263 germinal center kinase TNK1 is required for canonical NF- κ B and JNK signaling in B-cells by the
1264 EBV oncoprotein LMP1 and the CD40 receptor. *PLoS Biol* 10:e1001376.

- 1265 21. Schultheiss U, Püschner S, Kremmer E, Mak TW, Engelmann H, Hammerschmidt W, Kieser A.
1266 2001. TRAF6 is a critical mediator of signal transduction by the viral oncogene latent membrane
1267 protein 1. *Embo j* 20:5678-91.
- 1268 22. Arcipowski KM, Stunz LL, Bishop GA. 2014. TRAF6 is a critical regulator of LMP1 functions in vivo.
1269 *Int Immunol* 26:149-58.
- 1270 23. Arcipowski KM, Stunz LL, Graham JP, Kraus ZJ, Vanden Bush TJ, Bishop GA. 2011. Molecular
1271 mechanisms of TNFR-associated factor 6 (TRAF6) utilization by the oncogenic viral mimic of
1272 CD40, latent membrane protein 1 (LMP1). *J Biol Chem* 286:9948-55.
- 1273 24. Wang L, Howell MEA, Sparks-Wallace A, Zhao J, Hensley CR, Nicksic CA, Horne SR, Mohr KB,
1274 Moorman JP, Yao ZQ, Ning S. 2021. The Ubiquitin Sensor and Adaptor Protein p62 Mediates
1275 Signal Transduction of a Viral Oncogenic Pathway. *mBio* 12:e0109721.
- 1276 25. Ma Y, Walsh MJ, Bernhardt K, Ashbaugh CW, Trudeau SJ, Ashbaugh IY, Jiang S, Jiang C, Zhao B,
1277 Root DE, Doench JG, Gewurz BE. 2017. CRISPR/Cas9 Screens Reveal Epstein-Barr Virus-
1278 Transformed B Cell Host Dependency Factors. *Cell Host Microbe* 21:580-591.e7.
- 1279 26. Gewurz BE, Towfic F, Mar JC, Shinnars NP, Takasaki K, Zhao B, Cahir-McFarland ED,
1280 Quackenbush J, Xavier RJ, Kieff E. 2012. Genome-wide siRNA screen for mediators of NF- κ B
1281 activation. *Proc Natl Acad Sci U S A* 109:2467-72.
- 1282 27. Gewurz BE, Mar JC, Padi M, Zhao B, Shinnars NP, Takasaki K, Bedoya E, Zou JY, Cahir-McFarland
1283 E, Quackenbush J, Kieff E. 2011. Canonical NF- κ B activation is essential for Epstein-Barr
1284 virus latent membrane protein 1 TES2/CTAR2 gene regulation. *J Virol* 85:6764-73.
- 1285 28. Bentz GL, Moss CR, 2nd, Whitehurst CB, Moody CA, Pagano JS. 2015. LMP1-Induced
1286 Sumoylation Influences the Maintenance of Epstein-Barr Virus Latency through KAP1. *J Virol*
1287 89:7465-77.
- 1288 29. Selby TL, Biel N, Varn M, Patel S, Patel A, Hilding L, Ray A, Ross T, Cramblet WT, Moss CR, Lowrey
1289 AJ, Bentz GL. 2019. The Epstein-Barr Virus Oncoprotein, LMP1, Regulates the Function of SENP2,
1290 a SUMO-protease. *Sci Rep* 9:9523.
- 1291 30. Gires O, Kohlhuber F, Kilger E, Baumann M, Kieser A, Kaiser C, Zeidler R, Scheffer B, Ueffing M,
1292 Hammerschmidt W. 1999. Latent membrane protein 1 of Epstein-Barr virus interacts with JAK3
1293 and activates STAT proteins. *Embo j* 18:3064-73.
- 1294 31. Izumi KM, Cahir McFarland ED, Riley EA, Rizzo D, Chen Y, Kieff E. 1999. The residues between the
1295 two transformation effector sites of Epstein-Barr virus latent membrane protein 1 are not
1296 critical for B-lymphocyte growth transformation. *J Virol* 73:9908-16.
- 1297 32. Zhao B, Barrera LA, Ersing I, Willox B, Schmidt SC, Greenfeld H, Zhou H, Mollo SB, Shi TT,
1298 Takasaki K, Jiang S, Cahir-McFarland E, Kellis M, Bulyk ML, Kieff E, Gewurz BE. 2014. The NF- κ B
1299 genomic landscape in lymphoblastoid B cells. *Cell Rep* 8:1595-606.
- 1300 33. Wang D, Liebowitz D, Kieff E. 1985. An EBV membrane protein expressed in immortalized
1301 lymphocytes transforms established rodent cells. *Cell* 43:831-40.
- 1302 34. Baichwal VR, Sugden B. 1988. Transformation of Balb 3T3 cells by the BNLF-1 gene of Epstein-
1303 Barr virus. *Oncogene* 2:461-7.
- 1304 35. Moorthy RK, Thorley-Lawson DA. 1993. All three domains of the Epstein-Barr virus-encoded
1305 latent membrane protein LMP-1 are required for transformation of rat-1 fibroblasts. *J Virol*
1306 67:1638-46.
- 1307 36. Minamitani T, Ma Y, Zhou H, Kida H, Tsai CY, Obana M, Okuzaki D, Fujio Y, Kumanogoh A, Zhao B,
1308 Kikutani H, Kieff E, Gewurz BE, Yasui T. 2017. Mouse model of Epstein-Barr virus LMP1- and
1309 LMP2A-driven germinal center B-cell lymphoproliferative disease. *Proc Natl Acad Sci U S A*
1310 114:4751-4756.
- 1311 37. Wirtz T, Weber T, Kracker S, Sommermann T, Rajewsky K, Yasuda T. 2016. Mouse model for
1312 acute Epstein-Barr virus infection. *Proc Natl Acad Sci U S A* 113:13821-13826.

- 1313 38. Zhang B, Kracker S, Yasuda T, Casola S, Vanneman M, Hömig-Hölzel C, Wang Z, Derudder E, Li S,
1314 Chakraborty T, Cotter SE, Koyama S, Currie T, Freeman GJ, Kutok JL, Rodig SJ, Dranoff G,
1315 Rajewsky K. 2012. Immune surveillance and therapy of lymphomas driven by Epstein-Barr virus
1316 protein LMP1 in a mouse model. *Cell* 148:739-51.
- 1317 39. Thornburg NJ, Kulwichit W, Edwards RH, Shair KH, Bendt KM, Raab-Traub N. 2006. LMP1
1318 signaling and activation of NF-kappaB in LMP1 transgenic mice. *Oncogene* 25:288-97.
- 1319 40. Pich D, Mrozek-Gorska P, Bouvet M, Sugimoto A, Akidil E, Grundhoff A, Hamperl S, Ling PD,
1320 Hammerschmidt W. 2019. First Days in the Life of Naive Human B Lymphocytes Infected with
1321 Epstein-Barr Virus. *mBio* 10.
- 1322 41. Kaye KM, Izumi KM, Kieff E. 1993. Epstein-Barr virus latent membrane protein 1 is essential for
1323 B-lymphocyte growth transformation. *Proc Natl Acad Sci U S A* 90:9150-4.
- 1324 42. Dirmeier U, Neuhierl B, Kilger E, Reisbach G, Sandberg ML, Hammerschmidt W. 2003. Latent
1325 membrane protein 1 is critical for efficient growth transformation of human B cells by epstein-
1326 barr virus. *Cancer Res* 63:2982-9.
- 1327 43. Cohen JI, Wang F, Kieff E. 1991. Epstein-Barr virus nuclear protein 2 mutations define essential
1328 domains for transformation and transactivation. *J Virol* 65:2545-54.
- 1329 44. Kaye KM, Izumi KM, Mosialos G, Kieff E. 1995. The Epstein-Barr virus LMP1 cytoplasmic carboxy
1330 terminus is essential for B-lymphocyte transformation; fibroblast cocultivation complements a
1331 critical function within the terminal 155 residues. *J Virol* 69:675-83.
- 1332 45. Izumi KM, Kaye KM, Kieff ED. 1997. The Epstein-Barr virus LMP1 amino acid sequence that
1333 engages tumor necrosis factor receptor associated factors is critical for primary B lymphocyte
1334 growth transformation. *Proc Natl Acad Sci U S A* 94:1447-52.
- 1335 46. Jiang S, Wang LW, Walsh MJ, Trudeau SJ, Gerdt C, Zhao B, Gewurz BE. 2018. CRISPR/Cas9-
1336 Mediated Genome Editing in Epstein-Barr Virus-Transformed Lymphoblastoid B-Cell Lines. *Curr*
1337 *Protoc Mol Biol* 121:31.12.1-31.12.23.
- 1338 47. Kuleshov MV, Jones MR, Rouillard AD, Fernandez NF, Duan Q, Wang Z, Koplev S, Jenkins SL,
1339 Jagodnik KM, Lachmann A, McDermott MG, Monteiro CD, Gundersen GW, Ma'ayan A. 2016.
1340 Enrichr: a comprehensive gene set enrichment analysis web server 2016 update. *Nucleic Acids*
1341 *Res* 44:W90-7.
- 1342 48. Forte E, Luftig MA. 2009. MDM2-dependent inhibition of p53 is required for Epstein-Barr virus
1343 B-cell growth transformation and infected-cell survival. *J Virol* 83:2491-9.
- 1344 49. Cahir-McFarland ED, Carter K, Rosenwald A, Giltnane JM, Henrickson SE, Staudt LM, Kieff E.
1345 2004. Role of NF-kappa B in cell survival and transcription of latent membrane protein 1-
1346 expressing or Epstein-Barr virus latency III-infected cells. *J Virol* 78:4108-19.
- 1347 50. Nakayama T, Hieshima K, Nagakubo D, Sato E, Nakayama M, Kawa K, Yoshie O. 2004. Selective
1348 induction of Th2-attracting chemokines CCL17 and CCL22 in human B cells by latent membrane
1349 protein 1 of Epstein-Barr virus. *J Virol* 78:1665-74.
- 1350 51. Jorapur A, Marshall LA, Jacobson S, Xu M, Marubayashi S, Zibinsky M, Hu DX, Robles O, Jackson
1351 JJ, Baloche V, Busson P, Wustrow D, Brockstedt DG, Talay O, Kassner PD, Cutler G. 2022. EBV+
1352 tumors exploit tumor cell-intrinsic and -extrinsic mechanisms to produce regulatory T cell-
1353 recruiting chemokines CCL17 and CCL22. *PLoS Pathog* 18:e1010200.
- 1354 52. Demetriades C, Mosialos G. 2009. The LMP1 promoter can be transactivated directly by NF-
1355 kappaB. *J Virol* 83:5269-77.
- 1356 53. Johansson P, Jansson A, Rüetschi U, Rymo L. 2009. Nuclear factor-kappaB binds to the Epstein-
1357 Barr Virus LMP1 promoter and upregulates its expression. *J Virol* 83:1393-401.
- 1358 54. Devergne O, Cahir McFarland ED, Mosialos G, Izumi KM, Ware CF, Kieff E. 1998. Role of the TRAF
1359 binding site and NF-kappaB activation in Epstein-Barr virus latent membrane protein 1-induced
1360 cell gene expression. *J Virol* 72:7900-8.

- 1361 55. Izumi KM, Kieff ED. 1997. The Epstein-Barr virus oncogene product latent membrane protein 1
1362 engages the tumor necrosis factor receptor-associated death domain protein to mediate B
1363 lymphocyte growth transformation and activate NF-kappaB. *Proc Natl Acad Sci U S A* 94:12592-
1364 7.
- 1365 56. Lee DY, Sugden B. 2008. The LMP1 oncogene of EBV activates PERK and the unfolded protein
1366 response to drive its own synthesis. *Blood* 111:2280-9.
- 1367 57. Bentz GL, Whitehurst CB, Pagano JS. 2011. Epstein-Barr virus latent membrane protein 1 (LMP1)
1368 C-terminal-activating region 3 contributes to LMP1-mediated cellular migration via its
1369 interaction with Ubc9. *J Virol* 85:10144-53.
- 1370 58. Luftig M, Yasui T, Soni V, Kang MS, Jacobson N, Cahir-McFarland E, Seed B, Kieff E. 2004. Epstein-
1371 Barr virus latent infection membrane protein 1 TRAF-binding site induces NIK/IKK alpha-
1372 dependent noncanonical NF-kappaB activation. *Proc Natl Acad Sci U S A* 101:141-6.
- 1373 59. Tsai K, Thikmyanova N, Wojcechowskyj JA, Delecluse HJ, Lieberman PM. 2011. EBV tegument
1374 protein BHRF1 disrupts DAXX-ATRX to activate viral early gene transcription. *PLoS Pathog*
1375 7:e1002376.
- 1376 60. Zhang Y, Jiang C, Trudeau SJ, Narita Y, Zhao B, Teng M, Guo R, Gewurz BE. 2020. Histone Loaders
1377 CAF1 and HIRA Restrict Epstein-Barr Virus B-Cell Lytic Reactivation. *mBio* 11.
- 1378 61. Takada K, Horinouchi K, Ono Y, Aya T, Osato T, Takahashi M, Hayasaka S. 1991. An Epstein-Barr
1379 virus-producer line Akata: establishment of the cell line and analysis of viral DNA. *Virus Genes*
1380 5:147-56.
- 1381 62. Shimizu N, Tanabe-Tochikura A, Kuroiwa Y, Takada K. 1994. Isolation of Epstein-Barr virus (EBV)-
1382 negative cell clones from the EBV-positive Burkitt's lymphoma (BL) line Akata: malignant
1383 phenotypes of BL cells are dependent on EBV. *J Virol* 68:6069-73.
- 1384 63. Anonymous. 1985. Burkitt's lymphoma: a human cancer model. Proceedings of a symposium.
1385 Lyon, 6-9 December 1983. *IARC Sci Publ*:1-484.
- 1386 64. Song YJ, Izumi KM, Shinnars NP, Gewurz BE, Kieff E. 2008. IRF7 activation by Epstein-Barr virus
1387 latent membrane protein 1 requires localization at activation sites and TRAF6, but not TRAF2 or
1388 TRAF3. *Proc Natl Acad Sci U S A* 105:18448-53.
- 1389 65. Huye LE, Ning S, Kelliher M, Pagano JS. 2007. Interferon regulatory factor 7 is activated by a viral
1390 oncoprotein through RIP-dependent ubiquitination. *Mol Cell Biol* 27:2910-8.
- 1391 66. Ning S, Hahn AM, Huye LE, Pagano JS. 2003. Interferon regulatory factor 7 regulates expression
1392 of Epstein-Barr virus latent membrane protein 1: a regulatory circuit. *J Virol* 77:9359-68.
- 1393 67. Ning S, Pagano JS. 2010. The A20 deubiquitinase activity negatively regulates LMP1 activation of
1394 IRF7. *J Virol* 84:6130-8.
- 1395 68. Thomas N, Dreval K, Gerhard DS, Hilton LK, Abramson JS, Ambinder RF, Barta S, Bartlett NL,
1396 Bethony J, Bhatia K, Bowen J, Bryan AC, Cesarman E, Casper C, Chadburn A, Cruz M, Dittmer DP,
1397 Dyer MA, Farinha P, Gastier-Foster JM, Gerrie AS, Grande BM, Greiner T, Griner NB, Gross TG,
1398 Harris NL, Irvin JD, Jaffe ES, Henry D, Huppi R, Leal FE, Lee MS, Martin JP, Martin MR, Mbulaiteye
1399 SM, Mitsuyasu R, Morris V, Mullighan CG, Mungall AJ, Mungall K, Mutyaba I, Nokta M,
1400 Namirembe C, Noy A, Ogwang MD, Omoding A, Orem J, Ott G, Petrello H, Pittaluga S, et al. 2023.
1401 Genetic subgroups inform on pathobiology in adult and pediatric Burkitt lymphoma. *Blood*
1402 141:904-916.
- 1403 69. Grande BM, Gerhard DS, Jiang A, Griner NB, Abramson JS, Alexander TB, Allen H, Ayers LW,
1404 Bethony JM, Bhatia K, Bowen J, Casper C, Choi JK, Culibrk L, Davidsen TM, Dyer MA, Gastier-
1405 Foster JM, Gesuwan P, Greiner TC, Gross TG, Hanf B, Harris NL, He Y, Irvin JD, Jaffe ES, Jones
1406 SJM, Kerchan P, Knoetze N, Leal FE, Lichtenberg TM, Ma Y, Martin JP, Martin MR, Mbulaiteye
1407 SM, Mullighan CG, Mungall AJ, Namirembe C, Novik K, Noy A, Ogwang MD, Omoding A, Orem J,
1408 Reynolds SJ, Rushton CK, Sandlund JT, Schmitz R, Taylor C, Wilson WH, Wright GW, Zhao EY, et

- 1409 al. 2019. Genome-wide discovery of somatic coding and noncoding mutations in pediatric
1410 endemic and sporadic Burkitt lymphoma. *Blood* 133:1313-1324.
- 1411 70. Guo R, Zhang Y, Teng M, Jiang C, Schineller M, Zhao B, Doench JG, O'Reilly RJ, Cesarman E,
1412 Giulino-Roth L, Gewurz BE. 2020. DNA methylation enzymes and PRC1 restrict B-cell Epstein-
1413 Barr virus oncoprotein expression. *Nat Microbiol* 5:1051-1063.
- 1414 71. Wang F, Gregory C, Sample C, Rowe M, Liebowitz D, Murray R, Rickinson A, Kieff E. 1990.
1415 Epstein-Barr virus latent membrane protein (LMP1) and nuclear proteins 2 and 3C are effectors
1416 of phenotypic changes in B lymphocytes: EBNA-2 and LMP1 cooperatively induce CD23. *J Virol*
1417 64:2309-18.
- 1418 72. Gregory CD, Rowe M, Rickinson AB. 1990. Different Epstein-Barr virus-B cell interactions in
1419 phenotypically distinct clones of a Burkitt's lymphoma cell line. *J Gen Virol* 71 (Pt 7):1481-95.
- 1420 73. Jin J, Hu H, Li HS, Yu J, Xiao Y, Brittain GC, Zou Q, Cheng X, Mallette FA, Watowich SS, Sun SC.
1421 2014. Noncanonical NF- κ B pathway controls the production of type I interferons in antiviral
1422 innate immunity. *Immunity* 40:342-54.
- 1423 74. DeKroon RM, Gunawardena HP, Edwards R, Raab-Traub N. 2018. Global Proteomic Changes
1424 Induced by the Epstein-Barr Virus Oncoproteins Latent Membrane Protein 1 and 2A. *mBio* 9.
- 1425 75. Devergne O, Hatzivassiliou E, Izumi KM, Kaye KM, Kleijnen MF, Kieff E, Mosialos G. 1996.
1426 Association of TRAF1, TRAF2, and TRAF3 with an Epstein-Barr virus LMP1 domain important for
1427 B-lymphocyte transformation: role in NF-kappaB activation. *Mol Cell Biol* 16:7098-108.
- 1428 76. Shair KH, Raab-Traub N. 2012. Transcriptome changes induced by Epstein-Barr virus LMP1 and
1429 LMP2A in transgenic lymphocytes and lymphoma. *mBio* 3.
- 1430 77. Faumont N, Durand-Panteix S, Schlee M, Grömminger S, Schuhmacher M, Hölzel M, Laux G,
1431 Mailhammer R, Rosenwald A, Staudt LM, Bornkamm GW, Feuillard J. 2009. c-Myc and Rel/NF-
1432 kappaB are the two master transcriptional systems activated in the latency III program of
1433 Epstein-Barr virus-immortalized B cells. *J Virol* 83:5014-27.
- 1434 78. Wang L, Ren J, Li G, Moorman JP, Yao ZQ, Ning S. 2017. LMP1 signaling pathway activates IRF4 in
1435 latent EBV infection and a positive circuit between PI3K and Src is required. *Oncogene* 36:2265-
1436 2274.
- 1437 79. Wang L, Ning S. 2013. Interferon regulatory factor 4 is activated through c-Src-mediated tyrosine
1438 phosphorylation in virus-transformed cells. *J Virol* 87:9672-9.
- 1439 80. Glasmacher E, Agrawal S, Chang AB, Murphy TL, Zeng W, Vander Lugt B, Khan AA, Ciofani M,
1440 Spooner CJ, Rutz S, Hackney J, Nurieva R, Escalante CR, Ouyang W, Littman DR, Murphy KM,
1441 Singh H. 2012. A genomic regulatory element that directs assembly and function of immune-
1442 specific AP-1-IRF complexes. *Science* 338:975-80.
- 1443 81. Hnisz D, Abraham BJ, Lee TI, Lau A, Saint-André V, Sigova AA, Hoke HA, Young RA. 2013. Super-
1444 enhancers in the control of cell identity and disease. *Cell* 155:934-47.
- 1445 82. Jiang S, Zhou H, Liang J, Gerdt C, Wang C, Ke L, Schmidt SCS, Narita Y, Ma Y, Wang S, Colson T,
1446 Gewurz B, Li G, Kieff E, Zhao B. 2017. The Epstein-Barr Virus Regulome in Lymphoblastoid Cells.
1447 *Cell Host Microbe* 22:561-573.e4.
- 1448 83. Zhou H, Schmidt SC, Jiang S, Willox B, Bernhardt K, Liang J, Johannsen EC, Kharchenko P, Gewurz
1449 BE, Kieff E, Zhao B. 2015. Epstein-Barr virus oncoprotein super-enhancers control B cell growth.
1450 *Cell Host Microbe* 17:205-16.
- 1451 84. Yan B, Wang C, Chakravorty S, Zhang Z, Kadadi SD, Zhuang Y, Sirit I, Hu Y, Jung M, Sahoo SS,
1452 Wang L, Shao K, Anderson NL, Trujillo-Ochoa JL, Briggs SD, Liu X, Olson MR, Afzali B, Zhao B,
1453 Kazemian M. 2023. A comprehensive single cell data analysis of lymphoblastoid cells reveals the
1454 role of super-enhancers in maintaining EBV latency. *J Med Virol* 95:e28362.
- 1455 85. Hanahan D, Weinberg RA. 2000. The hallmarks of cancer. *Cell* 100:57-70.

- 1456 86. Kung CP, Raab-Traub N. 2010. Epstein-Barr virus latent membrane protein 1 modulates
1457 distinctive NF- κ B pathways through C-terminus-activating region 1 to regulate epidermal
1458 growth factor receptor expression. *J Virol* 84:6605-14.
- 1459 87. Johansen LM, Deppmann CD, Erickson KD, Coffin WF, 3rd, Thornton TM, Humphrey SE, Martin
1460 JM, Taparowsky EJ. 2003. EBNA2 and activated Notch induce expression of BATF. *J Virol*
1461 77:6029-40.
- 1462 88. Banerjee S, Lu J, Cai Q, Saha A, Jha HC, Dzeng RK, Robertson ES. 2013. The EBV Latent Antigen 3C
1463 Inhibits Apoptosis through Targeted Regulation of Interferon Regulatory Factors 4 and 8. *PLoS*
1464 *Pathog* 9:e1003314.
- 1465 89. Edwards RH, Marquitz AR, Raab-Traub N. 2015. Changes in expression induced by Epstein-Barr
1466 Virus LMP1-CTAR1: potential role of bcl3. *mBio* 6.
- 1467 90. Burton EM, Voyer J, Gewurz BE. 2022. Epstein-Barr virus latency programs dynamically sensitize
1468 B cells to ferroptosis. *Proc Natl Acad Sci U S A* 119:e2118300119.
- 1469 91. Wang LW, Shen H, Nobre L, Ersing I, Paulo JA, Trudeau S, Wang Z, Smith NA, Ma Y, Reinstadler B,
1470 Nomburg J, Sommermann T, Cahir-McFarland E, Gygi SP, Mootha VK, Weekes MP, Gewurz BE.
1471 2019. Epstein-Barr-Virus-Induced One-Carbon Metabolism Drives B Cell Transformation. *Cell*
1472 *Metab* 30:539-555.e11.
- 1473 92. Guo R, Liang JH, Zhang Y, Lutchenkov M, Li Z, Wang Y, Trujillo-Alonso V, Puri R, Giulino-Roth L,
1474 Gewurz BE. 2022. Methionine metabolism controls the B cell EBV epigenome and viral latency.
1475 *Cell Metab* 34:1280-1297.e9.
- 1476 93. Bonglack EN, Messinger JE, Cable JM, Ch'ng J, Parnell KM, Reinoso-Vizcaino NM, Barry AP,
1477 Russell VS, Dave SS, Christofk HR, Luftig MA. 2021. Monocarboxylate transporter antagonism
1478 reveals metabolic vulnerabilities of viral-driven lymphomas. *Proc Natl Acad Sci U S A* 118.
- 1479 94. Correia S, Palser A, Elgueta Karstegl C, Middeldorp JM, Ramayanti O, Cohen JI, Hildesheim A,
1480 Fellner MD, Wiels J, White RE, Kellam P, Farrell PJ. 2017. Natural Variation of Epstein-Barr Virus
1481 Genes, Proteins, and Primary MicroRNA. *J Virol* 91.
- 1482 95. Hu LF, Zabarovsky ER, Chen F, Cao SL, Ernberg I, Klein G, Winberg G. 1991. Isolation and
1483 sequencing of the Epstein-Barr virus BNLF-1 gene (LMP1) from a Chinese nasopharyngeal
1484 carcinoma. *J Gen Virol* 72 (Pt 10):2399-409.
- 1485 96. Chen ML, Tsai CN, Liang CL, Shu CH, Huang CR, Sulitzeanu D, Liu ST, Chang YS. 1992. Cloning and
1486 characterization of the latent membrane protein (LMP) of a specific Epstein-Barr virus variant
1487 derived from the nasopharyngeal carcinoma in the Taiwanese population. *Oncogene* 7:2131-40.
- 1488 97. Knecht H, Bachmann E, Brousset P, Sandvej K, Nadal D, Bachmann F, Odermatt BF, Delsol G,
1489 Pallesen G. 1993. Deletions within the LMP1 oncogene of Epstein-Barr virus are clustered in
1490 Hodgkin's disease and identical to those observed in nasopharyngeal carcinoma. *Blood* 82:2937-
1491 42.
- 1492 98. Kingma DW, Weiss WB, Jaffe ES, Kumar S, Frekko K, Raffeld M. 1996. Epstein-Barr virus latent
1493 membrane protein-1 oncogene deletions: correlations with malignancy in Epstein-Barr virus--
1494 associated lymphoproliferative disorders and malignant lymphomas. *Blood* 88:242-51.
- 1495 99. Knecht H, Bachmann E, Joske DJ, Sahli R, Eméry-Goodman A, Casanova JL, Zilić M, Bachmann F,
1496 Odermatt BF. 1993. Molecular analysis of the LMP (latent membrane protein) oncogene in
1497 Hodgkin's disease. *Leukemia* 7:580-5.
- 1498 100. da Costa VG, Marques-Silva AC, Moreli ML. 2015. The Epstein-Barr virus latent membrane
1499 protein-1 (LMP1) 30-bp deletion and XhoI-polymorphism in nasopharyngeal carcinoma: a meta-
1500 analysis of observational studies. *Syst Rev* 4:46.
- 1501 101. Li SN, Chang YS, Liu ST. 1996. Effect of a 10-amino acid deletion on the oncogenic activity of
1502 latent membrane protein 1 of Epstein-Barr virus. *Oncogene* 12:2129-35.

- 1503 102. Trivedi P, Winberg G, Klein G. 1997. Differential immunogenicity of Epstein-Barr virus (EBV)
1504 encoded growth transformation-associated antigens in a murine model system. *Eur J Cancer*
1505 33:912-7.
- 1506 103. Miller WE, Cheshire JL, Baldwin AS, Jr., Raab-Traub N. 1998. The NPC derived C15 LMP1 protein
1507 confers enhanced activation of NF-kappa B and induction of the EGFR in epithelial cells.
1508 *Oncogene* 16:1869-77.
- 1509 104. Mann KP, Staunton D, Thorley-Lawson DA. 1985. Epstein-Barr virus-encoded protein found in
1510 plasma membranes of transformed cells. *J Virol* 55:710-20.
- 1511 105. Dobin A, Davis CA, Schlesinger F, Drenkow J, Zaleski C, Jha S, Batut P, Chaisson M, Gingeras TR.
1512 2012. STAR: ultrafast universal RNA-seq aligner. *Bioinformatics* 29:15-21.
- 1513 106. Liao Y, Smyth GK, Shi W. 2013. featureCounts: an efficient general purpose program for
1514 assigning sequence reads to genomic features. *Bioinformatics* 30:923-930.
- 1515 107. Love MI, Huber W, Anders S. 2014. Moderated estimation of fold change and dispersion for
1516 RNA-seq data with DESeq2. *Genome Biol* 15:550.
- 1517

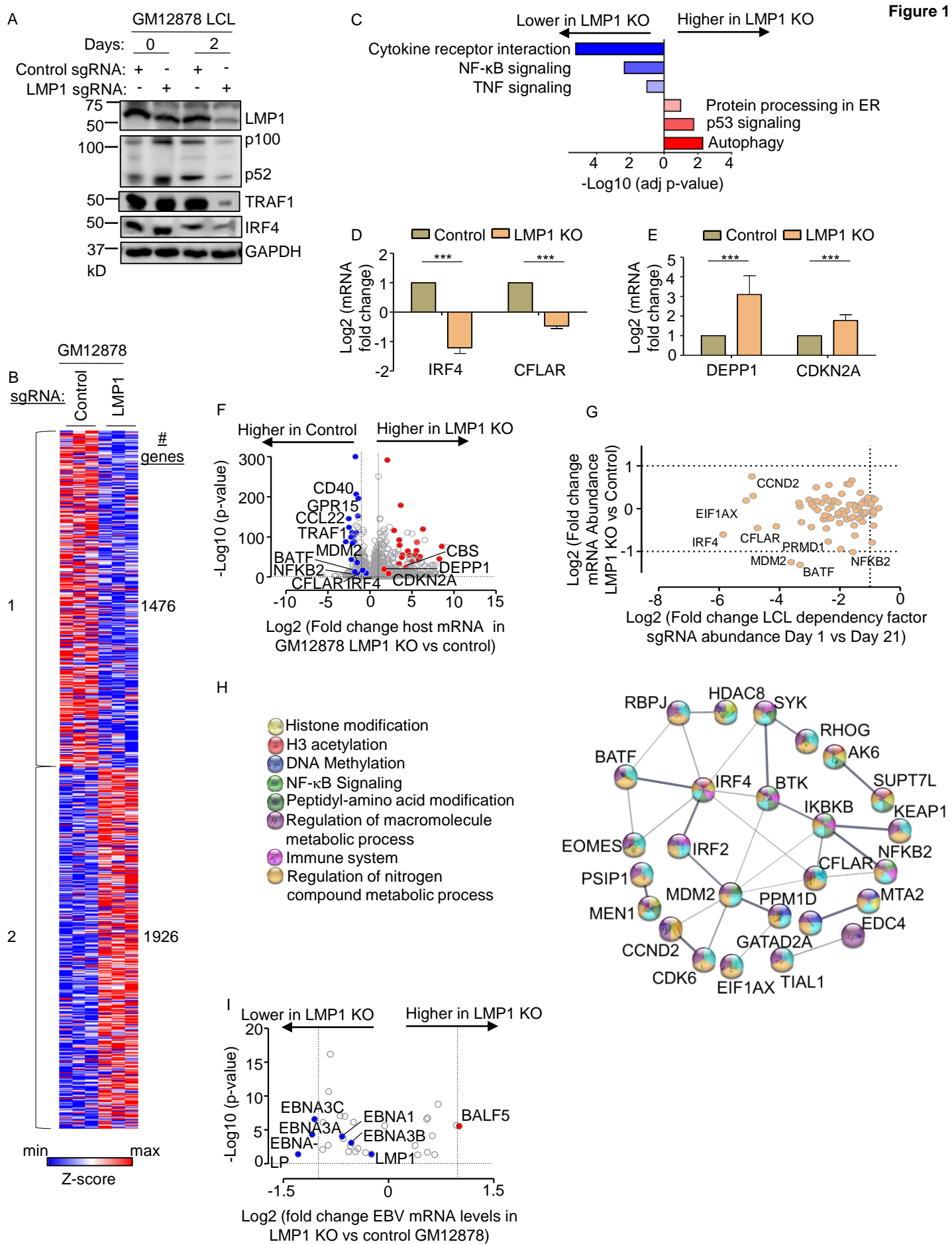


Fig. 1. Characterization of LMP1 KO effects on GM12878 LCL target gene regulation

(A) Immunoblot analysis of whole cell lysates (WCL) from GM12878 LCLs transduced with lentiviruses that express control or LMP1 targeting single guide RNAs (sgRNAs). Transduced cells were puromycin selected for 0 vs 2 days, as indicated. Blots for LMP1, for LMP1 target genes TRAF1 and IRF4, and for LMP1-driven non-canonical NF- κ B pathway p100/p52 processing are shown. Blots are representative of n=3 experiments.

(B) K-means heatmap analysis of GM12878 LCLs transduced as in (A) with lentivirus expressing control or LMP1 sgRNA and puromycin selected for 48 hours. The heatmap depicts relative Z-scores in each row from n=3 independent RNAseq replicates, divided into two clusters. The Z-score scale is shown at bottom, where blue and red colors indicate lower versus higher relative expression, respectively. Two-way ANOVA P-value cutoff of <0.01 and >2-fold gene expression cutoffs were used.

(C) Enrichr analysis of KEGG pathways most highly changed in GM12878 expressing control versus LMP1 sgRNA (LMP1 KO), as in (A). The X-axis depicts the -Log₁₀ adjusted p-value (adj p-value) scale. The top three most enriched KEGG pathways are shown.

(D) Abundances of two representative Cluster 1 genes from n=3 RNAseq analyses in cells with control vs LMP1 sgRNA. p-values were determined by one-sided Fisher's exact test. *p<0.05, **p<0.01.

(E) Abundances of two representative Cluster 2 genes from n=3 RNAseq analyses in cells with control vs LMP1 sgRNA. p-values were determined by one-sided Fisher's exact test. ***p<0.001.

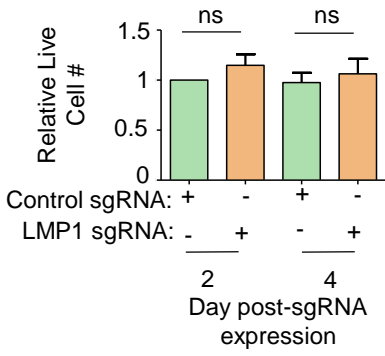
(F) Volcano plot analysis of host transcriptome-wide GM12878 genes differentially expressed in cells with control versus LMP1 sgRNA expression, as in (B), using data from n=3 RNAseq datasets.

(G) Scatter plot cross comparison of log₂ transformed fold change mRNA abundances in GM12878 expressing LMP1 vs. control sgRNA (Y-axis) versus log₂ transformed fold change abundances of sgRNAs at Day 21 versus Day 1 post-transduction of GM12878 LCLs in a genome-wide CRISPR screen (25) (X-axis).

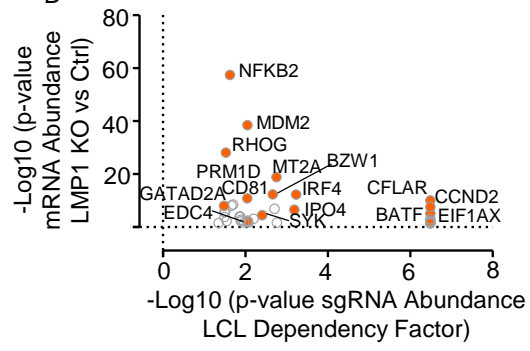
(H) String analysis of genes shown in (G). Pathway identifiers for each gene and interaction are colored coded.

(I) Volcano plot analysis of EBV mRNA values in GM12878 expressing LMP1 vs control sgRNAs, as in (B). p-value <0.05 and >2-fold change mRNA abundance cutoffs were used.

A



B



C

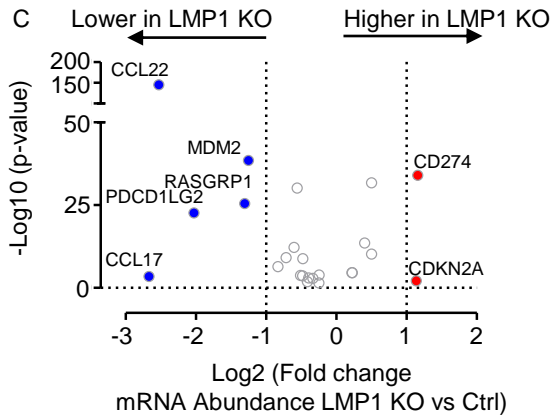


Fig. S1. Characterization of LMP1 KO effects on GM12878 LCL target gene regulation.

(A) Relative mean + standard deviation (SD) live cell numbers from CellTitreGlo analysis of n=3 replicates of Cas9+ GM12878 LCLs, transduced with lentiviruses that expressed control or LMP1 sgRNAs and puromycin selected, for 2 versus 4 days.

(B) Scatter plot analysis cross-comparing the significance of changes in LCL dependency factor expression upon GM12878 LMP1 KO versus the CRISPR screen significance score for selection against sgRNAs in LCL vs Burkitt dependency factor analysis (25). Shown on the Y-axis are $-\log_{10}$ transformed P-values from RNAseq analysis of GM12878 LCLs transduced with lentiviruses expressing LMP1 versus control sgRNA (as in **Fig. 1F**), versus $-\log_{10}$ transformed P-values from CRISPR LCL vs Burkitt cell dependency factor analysis (25). Higher Y-axis scores indicate more significant differences in expression for the indicated genes in GM12878 with LMP1 vs control sgRNA. Higher X-axis scores indicate a stronger selection against sgRNA targeting the indicated genes in GM12878 LCLs versus P3HR1 Burkitt cells over 21 days of cell culture. Shown are genes with $p < 0.05$ in both analyses.

(C) Volcano plot analysis visualizing KEGG Hodgkin lymphoma pathway gene $-\log_{10}$ (P-value) on the y-axis versus \log_2 transformed fold change in mRNA abundances on the x-axis of GM12878 genes in cells expressing LMP1 versus control sgRNA (as in **Fig. 1F**). P-value < 0.05 and > 2 -fold change mRNA abundance cutoffs were used.

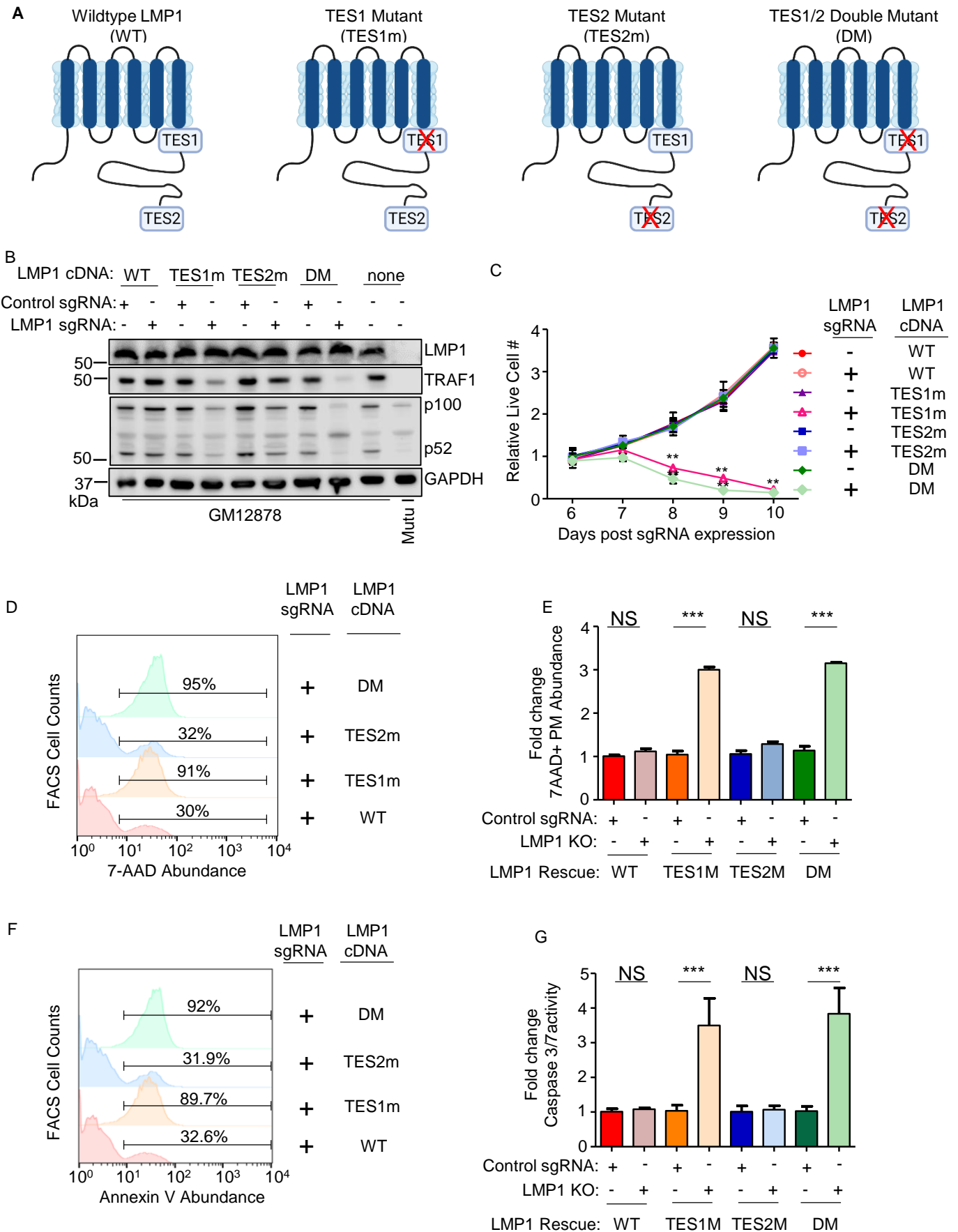


Fig. 2. Loss of TES1 but not TES2 signaling triggers LCL apoptosis.

(A) Schematic diagram of LMP1 WT with TES1 and TES2 domains highlighted. Wildtype (WT) or point mutants abrogated for signaling from TES1 (TES1m), TES2 (TES2m) or double TES1/TES2 mutant (DM) are shown.

(B) Immunoblot analysis of WCL from GM12878 LCLs that expressed control or LMP1 sgRNAs and puromycin selected for 3 days, then induced for expression with the indicated LMP1 rescue cDNA construct for 6 days. Blots are representative of n = 3 experiments.

(C) Growth curve analysis of GM12878 LCLs at the indicated day post expression of control or LMP1 sgRNAs and the indicated LMP1 WT, TES1m, TES2m or DM rescue cDNA. Shown are mean \pm SD from n=3 independent experiments. **p<0.01.

(D) FACS analysis of 7-AAD vital dye uptake in GM12878 on day 7 post- expression of LMP1 sgRNAs and the indicated LMP1 rescue cDNA. Shown are percentages of 7-AAD+ cells within the indicated gates. Representative of n=3 experiments.

(E) Mean \pm SD of fold change 7-AAD values from n=3 independent experiments of GM12878 with the indicated control or LMP1 sgRNA and rescue cDNA expression, as in (D). Values in GM12878 with control sgRNA and no LMP1 rescue cDNA were set to 1.

(F) FACS analysis of plasma membrane annexin V abundance in GM12878 on day 7 post- expression of control or LMP1 sgRNAs and the indicated LMP1 rescue cDNA. Shown are percentages of 7-AAD+ cells within the indicated gates. Representative of n=3 experiments.

(G) Mean \pm SD of fold-change caspase 3/7 activity levels, as determined by caspase 3/7 Glo assay, from n=3 independent experiments of GM12878 with the indicated control or LMP1 sgRNA and rescue cDNA expression. Values in GM12878 with control sgRNA and no LMP1 rescue cDNA were set to 1.

A

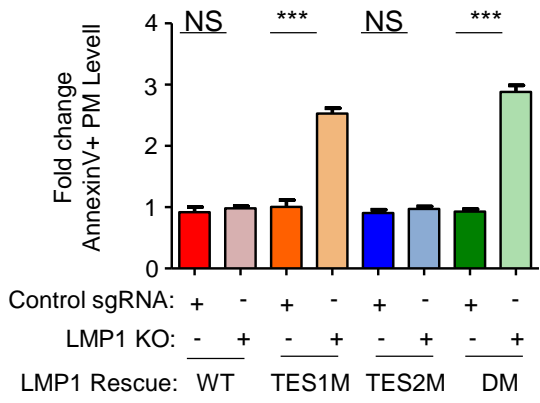


Fig. S2. Loss of TES1 but not TES2 signaling triggers LCL apoptosis.

Mean \pm SD of fold change plasma membrane Annexin V values from n=3 independent experiments, using GM12878 with the indicated control or LMP1 sgRNA and rescue cDNA expression. Values in GM12878 with control sgRNA and no LMP1 rescue cDNA were set to 1.

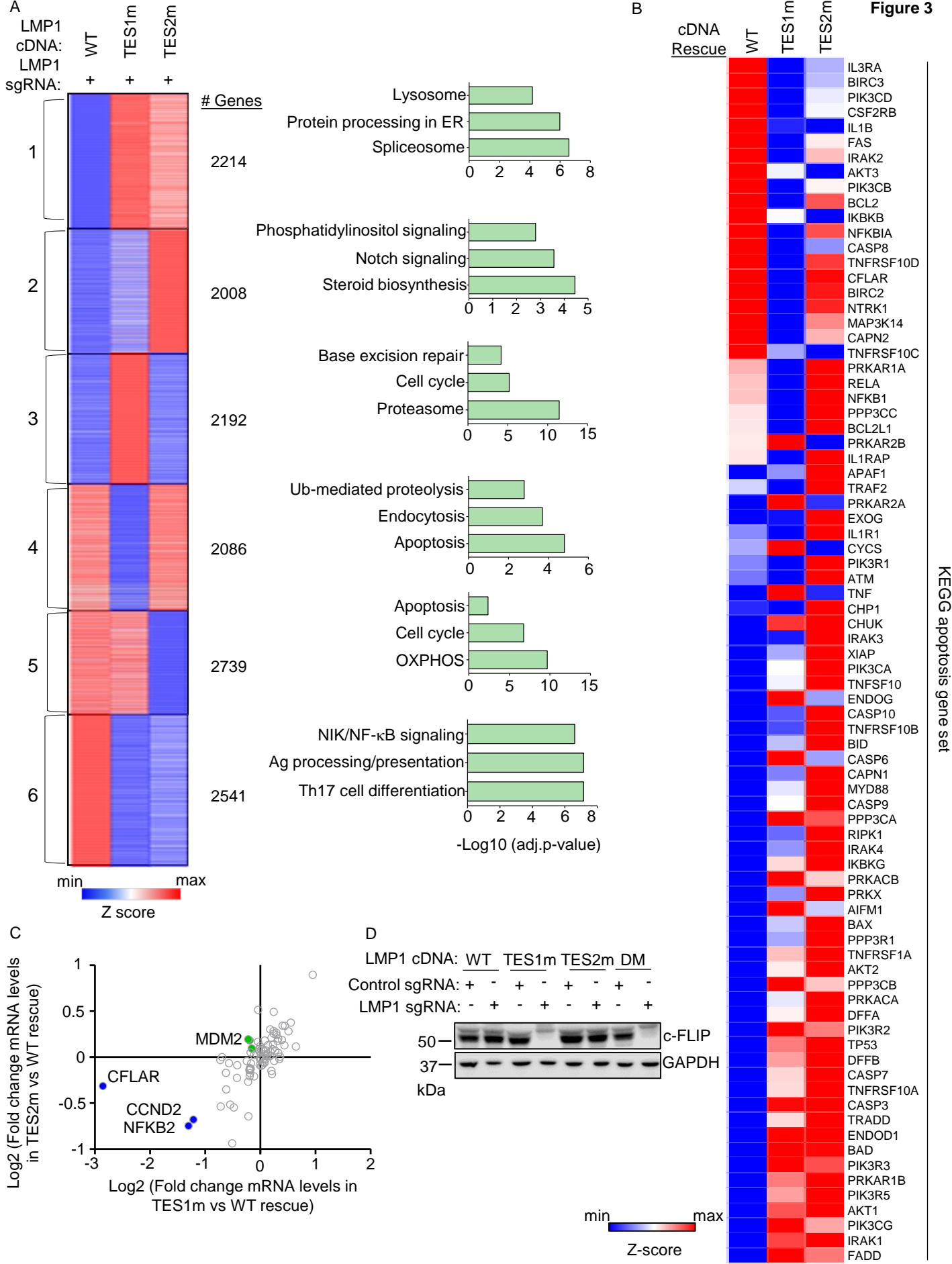


Fig. 3. Characterization of host genome-wide TES1 vs TES2 LCL target genes

(A) RNAseq K-means heatmap analysis of GM12878 LCLs transduced with lentivirus expressing LMP1 sgRNA and induced for WT, TES1m or TES2m rescue cDNA expression for 6 days. The heatmap depicts relative Z-scores in each row from n=3 independent RNAseq datasets, divided into six clusters. The Z-score scale is shown at bottom, where blue and red colors indicate lower versus higher relative expression, respectively. Two-way ANOVA P-value cutoff of <0.05 and >2-fold gene expression cutoffs were used. The top three most highly enriched KEGG pathways amongst genes within each cluster are shown at right.

(B) Heatmap analysis of KEGG apoptosis pathway gene relative row Z-scores from RNAseq analysis as in (A). The Z-score scale is shown at bottom, where blue and red colors indicate lower versus higher relative expression, respectively. Two-way ANOVA P-value cutoff of <0.05 and >2-fold gene expression cutoffs were used.

(C) Scatter plot analysis cross comparing log₂ transformed fold change of LCL dependency factor mRNA abundances in GM12878 expressing LMP1 sgRNA together with TES2 mutant versus wildtype cDNA rescue (Y-axis) and TES1 mutant versus wildtype cDNA rescue (X-axis) from triplicate RNAseq datasets, as in (A). This analysis highlighted that CFLAR and to a lesser extent NFKB2 and CCND2 mRNAs were more highly downmodulated by TES1m than TES2m rescue, relative to levels in cells with WT LMP1 rescue. Shown are genes differentially regulated by >2 fold with either TES1m or TES2m rescue, relative to levels with WT LMP1 rescue.

(D) Immunoblot analysis of c-FLIP and load control GAPDH expression in WCL from GM12878 LCLs with the indicated control or LMP1 sgRNA and LMP1 rescue cDNA expression. Representative of n=3 experiments.

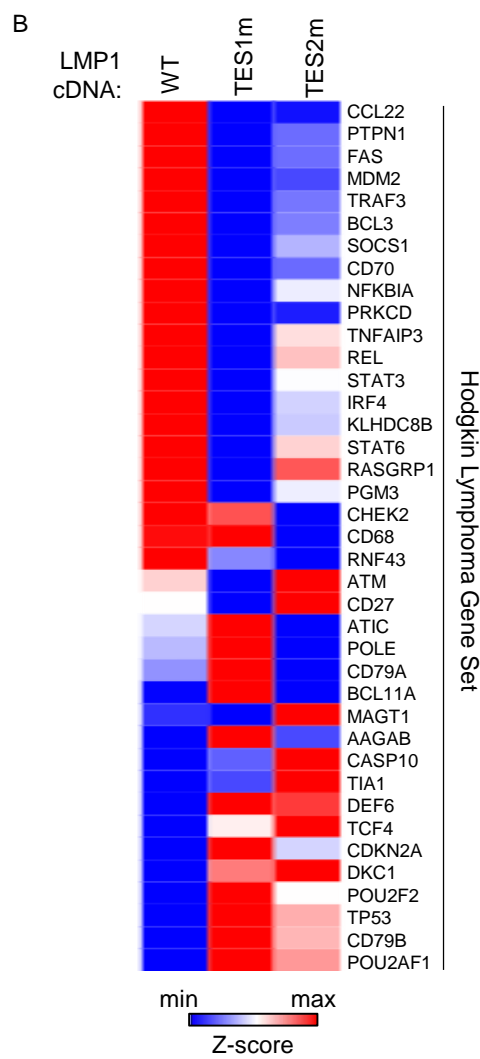
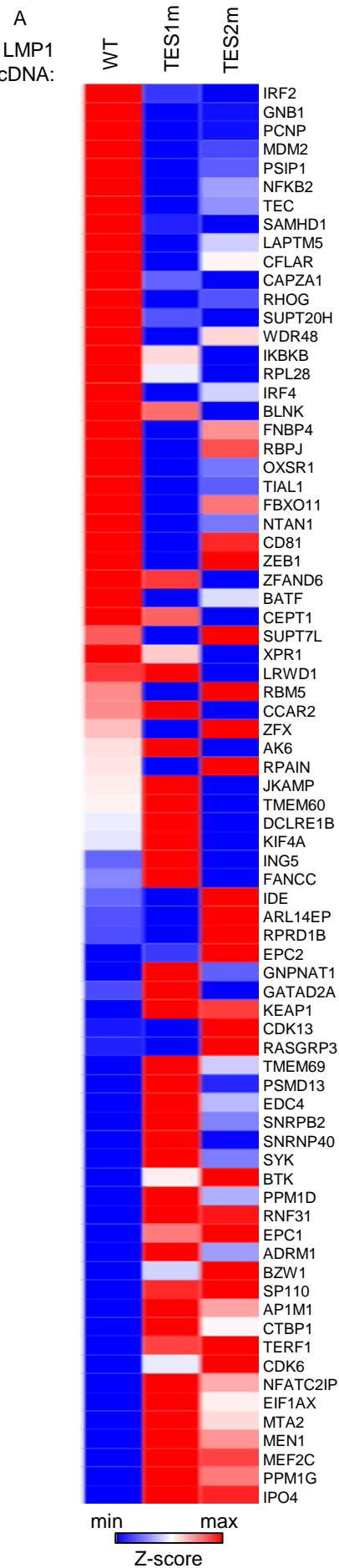


Figure S3. Characterization of TES1 vs TES2 LCL dependency factor and Hodgkin lymphoma pathway targets.

(A) Heatmap analysis of CRISPR defined LCL dependency factor gene relative row Z-scores from RNAseq of GM12878 expressing LMP1 sgRNA and the indicated rescue cDNA, as in **Fig. 3**. The Z-score scale is shown at bottom, where blue and red colors indicate lower versus higher relative expression, respectively. Two-way ANOVA P-value cutoff of <0.05 and >2 -fold gene expression cutoffs were used.

(B) Heatmap analysis of KEGG Hodgkin Lymphoma pathway gene relative row Z-scores from RNAseq of GM12878 expressing LMP1 sgRNA and the indicated rescue cDNA, as in **Fig. 3**. Two-way ANOVA P-value cutoff of <0.05 and >2 -fold gene expression cutoffs were used.

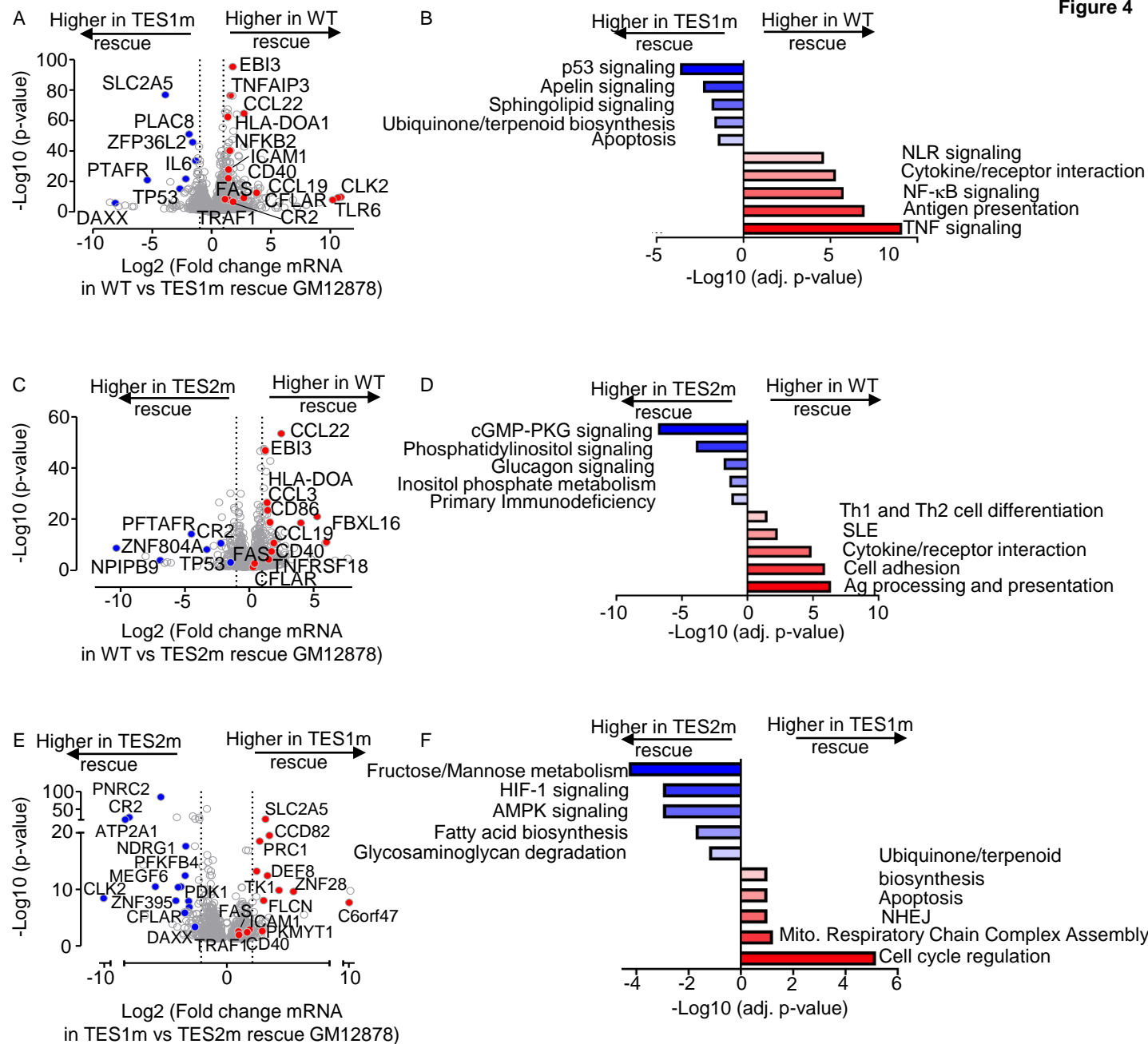


Fig. 4. Characterization of LCL pathways targeted by TES1 vs TES2 signaling

(A) Volcano plot analysis of host transcriptome-wide GM12878 genes differentially expressed in LMP1 KO GM12878 with WT vs TES1 mutant cDNA rescue. Higher X-axis fold changes indicate higher expression with WT LMP1 rescue, whereas lower X-axis fold changes indicate higher expression with TES1m rescue. Data are from n=3 RNAseq datasets, as in **Fig. 3**.

(B) Enrichr analysis of KEGG pathways most highly enriched in RNAseq data as in (A) amongst genes more highly expressed in LMP1 KO GM12878 with WT than TES1m rescue (red) vs amongst genes more highly expressed with TES1m than WT rescue (blue).

(C) Volcano plot analysis of host transcriptome-wide GM12878 genes differentially expressed in LMP1 KO GM12878 with WT vs TES2 mutant cDNA rescue. Higher X-axis fold changes indicate higher expression with WT LMP1 rescue, whereas lower X-axis fold changes indicate higher expression with TES2m rescue. Data are from n=3 RNAseq datasets, as in **Fig. 3**.

(D) Enrichr analysis of KEGG pathways most highly enriched in RNAseq data as in (C) amongst genes more highly expressed in LMP1 KO GM12878 with WT than TES2m rescue (red) vs amongst genes more highly expressed with TES2m than WT rescue (blue).

(E) Volcano plot analysis of host transcriptome-wide GM12878 genes differentially expressed in LMP1 KO GM12878 with TES1 vs TES2 mutant cDNA rescue. Higher X-axis fold changes indicate higher expression with TES1m rescue, whereas lower X-axis fold changes indicate higher expression with TES2m rescue. Data are from n=3 RNAseq datasets, as in **Fig. 3**.

(F) Enrichr analysis of KEGG pathways most highly enriched in RNAseq data as in (E) amongst genes more highly expressed in LMP1 KO GM12878 with TES1m than TES2m rescue (red) vs amongst genes more highly expressed with TES2m than TES1m rescue (blue).

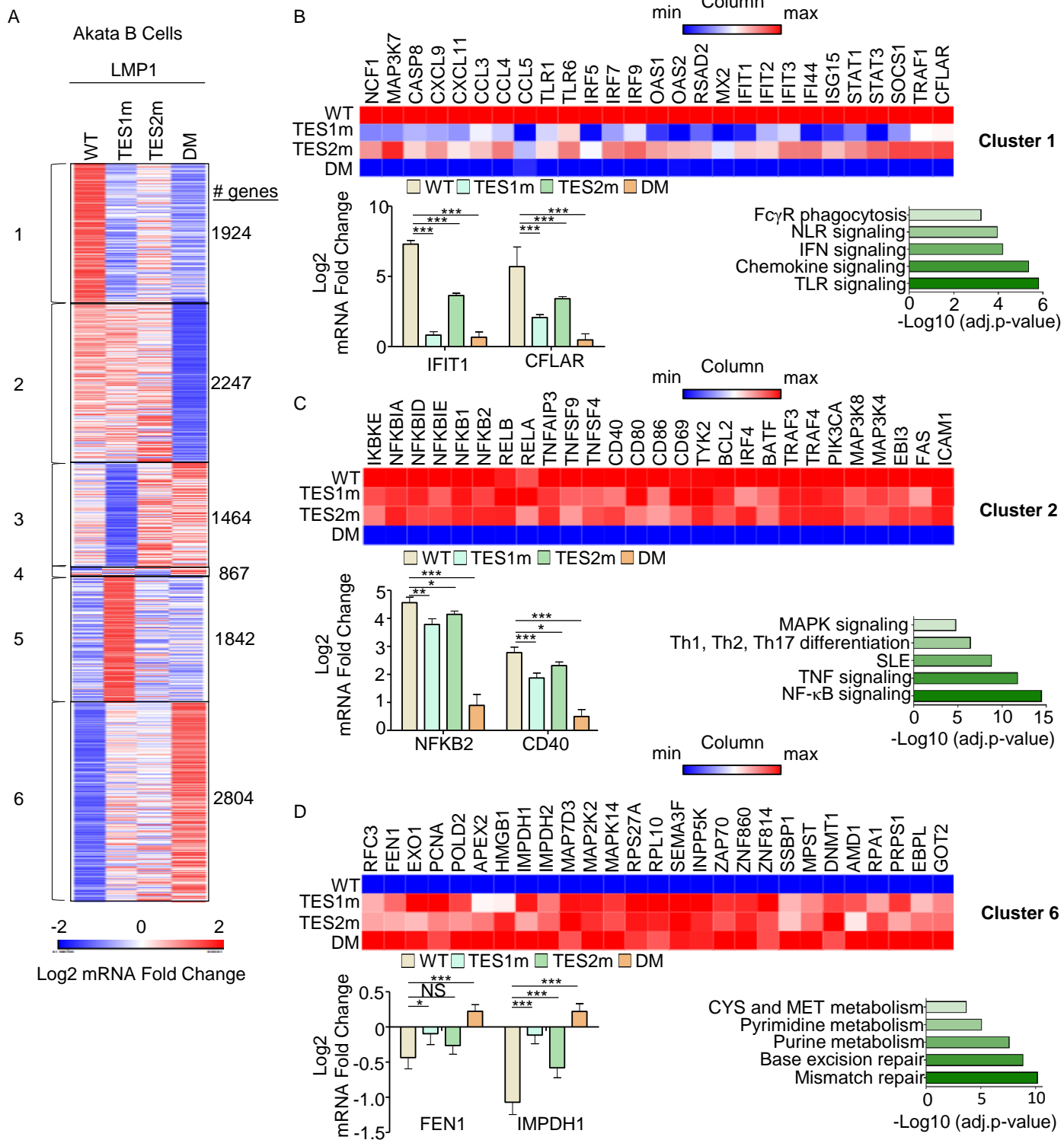


Fig. 5. Characterization of host genome-wide Akata B-cell LMP1 target genes.

(A) K-means heatmap analysis of RNAseq datasets from n=3 replicates generated in EBV- Akata Burkitt cells with conditional LMP1 WT, TES1m, TES2m or DM expression induced by 250 ng/ml doxycycline for 24 hours. The heatmap visualizes host gene Log2 Fold change across the four conditions, divided into six clusters. A two-way ANOVA P value cutoff of <0.01 and >2-fold gene expression were used. # of genes in each cluster is indicated at right.

(B) Heatmaps of representative Cluster 1 differentially regulated genes (top), with column maximum (max) colored red and minimum (min) colored blue, as shown by the scalebar. Also shown are expression values of two representative Cluster 1 genes (lower left) and Enrichr analysis of KEGG pathways significantly enriched in Cluster 1 gene sets (lower right). p-values were determined by one-sided Fisher's exact test. ***p<0.001.

(C) Heatmaps of representative Cluster 2 differentially regulated genes (top), as in (B). Also shown are expression values of two representative Cluster 2 genes (lower left) and Enrichr analysis of KEGG pathways significantly enriched in Cluster 2 gene sets (lower right). p-values were determined by one-sided Fisher's exact test. *p<0.05, **p<0.01, ***p<0.001.

(D) Heatmaps of representative Cluster 6 differentially regulated genes (top), as in (B). Also shown are expression values of two representative Cluster 6 genes (lower left) and Enrichr analysis of KEGG pathways significantly enriched in Cluster 6 gene sets (lower right). p-values were determined by one-sided Fisher's exact test. *p<0.05, ***p<0.001.

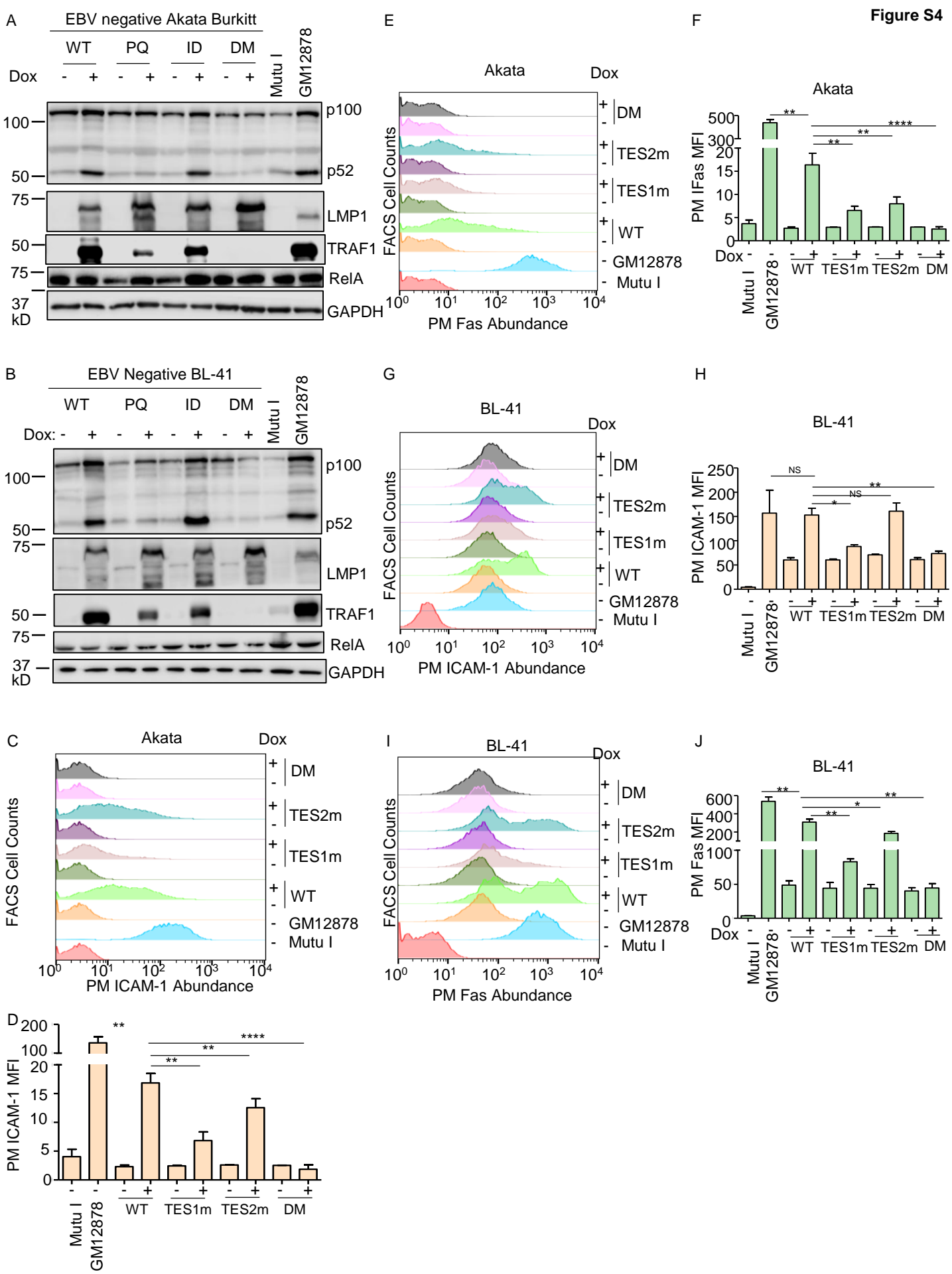


Fig. S4. Validation of LMP1 WT, TES1m, TES2m and DM conditional expression system in EBV-negative Akata Burkitt B-cells.

(A) Immunoblot analysis of WCL from Akata cells induced for LMP1 WT, TES1m, TES2m or DM expression by addition of 250 ng/ml doxycycline (Dox) for 24 hours, as indicated. For cross-comparison, WCL from equal numbers of Mutu I Burkitt lymphoma (latency I, lacks LMP1 expression) and GM12878 were also included at right. Blots are representative of n = 3 experiments.

(B) Immunoblot analysis of WCL from BL-41 cells induced for WT, TES1m, TES2m or DM LMP1 by addition of 250 ng/ml Dox for 24 hours, as indicated. For cross-comparison, WCL from equal numbers of Mutu I Burkitt and GM12878 were also included at right. Blots are representative of n = 3 experiments.

(C) FACS analysis of plasma membrane (PM) ICAM-1 abundance in Akata cells induced for LMP1 by 250 ng/ml Dox for 24 hours, as indicated. Y-axis are histogram cell counts, X-axis represents PM ICAM-1 abundance. For comparison, levels in GM12878 LCLs or latency I Mutu I Burkitt cells are shown.

(D) PM ICAM-1 Mean Fluorescence Intensity (MFI) + standard deviation (SD) from n=3 replicates in Akata cells with the indicated LMP1 expression, as in (C). p-values were determined by one-sided Fisher's exact test. **p<0.001, ***p<0.0001.

(E) FACS analysis of PM Fas abundance in Akata cells induced for LMP1 by 250ng/ml of Dox for 24 hours as indicated. For comparison, GM12878 LCLs or latency I Mutu I Burkitt cells were also analyzed.

(F) PM Fas MFI + SD from n=3 replicates in Akata cells with the indicated LMP1 expression, as in (E). P-values were determined by one-sided Fisher's exact test. **p<0.001, ***p<0.0001.

(G) FACS analysis of PM ICAM-1 in BL-41 cells induced for LMP1 expression by 250ng/ml Dox for 24 hours, as indicated. For comparison, GM12878 and Mutu I were also analyzed. p-values were determined by one-sided Fisher's exact test. **p<0.001, ***p<0.0001.

(H) PM ICAM-1 MFI + SD from n=3 replicates in BL-41 cells with the indicated LMP1 expression, as in (G). P-values were determined by one-sided Fisher's exact test. **p<0.001, ***p<0.0001.

(I) FACS analysis of PM Fas levels in BL-41 cells induced for LMP1 expression by 250 ng/ml dox for 24 hours, as indicated. GM12878 and Mutu I were analyzed for cross-comparison. p-values were determined by one-sided Fisher's exact test. **p<0.001, ***p<0.0001.

(J) PM Fas MFI + SD from n=3 replicates of BL-41-LMP1 with the indicated LMP1 expression, as in (I). Mutu I and GM12878 were analyzed for comparison. p-values were determined by one-sided Fisher's exact test. **p<0.001, ***p<0.0001.

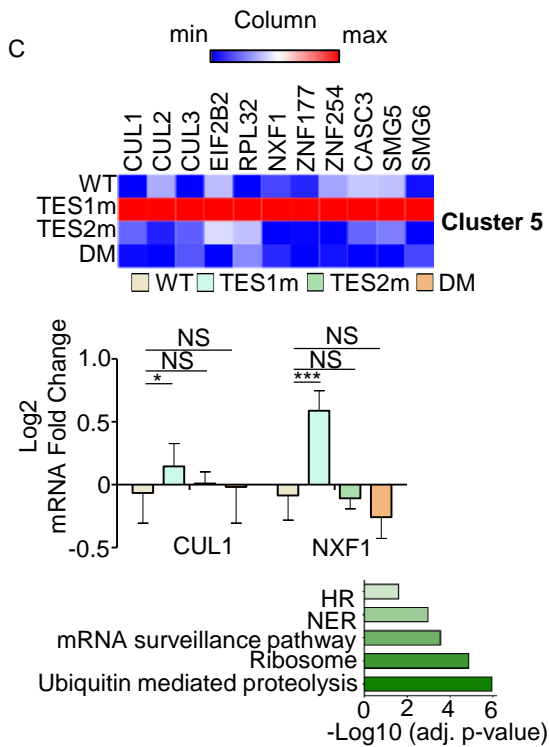
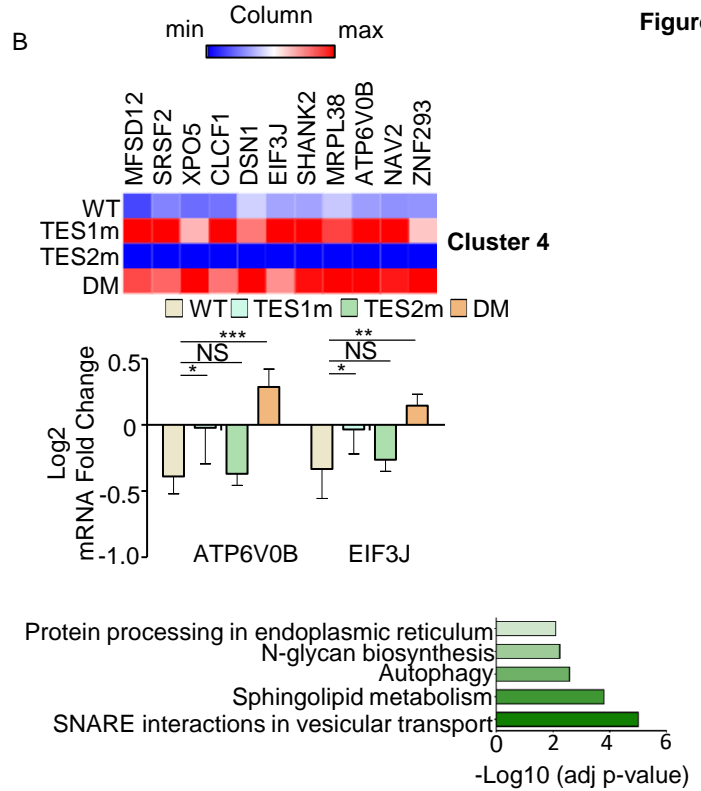
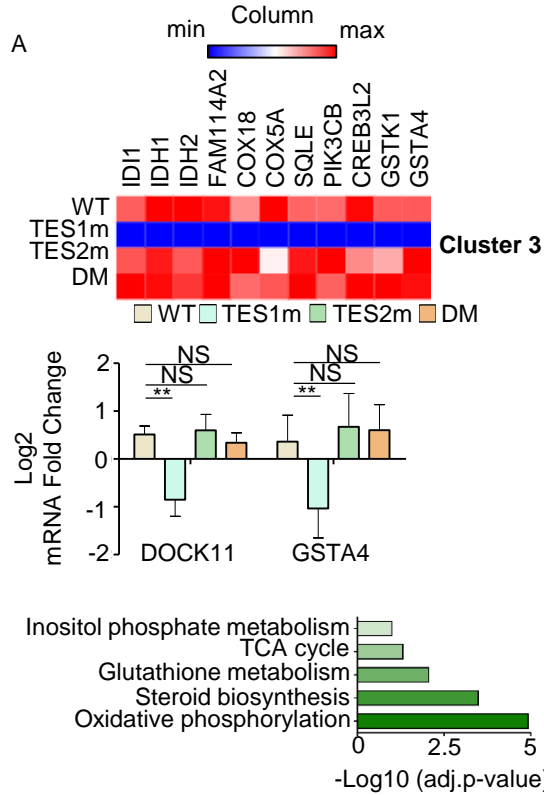


Fig. S5. Characterization of host genome-wide Akata B-cell LMP1 target genes, related to Figure 4.

(A) Heatmaps of representative **Figure 4** Cluster 3 differentially regulated genes (top), with column maximum colored red and minimum colored blue, as shown by the scalebar. Also shown are expression values of two representative Clusters 3 genes (lower left) and Enrichr analysis of KEGG pathways most significantly enriched Cluster 3 gene sets (lower right). p-values were determined by one-sided Fisher's exact test. ** $p < 0.01$.

(B) Heatmaps of representative **Figure 4** Cluster 4 differentially regulated genes (top), with column maximum colored red and minimum colored blue, as shown by the scalebar. Also shown are expression values of two representative Clusters 4 genes (lower left) and Enrichr analysis of KEGG pathways most significantly enriched Cluster 4 gene sets (lower right). p-values were determined by one-sided Fisher's exact test. * $p < 0.05$, ** $p < 0.01$, *** $p < 0.001$.

(C) Heatmaps of representative **Figure 4** Cluster 5 differentially regulated genes (top), with column maximum colored red and minimum colored blue, as shown by the scalebar. Also shown are expression values of two representative Clusters 5 genes (lower left) and Enrichr analysis of KEGG pathways most significantly enriched Cluster 5 gene sets (lower right). p-values were determined by one-sided Fisher's exact test. * $p < 0.05$, *** $p < 0.001$.

Fig. S6. RNAseq analysis of BL-41 B-cell responses to WT, TES1, TES2 or DM LMP1.

(A) K-means heatmap analysis of RNAseq datasets from n=3 replicates generated in EBV- BL-41 Burkitt cells with conditional LMP1 WT, TES1m, TES2m or DM expression induced by 250 ng/ml doxycycline for 24 hours. The heatmap visualizes host gene Log2 Fold change across the four conditions, divided into six clusters. A two-way ANOVA P value cutoff of <0.01 and >2-fold gene expression were used. # of genes in each cluster is indicated at right.

(B) Heatmaps of representative Cluster 1 differentially regulated genes (top), with column maximum (max) colored red and minimum (min) colored blue, as shown by the scalebar. Also shown are expression values of two representative Cluster 1 genes (lower left) and Enrichr analysis of KEGG pathways significantly enriched in Cluster 1 gene sets (lower right). p-values were determined by one-sided Fisher's exact test. ***p<0.001.

(C) Heatmaps of representative Cluster 2 differentially regulated genes (top). Also shown are expression values of two representative Cluster 2 genes (lower left) and Enrichr analysis of KEGG pathways significantly enriched in Cluster 2 gene sets (lower right). p-values were determined by one-sided Fisher's exact test. ***p<0.001.

(D) Heatmaps of representative Cluster 4 differentially regulated genes (top). Also shown are expression values of two representative Cluster 4 genes (lower left) and Enrichr analysis of KEGG pathways significantly enriched in Cluster 4 gene sets (lower right). p-values were determined by one-sided Fisher's exact test. *p<0.05, ***p<0.001.

(E) Heatmaps of representative Cluster 6 differentially regulated genes (top). Also shown are expression values of two representative Cluster 6 genes (lower left) and Enrichr analysis of KEGG pathways significantly enriched in Cluster 6 gene sets (lower right). p-values were determined by one-sided Fisher's exact test. *p<0.05, **p<0.01, ***p<0.001.

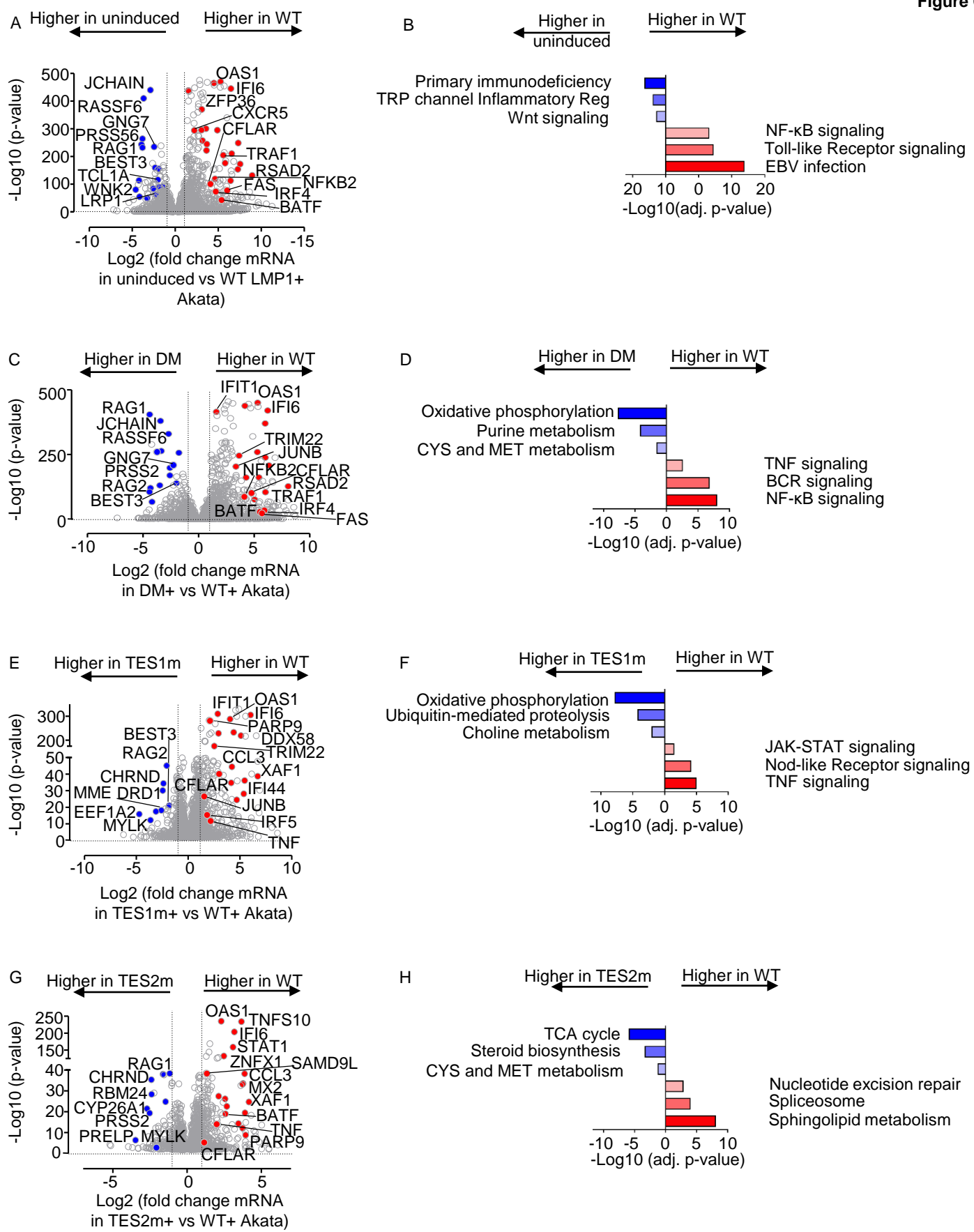


Fig. 6. Characterization of Akata B-cell pathways targeted by TES1 vs TES2 signaling.

(A) Volcano plot analysis of host transcriptome-wide genes differentially expressed in Akata cells conditionally induced for WT LMP1 expression for 24h by 250 ng/ml Dox versus in mock induced cells. Higher X-axis fold changes indicate genes more highly expressed in cells with WT LMP1 expression, whereas lower X-axis fold changes indicate higher expression in cells mock induced for LMP1. Data are from n=3 RNAseq datasets, as in **Fig. 5**.

(B) Enrichr analysis of KEGG pathways most highly enriched in RNAseq data as in (A) amongst genes more highly expressed in Akata with WT LMP1 (red) vs amongst genes more highly expressed with mock LMP1 induction (blue).

(C) Volcano plot analysis of host transcriptome-wide genes differentially expressed in Akata cells conditionally induced for WT vs DM LMP1 expression for 24h by 250 ng/ml Dox. Higher X-axis fold changes indicate genes more highly expressed in cells with WT LMP1 expression, whereas lower X-axis fold changes indicate higher expression in cells with DM LMP1. Data are from n=3 RNAseq datasets, as in **Fig. 5**.

(D) Enrichr analysis of KEGG pathways most highly enriched in RNAseq data as in (C) amongst genes more highly expressed in Akata with WT LMP1 (red) vs amongst genes more highly expressed with DM LMP1 induction (blue).

(E) Volcano plot analysis of host transcriptome-wide genes differentially expressed in Akata cells conditionally induced for WT vs TES1m LMP1 expression for 24h by 250 ng/ml Dox. Higher X-axis fold changes indicate genes more highly expressed in cells with WT LMP1 expression, whereas lower X-axis fold changes indicate higher expression in cells with TES1m LMP1. Data are from n=3 RNAseq datasets, as in **Fig. 5**.

(F) Enrichr analysis of KEGG pathways most highly enriched in RNAseq data as in (E) amongst genes more highly expressed in Akata with WT LMP1 (red) vs amongst genes more highly expressed with TES1m LMP1 induction (blue).

(G) Volcano plot analysis of host transcriptome-wide genes differentially expressed in Akata cells conditionally induced for WT vs TES2m LMP1 expression for 24h by 250 ng/ml Dox. Higher X-axis fold changes indicate genes more highly expressed in cells with WT LMP1 expression, whereas lower X-axis fold changes indicate higher expression in cells with TES2m LMP1. Data are from n=3 RNAseq datasets, as in **Fig. 5**.

(H) Enrichr analysis of KEGG pathways most highly enriched in RNAseq data as in (G) amongst genes more highly expressed in Akata with WT LMP1 (red) vs amongst genes more highly expressed with TES2m LMP1 induction (blue).

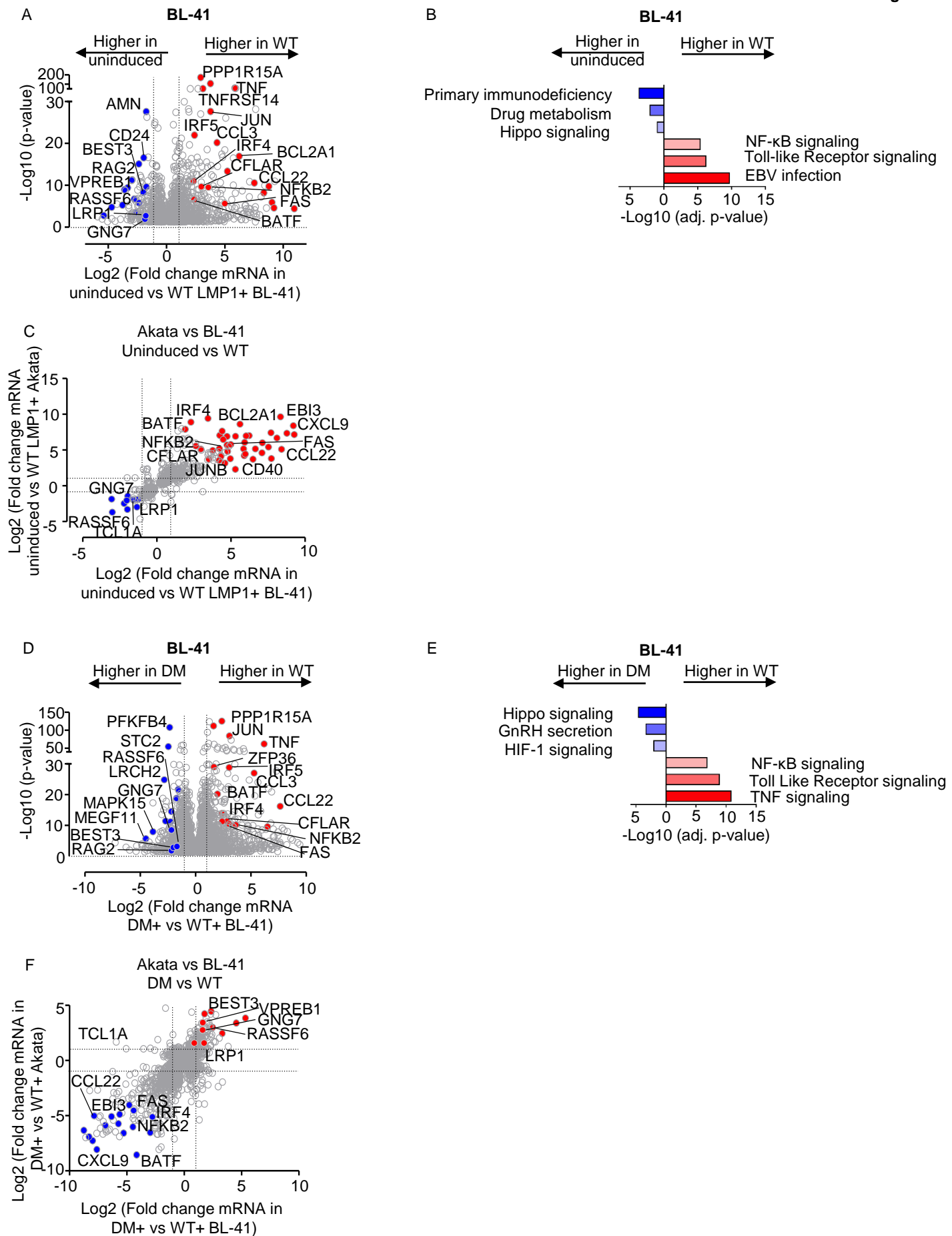


Fig. S7. Cross-comparison of WT and DM LMP1 effects on Akata vs BL-41 transcriptomes.

(A) Volcano plot analysis of host transcriptome-wide genes differentially expressed in BL-41 cells conditionally induced for WT LMP1 expression for 24h by 250 ng/ml Dox versus in mock induced cells. Higher X-axis fold changes indicate genes more highly expressed in cells with WT LMP1 expression, whereas lower X-axis fold changes indicate higher expression in cells mock induced for LMP1. Data are from n=3 RNAseq datasets.

(B) Enrichr analysis of KEGG pathways most highly enriched in RNAseq data as in (A) amongst genes more highly expressed in BL-41 with WT LMP1 (red) vs amongst genes more highly expressed with mock LMP1 induction (blue).

(C) Volcano plot cross-comparison of Log₂ transformed fold change of host mRNA levels in BL-41 cells (X-axis) versus Akata cells (Y-axis) uninduced versus induced for WT LMP1 by 250 ng/ml Dox for 24 hours. Selected genes highly WT LMP1 induced in both Burkitt contexts are highlighted in red, whereas selected genes suppressed by LMP1 in both Burkitt contexts are highlighted in blue.

(D) Volcano plot analysis of host transcriptome-wide genes differentially expressed in BL-41 cells conditionally induced for DM versus WT LMP1 expression for 24h by 250 ng/ml Dox. Higher X-axis fold changes indicate genes more highly expressed in cells with WT LMP1 expression, whereas lower X-axis fold changes indicate higher expression in cells induced for DM LMP1. Data are from n=3 RNAseq datasets.

(E) Enrichr analysis of KEGG pathways most highly enriched in RNAseq data as in (D) amongst genes more highly expressed in BL-41 with WT LMP1 (red) vs amongst genes more highly expressed with DM LMP1 induction (blue).

(F) Volcano plot cross-comparison of Log₂ transformed fold change of host mRNA levels in BL-41 cells (X-axis) versus Akata cells (Y-axis) induced for DM versus WT LMP1 by 250 ng/ml Dox for 24 hours. Selected genes highly WT LMP1 induced in both Burkitt contexts relative to levels in cells with DM LMP1 expression are highlighted in red, whereas selected genes suppressed by WT LMP1 in both Burkitt contexts are highlighted in blue.

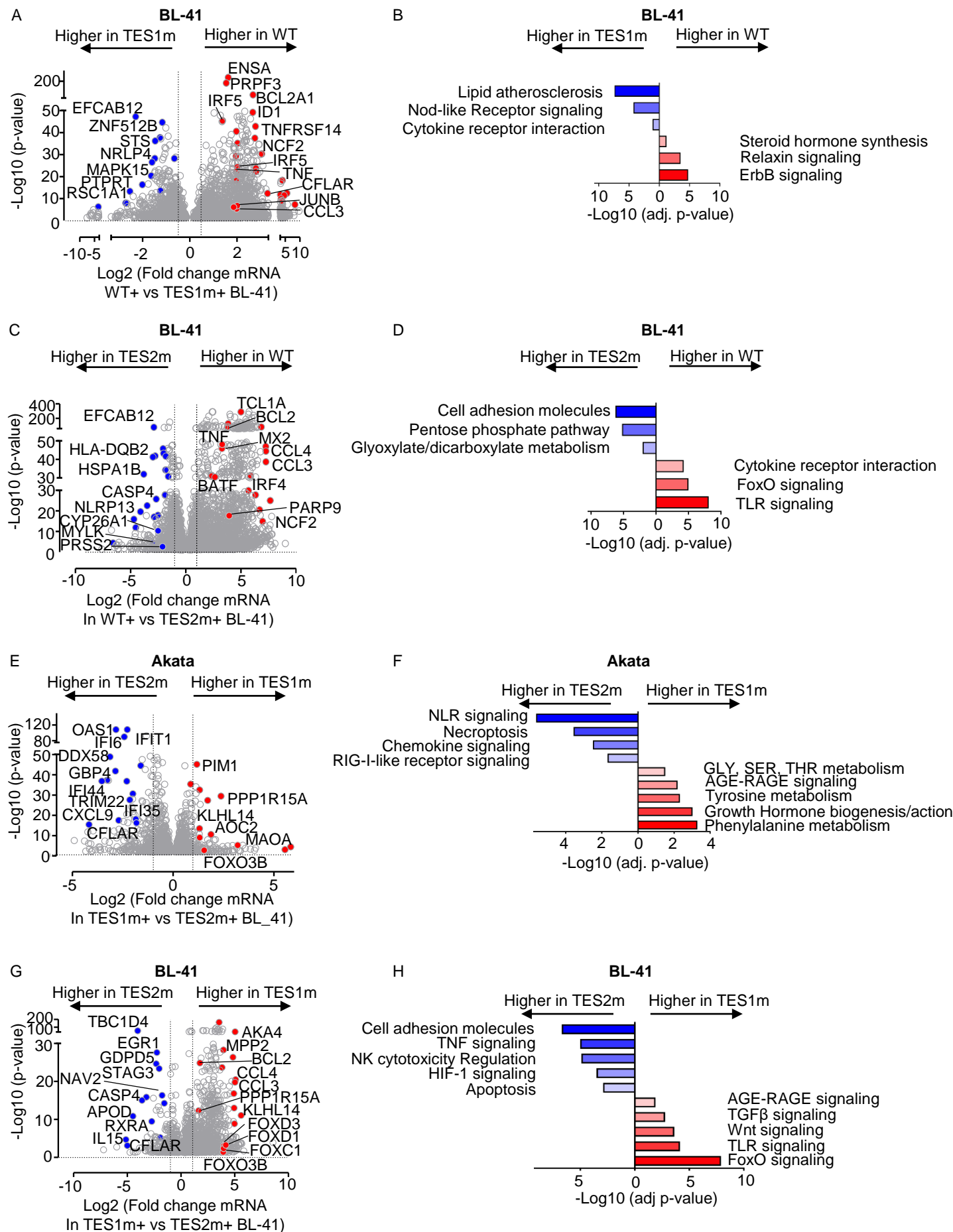


Fig. S8. Cross-comparison of TES1 and TES2 LMP1 effects on Akata vs BL-41 transcriptomes.

A) Volcano plot analysis of host transcriptome-wide genes differentially expressed in BL-41 cells conditionally induced for TES1m vs WT LMP1 expression for 24h by 250 ng/ml Dox. Higher X-axis fold changes indicate genes more highly expressed in cells with WT LMP1 expression, whereas lower X-axis fold changes indicate higher expression induced for TES1m LMP1. Data are from n=3 RNAseq datasets.

(B) Enrichr analysis of KEGG pathways most highly enriched in RNAseq data as in (A) amongst genes more highly expressed in BL-41 with WT LMP1 (red) vs amongst genes more highly expressed with TES1m LMP1 induction (blue).

(C) Volcano plot analysis of host transcriptome-wide genes differentially expressed in BL-41 cells conditionally induced for TES2m vs WT LMP1 expression for 24h by 250 ng/ml Dox. Higher X-axis fold changes indicate genes more highly expressed in cells with WT LMP1 expression, whereas lower X-axis fold changes indicate higher expression induced for TES2m LMP1. Data are from n=3 RNAseq datasets.

(D) Enrichr analysis of KEGG pathways most highly enriched in RNAseq data as in (A) amongst genes more highly expressed in BL-41 with WT LMP1 (red) vs amongst genes more highly expressed with TES2m LMP1 induction (blue).

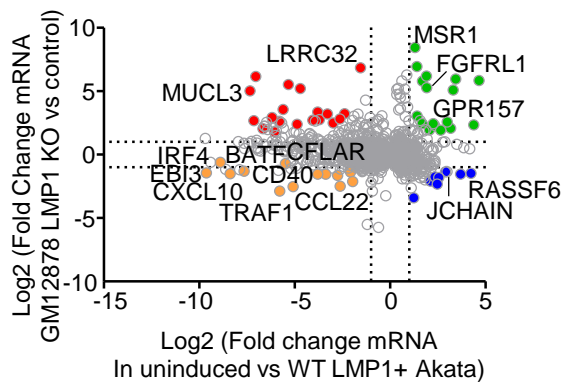
(E) Volcano plot analysis of host transcriptome-wide genes differentially expressed in Akata cells conditionally induced for TES1m vs TES2m LMP1 expression for 24h by 250 ng/ml Dox. Higher X-axis fold changes indicate genes more highly expressed in cells with TES1m LMP1 expression, whereas lower X-axis fold changes indicate higher expression induced for TES2m LMP1. Data are from n=3 RNAseq datasets.

(F) Enrichr analysis of KEGG pathways most highly enriched in RNAseq data as in (E) amongst genes more highly expressed in Akata with TES1m LMP1 (red) vs amongst genes more highly expressed with TES2m LMP1 induction (blue).

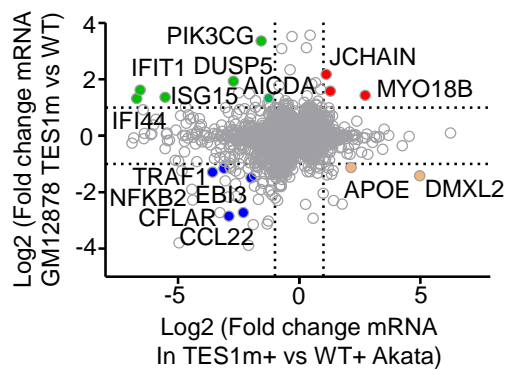
(G) Volcano plot analysis of host transcriptome-wide genes differentially expressed in BL-41 cells conditionally induced for TES1m vs TES2m LMP1 expression for 24h by 250 ng/ml Dox. Higher X-axis fold changes indicate genes more highly expressed in cells with TES1m LMP1 expression, whereas lower X-axis fold changes indicate higher expression induced for TES2m LMP1. Data are from n=3 RNAseq datasets.

(H) Enrichr analysis of KEGG pathways most highly enriched in RNAseq data as in (G) amongst genes more highly expressed in BL-41 with TES1m LMP1 (red) vs amongst genes more highly expressed with TES2m LMP1 induction (blue).

A



B



C

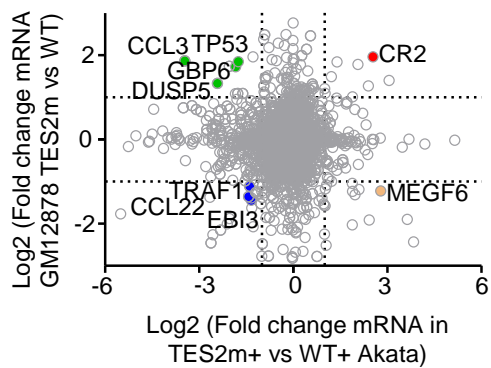


Figure S9. Cross-comparison of host genes differentially expressed upon perturbation of LCL LMP1 versus upon LMP1 induction in Akata cells.

(A) Volcano plot analysis of host genes differentially expressed upon WT LMP1 induction in Akata (X-axis) versus upon LMP1 KO in GM12878 (Y-axis). Shown are Log₂ transformed mRNA fold change values for Akata cells mock induced versus induced for LMP1 WT expression for 24 hours (X-axis) versus upon expression of LMP1 vs control sgRNA in GM12878 for 48 hours. Genes more highly expressed in mock-induced Akata have higher x-axis values, whereas genes more highly expressed in Akata induced for WT LMP1 have lower x-axis values. Likewise, genes with higher expression with control sgRNA expression have higher y-axis values, whereas genes with lower expression in GM12878 with LMP1 KO have lower Y-axis values. P value <0.05 and >2-fold gene expression cutoffs were used.

(B) Volcano plot analysis of host genes differentially expressed upon TES1m vs WT LMP1 induction in Akata (X-axis) versus upon rescue of LMP1 KO GM12878 with TES1m versus WT LMP1 (Y-axis). Shown are Log₂ transformed mRNA fold change values for Akata cells induced for TES1m versus WT LMP1 expression for 24 hours (X-axis) versus upon rescue of GM12878 LMP1 KO with TES1m vs WT LMP1 cDNA, as in **Fig 3**. Genes more highly expressed in Akata with TES1m than WT LMP1 expression have higher x-axis values, whereas genes more highly expressed in Akata induced for WT LMP1 than TES1m have lower x-axis values. Likewise, GM12878 genes with higher expression with TES1m rescue have higher y-axis values, whereas genes with lower expression in GM12878 with TES1m than WT rescue have lower Y-axis values. P value <0.05 and >2-fold gene expression cutoffs were used.

(C) Volcano plot analysis of host genes differentially expressed upon TES2m vs WT LMP1 induction in Akata (X-axis) versus upon rescue of LMP1 KO GM12878 with TES2m versus WT LMP1 (Y-axis). Shown are Log₂ transformed mRNA fold change values for Akata cells induced for TES2m versus WT LMP1 expression for 24 hours (X-axis) versus upon rescue of GM12878 LMP1 KO with TES2m vs WT LMP1 cDNA, as in **Fig 3**. Genes more highly expressed in Akata with TES2m than WT LMP1 expression have higher x-axis values, whereas genes more highly expressed in Akata induced for WT LMP1 than TES2m have lower x-axis values. Likewise, GM12878 genes with higher expression with TES2m rescue have higher y-axis values, whereas genes with lower expression in GM12878 with TES2m than WT rescue have lower Y-axis values. P value <0.05 and >2-fold gene expression cutoffs were used.

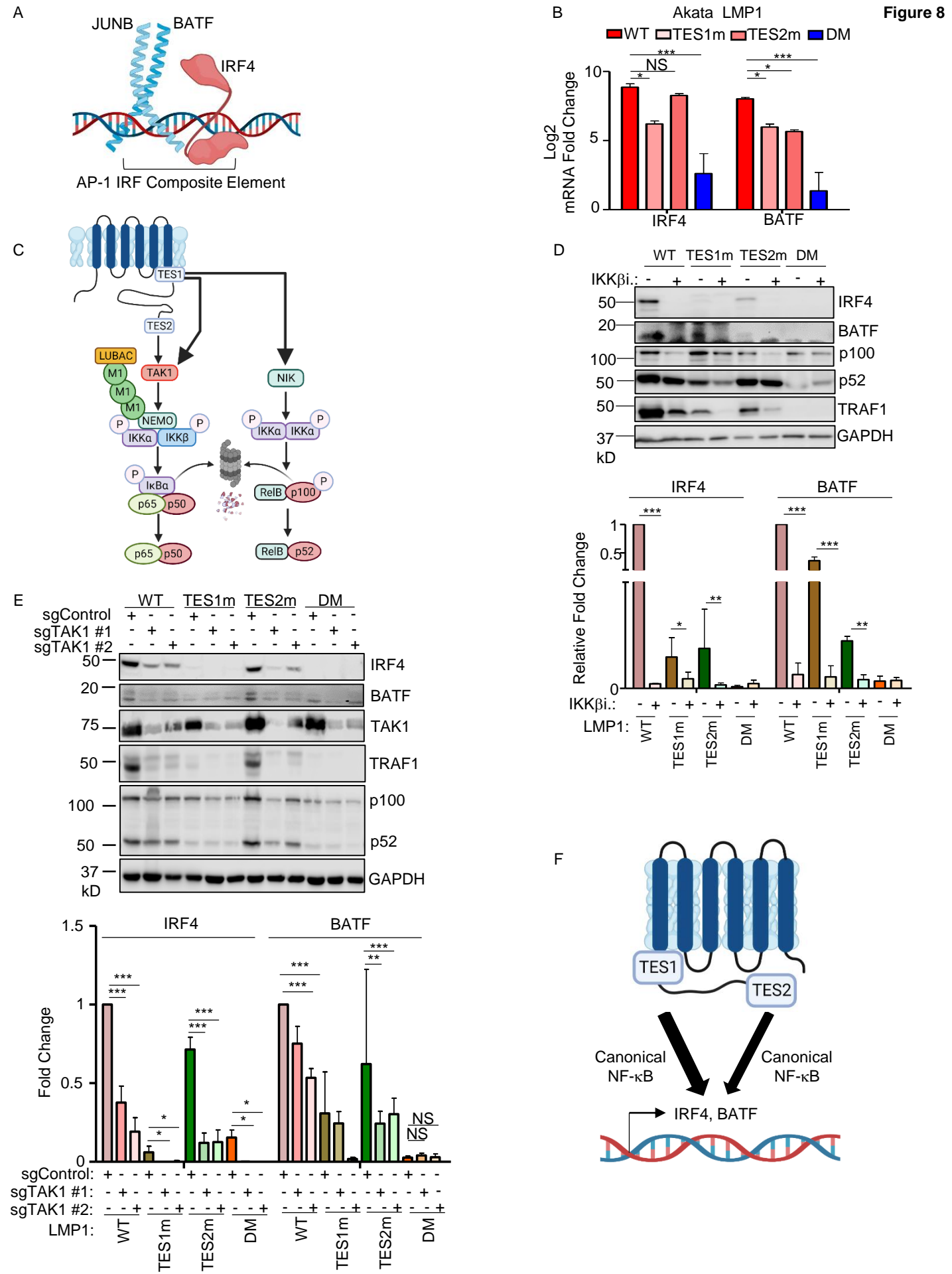


Fig. 8. Roles of TES1 and TES2 canonical NF- κ B pathways in LCL dependency factor BATF and IRF4 expression.

(A) Schematic diagram of JUNB, BATF and IRF4 at an AP-1/IRF composite DNA site.

(B) Mean + SD fold changes of IRF4, BATF and JUNB mRNA abundances from n=3 RNAseq replicates of Akata cells expressing the indicated LMP1 cDNA for 24 hours, as in Fig. 5. p-values were determined by one-sided Fisher's exact test. *p<0.05, ***p<0.001.

(C) Schematic diagram of LMP1 TES1 and TES2 NF- κ B pathways. TES1 and TES2 each activate canonical NF- κ B pathways, whereas TES1 also activates non-canonical NF- κ B.

(D) Immunoblot analysis of WCL from Akata cells induced for LMP1 expression by 250 ng/ml Dox for 24 hours, either without or with 1 μ M IKK β inhibitor VIII. Shown below are relative fold changes + SD from n=3 replicates of IRF4 or BATF vs GAPDH load control densitometry values. Values in vehicle control treated WT LMP1 expressing cells were set to 1. P-values were determined by one-sided Fisher's exact test. **p<0.001, ***p<0.0001.

(E) Immunoblot analysis of WCL from Cas9+ Akata cells expressing control or either of two *TAK1* targeting sgRNAs, induced for LMP1 expression by 250 ng/ml Dox for 24 hours. Shown below are relative foldchanges + SD from n=3 replicates of IRF4 or BATF vs GAPDH load control densitometry values. Levels in cells with control sgRNA (sgControl) and WT LMP1 were set to 1. **p<0.001, ***p<0.0001.

(F) Model of additive TES1 and TES2 canonical NF- κ B pathway effects on BATF and IRF4 induction.

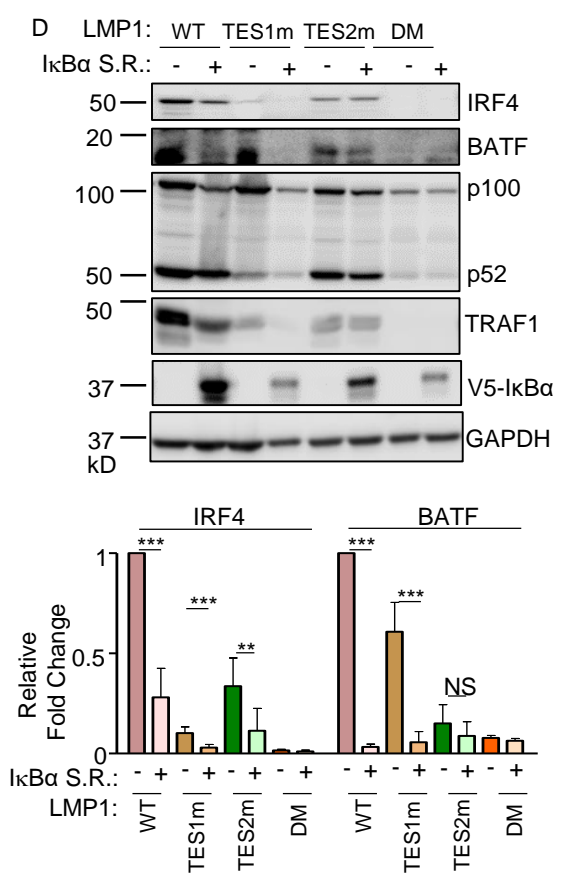
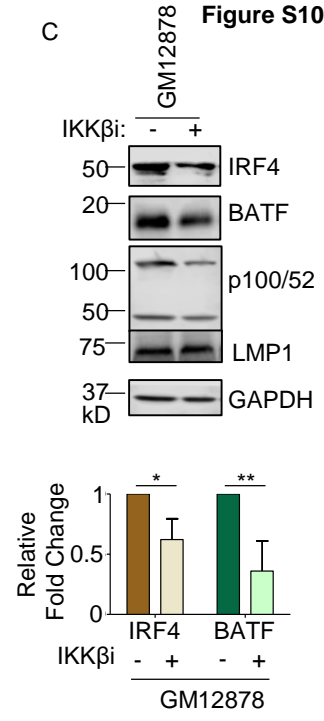
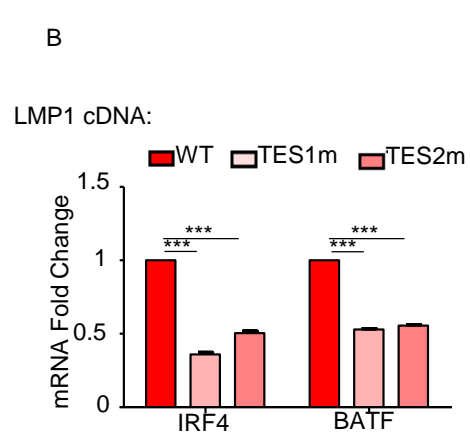
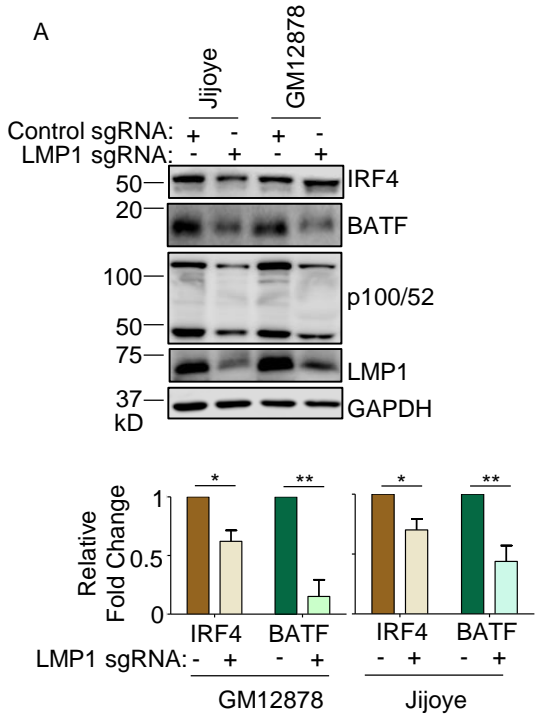


Fig. S10. Roles of TES1 and TES2 canonical NF- κ B pathways in BATF and IRF4 induction.

(A) Immunoblot analysis of WCL from latency III Jijoye Burkitt cells or GM12878 LCL expressing LMP1 targeting sgRNA, as indicated. Shown below are relative fold changes + SD from n=3 replicates of IRF4 or BATF vs GAPDH load control densitometry values, with values in sgRNA control expressing cells set to 1. P-values were determined by one-sided Fisher's exact test. **p<0.001, ***p<0.0001.

(B) Relative +SD BATF and IRF4 mRNA levels from n=3 RNAseq replicates from LMP1 KO GM12878 with TES1m, TES2m or WT LMP1 rescue cDNA expression, as in Fig 3-4. BATF or IRF4 levels in cells with WT LMP1 rescue were defined as 1. ***p<0.0001.

(C) Immunoblot analysis of WCL from GM12878 LCLs treated with vehicle control or 1 μ M IKK β inhibitor VIII for 24 hours. Shown below are relative foldchanges + SD from n=3 replicates of IRF4 or BATF vs GAPDH load control densitometry values. Levels in vehicle control treated WT LMP1 expressing cells were set to 1. P-values were determined by one-sided Fisher's exact test. **p<0.001, ***p<0.0001.

(D) Immunoblot analysis of WCL from Akata cells induced for the indicated LMP1 construct expression, either without or together with an I κ B α super-repressor (I κ B α -S.R.) that blocks canonical NF- κ B signaling. Shown below are relative foldchanges + SD of IRF4 or BATF vs GAPDH load control densitometry values from n=3 replicates, with values in cells expressing WT LMP1 but not I κ B α - set to 1. P-values were determined by one-sided Fisher's exact test. **p<0.001, ***p<0.0001.

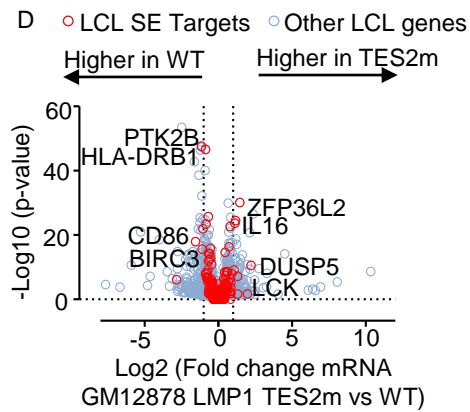
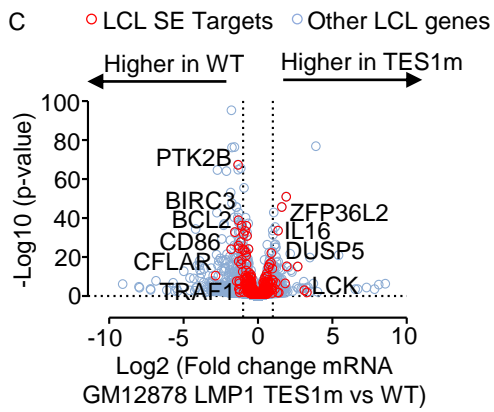
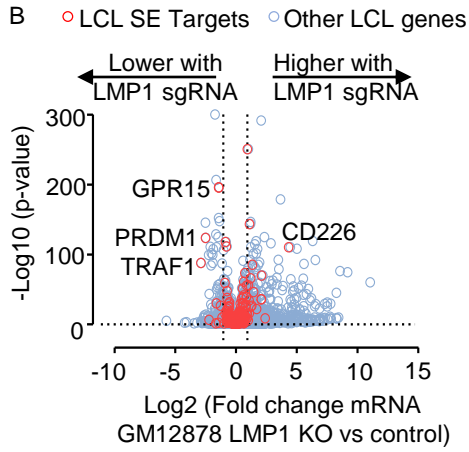
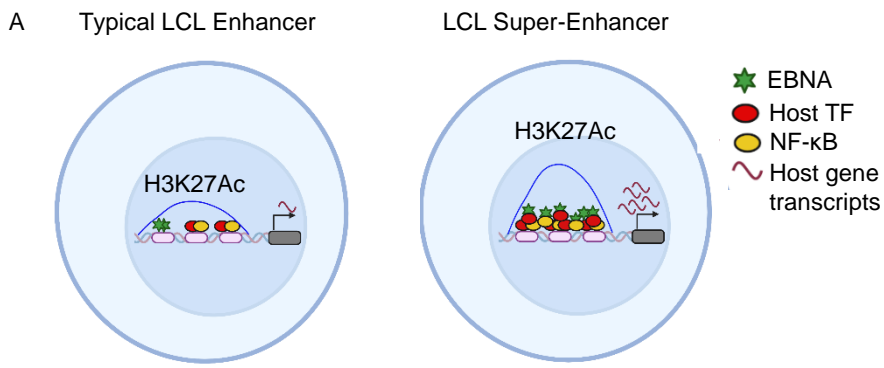


Fig. 9. LMP1 TES1 and TES2 roles in EBV super-enhancer target gene regulation in GM12878 LCLs.

(A) Schematic diagram of typical LCL enhancers vs super-enhancers. Super-enhancers have significantly broader and taller histone 3 lysine 27 acetyl (H3K27Ac) peaks. EBV SE are host genomic enhancer sites bound by all five LMP1-activated NF- κ B transcription factor subunits, EBNA-2, LP, 3A, and 3C.

(B) Volcano plot analysis of mRNA values in GM12878 expressing LMP1 vs control sgRNAs as in **Fig. 3**. Genes targeted by EBV super-enhancers (SE) are highlighted by red circles, whereas other LCL genes are indicated by blue circles. Genes more highly expressed with LMP1 KO have higher x-axis values, whereas those downmodulated by LMP1 KO have lower values. P value <0.05 and >2 -fold gene expression cutoffs were used.

(C) Volcano plot analysis of mRNA values in GM12878 expressing LMP1 sgRNA with TES1m versus WT LMP1 cDNA rescue, as in **Fig. 2-3**. Genes targeted by EBV super-enhancers (SE) are highlighted by red circles, whereas other LCL genes are indicated by blue circles. Genes more highly expressed with endogenous LMP1 KO and TES1m rescue have higher x-axis values, whereas those more highly expressed with WT LMP1 rescue have lower values. P value <0.05 and >2 -fold gene expression cutoffs were used.

(D) Volcano plot analysis of mRNA values in GM12878 expressing LMP1 sgRNA with TES2m versus WT LMP1 cDNA rescue, as in (C). Genes targeted by EBV super-enhancers (SE) are highlighted by red circles, whereas other LCL genes are indicated by blue circles. Genes more highly expressed with endogenous LMP1 KO and TES2m rescue have higher x-axis values, whereas those more highly expressed with WT LMP1 rescue have lower values. P value <0.05 and >2 -fold gene expression cutoffs were used.

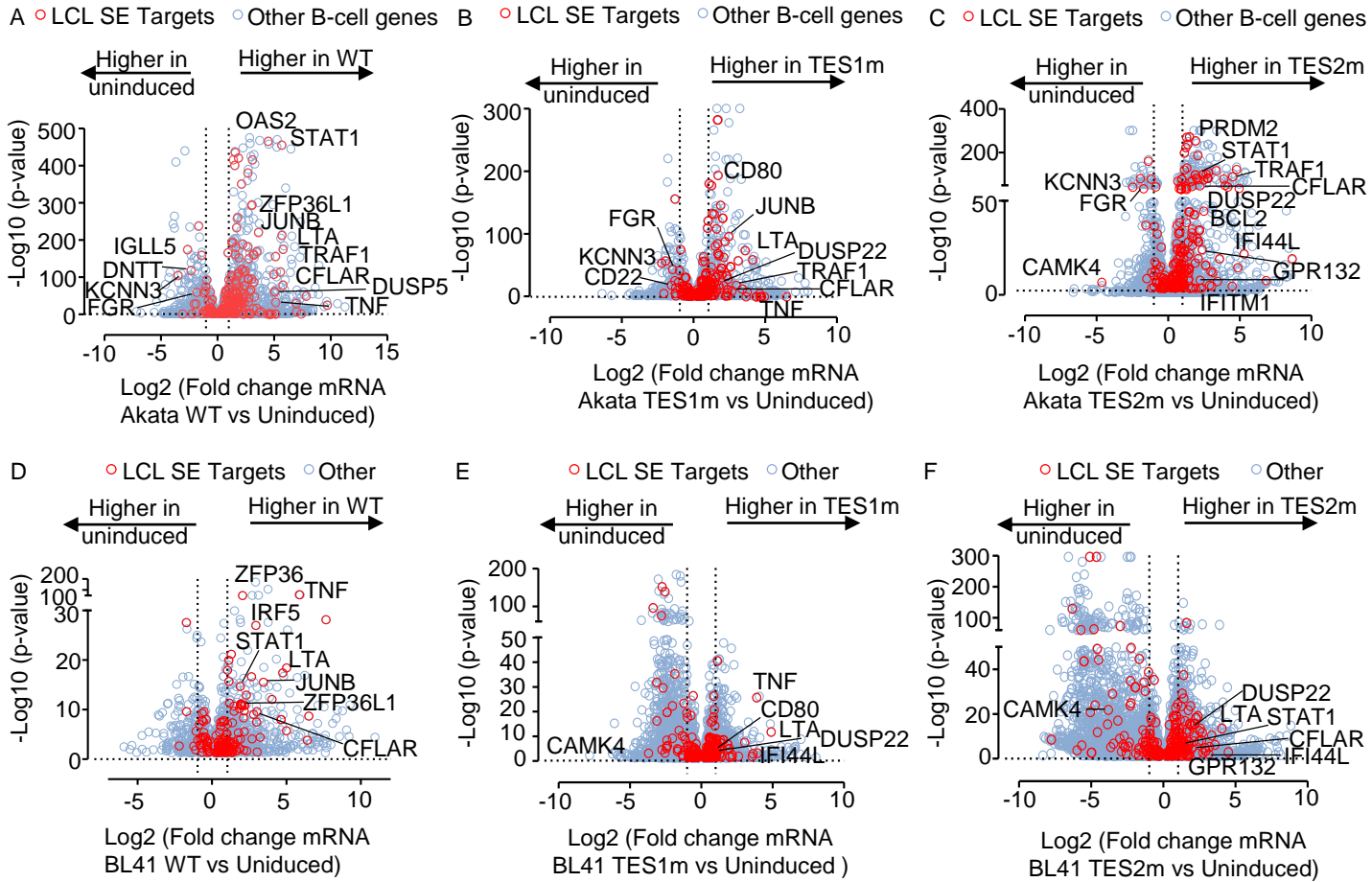


Figure S11. LMP1 TES1 and TES2 roles in EBV super-enhancer target gene regulation in Akata and BL-41 Burkitt B-cells.

- (A) Volcano plot analysis of Akata RNA-seq, comparing mRNA values in cells induced for LMP1 WT vs. mock-induced for 24 hours. SE targeted genes highlighted by red circles and other B-cell genes indicated by blue circles. P value <0.05 and >2 -fold gene expression cutoffs were used.
- (B) Volcano plot analysis of Akata RNA-seq, comparing mRNA values in cells induced for LMP1 TES1m vs. mock-induced for 24 hours. SE targeted genes highlighted by red circles and other B-cell genes indicated by blue circles. P value <0.05 and >2 -fold gene expression cutoffs were used.
- (C) Volcano plot analysis of Akata RNA-seq, comparing mRNA values in cells induced for LMP1 TES2m vs. mock-induced for 24 hours. SE targeted genes highlighted by red circles and other B-cell genes indicated by blue circles. P value <0.05 and >2 -fold gene expression cutoffs were used.
- (D) Volcano plot analysis of BL-41 RNA-seq, comparing mRNA values in cells induced for LMP1 WT vs. mock-induced for 24 hours. SE targeted genes highlighted by red circles and other B-cell genes indicated by blue circles. P value <0.05 and >2 -fold gene expression cutoffs were used.
- (E) Volcano plot analysis of BL-41 RNA-seq, comparing mRNA values in cells induced for LMP1 TES1m vs. mock-induced for 24 hours. SE targeted genes highlighted by red circles and other B-cell genes indicated by blue circles. P value <0.05 and >2 -fold gene expression cutoffs were used.
- (F) Volcano plot analysis of BL-41 RNA-seq, comparing mRNA values in cells induced for LMP1 TES2m vs. mock-induced for 24 hours. SE targeted genes highlighted by red circles and other B-cell genes indicated by blue circles. P value <0.05 and >2 -fold gene expression cutoffs were used.

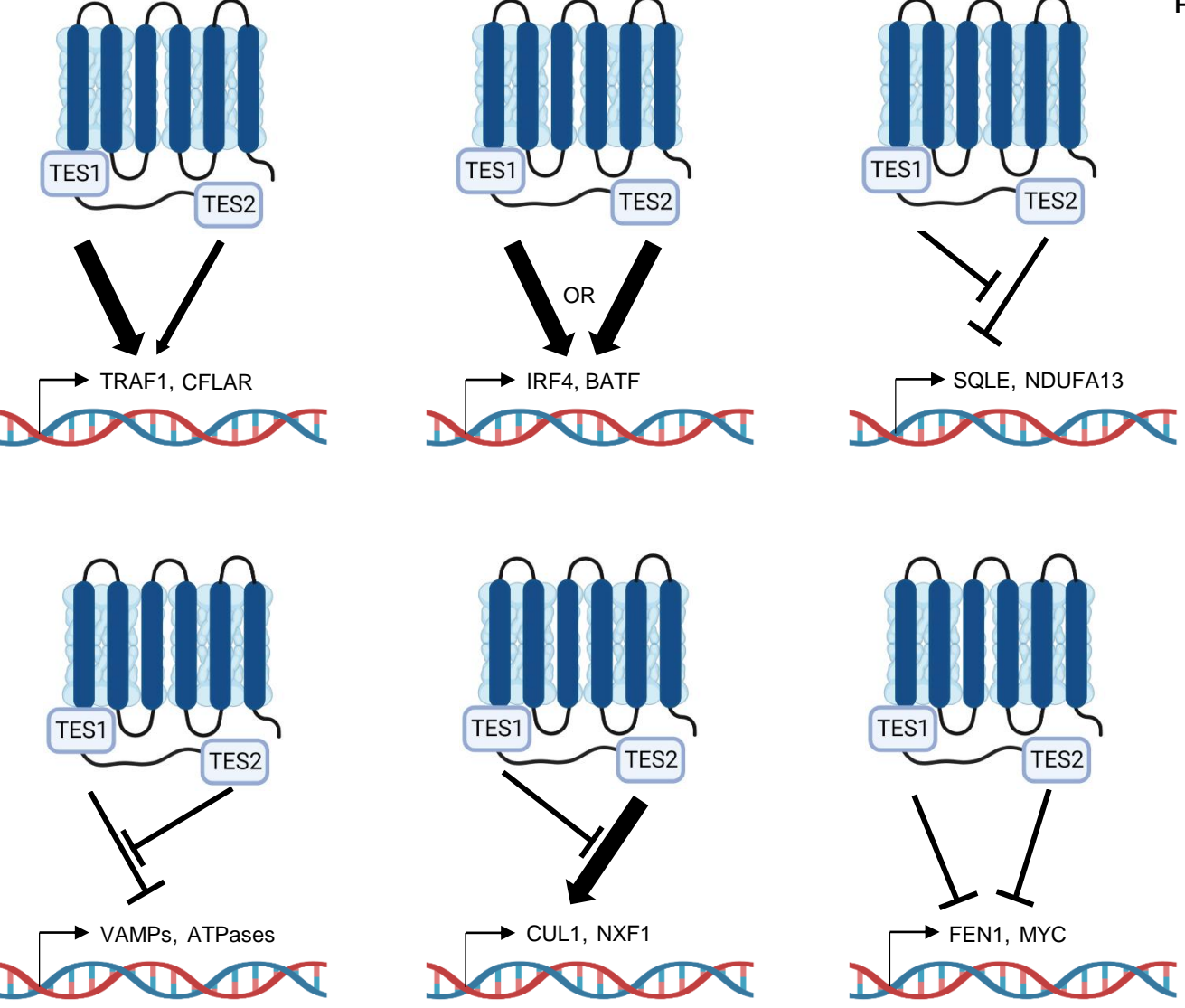


Fig. 10. Model highlighting different modes of LMP1 TES1 and TES2 cross-talk in B-cell target gene regulation.